# Receptor source apportionment of gaseous species at a site in the Mpumalanga Highveld

**E Cogho**

 **orcid.org / 0000-0001-9748-4184**

Thesis accepted for the degree Doctor of Philosophy in Science with Chemistry at the North-West University

| | |
|---|---|
| Promoter: | Prof PG van Zyl |
| Co-promoter: | Prof JP Beukes |
| Co-promoter: | Dr VT Vakkari |

# Acknowledgements

I would like to thank the following people without whom the completion of my dissertation would not have been possible.

- My supervisors, Professors Pieter van Zyl, Paul Beukes and Ville Vakkari for their guidance, input and support,
- My wife, Ezelna Germeshuisen-Cogho, and parents, Viktor and Anneke Cogho, for their unending belief, support and love,
- My Father in Heaven for providing me with the opportunity, perseverance and knowledge:

**“Yes, I am the vine, you are the branches. Those who remain in me, and I in them, will produce much fruit. For apart from me you can do nothing.” John 15:5**

# Abstract

To date, most source apportionment studies in South Africa, as well as globally, have focused on determining the chemical composition of aerosols/particulate matter (PM) or precipitation, with little consideration of the gaseous phase. This can be attributed to the methodologies available to perform source apportionment studies, which rely on the statistical analysis of large datasets with detailed assessments of the chemical composition of these types of atmospheric samples. However, a recent study performed by Chiloane *et al.* (2017) developed and utilised a method through which sources of equivalent black carbon (eBC) at the Elandsfontein atmospheric monitoring site in the Mpumalanga Highveld were identified by assessing the chemical composition of plumes measured at a receptor site. In this method, sources were identified by considering the air mass history associated with each plume and investigating the co-incidental appearances of peaks of typical atmospheric pollutant species measured at Elandsfontein. Therefore, plumes could be related to specific sources in this region.

This method was further developed and used to determine the predominant sources of hydrogen sulphide ($H_2S$), sulphur dioxide ($SO_2$), nitrogen oxide (NO) and nitrogen dioxide ($NO_2$) at Elandsfontein. An algorithm for this novel source quantification method introduced in this study for these atmospheric gaseous species was compiled, which could also be used in other studies. The Mpumalanga Highveld is a highly industrialised area in South Africa, with anthropogenic sources of atmospheric pollutants, including coal-fired power stations, as well as large petrochemical and pyrometallurgical smelters, while emissions from urban areas (e.g. household combustion, waste burning and traffic) are also well documented. Furthermore, the Mpumalanga Highveld has been included in the Highveld Priority Area as declared by the South African government, which is a region with high ambient concentrations of atmospheric pollutants that necessitate intervention. Measurements were conducted for two years at Elandsfontein in the European Integrated Project on Aerosol Cloud Climate and Air Quality Interactions.

The receptor method developed to enable the identification of sources and quantification of their contribution was applied to atmospheric concentrations of these trace gas levels above their baseline levels. The results indicate that emissions from urban areas on the Mpumalanga Highveld, associated with sources in towns, as well as semi- and informal settlements (e.g. ineffective household combustion of low-grade coal, sewage wastewater treatment facilities, landfills, small industries and traffic) contributed most to atmospheric $H_2S$ levels in excess of baseline concentrations (34.6%), followed by pyrometallurgical smelters (19.8%) and a petrochemical operation near Secunda (17.9%). The Johannesburg-Pretoria (Jhb-Pta) megacity, coal-fired power stations, burning coal dumps and cattle feedlots contributed 10.9%, 4.7%, 3.8% and 0.4%, respectively, to $H_2S$ concentrations in excess of the baseline levels. The contribution from urban areas is even more pronounced if the contributions from urban areas and the Jhb-Pta megacity on atmospheric $H_2S$ levels are combined. The largest contributor to $SO_2$ in excess of baseline levels was determined to be high-stack emissions associated with coal-fired power stations (62.8%), while the pyrometallurgical sector made the

second largest contribution (23.4%) and the third largest contribution was from the petrochemical sector (7.2%). Urban sources, the Jhb-Pta megacity and burning coal dumps contributed 4.6%, 1.1% and 0.4%, respectively, to atmospheric $SO_2$ concentrations determined at Elandsfontein. Only three high-stack sources were determined for NO with coal-fired power stations contributing the majority of measured NO (85.9%). NO is typically associated with fresher plumes with a large contribution originating from coal-fired power stations in the proximity of Elandsfontein. Coal-fired power stations also made the largest contribution to atmospheric $NO_2$ concentrations measured at Elandsfontein (59.4%), while the second and third largest contributions were from pyrometallurgical smelters (15%) and petrochemical operations (10.4%). Urban sources, traffic emissions, the Jhb-Pta and burning coal dumps contributed 6.1%, 5.7%, 1.6% and 0.3%, respectively. Although the contributions of these low-level emissions to $NO_2$ are relatively low, it is not insignificant, as reflected by the temporal patterns.

In addition to the new method introduced in this study to quantify sources of atmospheric gaseous species, a novel use of satellite data was also developed through which burning coal dumps could be identified and their impacts on concentrations of atmospheric pollutants could be determined. Satellite fire radiative power (FRP) data from the Moderate Resolution Imaging Spectro-Radiometer (MODIS) was used to determine the locations and durations of spontaneously combusted coal within the Mpumalanga Highveld. It was concluded that five mining sites, all opencast mines situated on old board-and-pillar mines, were prone to spontaneous combustion. Furthermore, a relatively well-defined seasonal pattern in the combustions was also observed, with combustion events being more prevalent during the winter months. Considering the active burning periods of the areas where spontaneous combustion was recorded, it was noted that burning coal dumps could be a major source of atmospheric pollutants on the Mpumalanga Highveld.

Mean concentrations of 3.1 ppbv, 11.5 ppbv, 2.7 ppbv and 12.5 ppbv were determined for $H_2S$, $SO_2$, NO and $NO_2$, respectively, for the entire sampling period. Well-defined seasonal and diurnal patterns indicated that low-level emission sources likely made the most significant contribution to the ambient $H_2S$ concentrations, whereas high-stack emissions were the dominant emission source for $SO_2$, NO and $NO_2$. However, the impact of high-stack emissions on $H_2S$ was also evident, while low-level emissions also contributed to ambient $NO_2$ concentrations, which supports the source results obtained through the application of the novel method.

**Keywords:** Hydrogen sulphide ($H_2S$), sulphur dioxide ($SO_2$), nitric oxide (NO), nitrogen dioxide ($NO_2$), seasonal and diurnal patterns, receptor source identification and quantification, South Africa, air quality management

# Contents

# List of abbreviations

| | |
|---|---|
| ACRG | Atmospheric Chemistry Research Group |
| ARL | Air Resources Laboratory |
| BIC | Bushveld Igneous Complex |
| CCN | Cloud condensation nuclei |
| $CH_4$ | Methane |
| CMB | Chemical mass balance |
| CO | Carbon monoxide |
| $CO_2$ | Carbon dioxide |
| DEA | Department of Environmental Affairs |
| DFFE | Department of Forestry, Fisheries and the Environment |
| eBC | Equivalent black carbon |
| EUCAARI | European Integrated Project on Cloud Climate, Aerosols and Air Quality |
| FA | Factor analysis |
| FLEXPART | FLEXible PARTicle dispersion model |
| GDAS | Global Data Assimilation Service |
| GHS | Greenhouse gases |
| $H_2S$ | Hydrogen sulphide |
| $H_2SO_4$ | Sulphuric acid |
| $HNO_3$ | Nitric acid |
| HYSPLIT | Hybrid Langrangian Integrated Trajectory |
| Jhb-Pta | Johannesburg-Pretoria |
| MAAP | Multi angle absorption photometer |
| NAAQS | National ambient air quality standard |
| NCD | Noncommunicable disease |
| NCEP | National Centre for Environmental Prediction |
| $NH_3$ | Ammonia |

| | |
|---|---|
| NMHC | Non-methane hydrocarbons |
| NO | Nitrous oxide |
| $NO_2$ | Nitrogen dioxide |
| $NO_x$ | Oxides of nitrogen |
| $NO_3^-$ | Nitrate |
| NOAA | National Oceanic and Atmospheric Administration |
| NWU | North-West University |
| $O_3$ | Ozone |
| PC | Principal component analysis |
| PM | Particulate matter |
| PMT | Photo multiplier tube |
| Ppbv | Parts per billion |
| Ppt | Parts per trillion |
| PSCF | Potential source contribution functions |
| $S^0$ | Elemental sulphur |
| $SO_2$ | Sulphur dioxide |
| $SO_4^{2-}$ | Sulphate |
| UNFCCC | United Nations framework Convention on Climate Change |
| UV | Ultra violet |
| VOC | Volatile organic compound |
| U.S EPA | United States Environmental Protection Agency |
| USNWS | United States National Weather Service |
| WHO | World Health Organisation |

# List of figures

## Chapter 2



## Chapter 3

## Chapter 4



## Chapter 5

# List of tables

## Chapter 3



## Chapter 4



## Chapter 5



## Chapter 6

# Chapter 1: Background, motivation, aim and objectives

**In this chapter,** this study is introduced by presenting a brief discussion on background information relevant to this study, while the motivation for performing this research is also discussed (section 1.1). In section 1.2, the general aim and specific objectives of the study are presented, while section 1.3 indicates the layout of the thesis.

## 1.1 Background and motivation

The atmosphere is the single largest resource shared by the entire world, which protects life on earth by absorbing solar radiation and regulating the temperature on earth (DEA, 2012). Anthropogenic emissions of gaseous species and aerosols alter the properties of the atmosphere, which subsequently impacts life and natural cycles on earth (IPCC, 2021). Furthermore, many of these compounds affect air quality and pose a threat to human health (e.g. Last *et al.,* 1994; Brunekreef & Holgate, 2002; Suwa *et al.,* 2002; Godish, 2004; Vallere, 2009; Di *et al.,* 2017; Manisalidis *et al.,* 2020). From an air quality perspective, nitric oxide (NO), nitrogen dioxide ($NO_2$), sulphur dioxide ($SO_2$) and hydrogen sulphide ($H_2S$) are among the most important gaseous species emitted in the atmosphere. These species can also act as precursors for the formation of secondary aerosol particles (e.g. Seinfeld & Pandis, 2006). Aerosols are an amalgamation of fine particles or liquids in the air, which can be emitted directly in particle phase or form in the atmosphere as secondary pollutants from gaseous precursor species through gas-to-particle conversions. World-wide, there is an increase in pollutant emissions, which contributes to the degradation of the atmosphere, as well as posing a serious threat to humans and the environment (Fenger, 1999). In a recent review of air quality papers over recent decades, it was found that air pollution has increased due to industrialisation, vehicular emissions, construction and biomass burning (Dhital & Rupakheti, 2019). However, in developed countries, air pollution has decreased, but it still remains relatively high in developing countries and Asian megacities (e.g. Beijing and Delhi) (Gurjar *et al*., 2016; Liu *et al.,* 2017). The direct and indirect effects of these pollutant species necessitate the need to conduct long-term measurements of emissions and concentrations of these species in the atmosphere in order to monitor changes in the atmospheric chemical compositions, and the general state of air quality in order to inform policymakers in their decision-making (Di *et al.,* 2017; Manisalidis *et al.,* 2020).

On a global scale, the measurement and improvement of air quality are a priority in developed countries, while developing countries, which in many instances also have emission and air quality targets, prioritise their resources to grow their economies (Venter *et al.,* 2012). South Africa is considered to have a two-tier economy, which is a combination between a developed- (Western industrialised countries) and a developing (emerging market) country (Venter *et al.,* 2012). On a global scale, Southern Africa is considered a major source of atmospheric pollutants, with the South African Highveld identified as a global hotspot for $NO_2$ and

$SO_2$ (Wenig *et al.,* 2003; Toenges-Schuller *et al.*, 2006). In addition to the aforementioned, a recent study by Shikawambana *et al.* (2020) found that sulphur emissions across the Limpopo, Gauteng and Mpumalanga Provinces of South Africa have shown an increasing trend from 1980 to 2018. Furthermore, large biomass burning activities in southern Africa contribute greatly to the global aerosol budget (Venter *et al.,* 2012; Swap *et al.,* 2003).

In order to improve air quality over any region or country, it is essential to evaluate the levels of atmospheric pollutants and to determine the contributions of different sources to the observed concentrations of these pollutants. In order to determine sources of atmospheric pollutants, numerous source apportionment methods have been developed and deployed throughout the realm of atmospheric chemistry, which have made significant contributions to improve our understanding of atmospheric chemistry and the main sources of pollutants (Viana *et al*., 2008; Belis *et al.,* 2015; Hopke, 2008; 2011; and 2016; Wold *et al.,* 1987; Adbi & Williams, 2010). However, most of these source apportionment methods rely on detailed chemical composition and meteorological information to model ambient concentrations based on emission profiles and rates (e.g. Maseko *et al*., 2021; de Lange *et al*., 2021) and are unsuitable to determine sources of atmospheric gaseous pollutants (e.g. $SO_2$ and $NO_2$) at a receptor site, especially in South Africa where up-to-date and regional-specific emission inventories are lacking. To date, most receptor source apportionment studies performed in South Africa have been based on the detailed chemical characterisation of aerosols, which was then subjected to statistical methods, e.g. principle component analysis or positive matrix factorisation (e.g. Maenhaut *et al*., 1996; Engelbrecht *et al*., 2002; Van Zyl *et al*., 2014; Tiitta *et al*., 2014; Venter *et al*., 2017; Jaars *et al*., 2018; Mathuthu *et al*., 2019; Meyemeki *et al*., 2021; Adeyemi *et al*., 2021; Alfeus *et al*., 2023). Furthermore, source apportionment was also conducted in South Africa through studies on precipitation chemistry (e.g. Mphepya *et al*., 2004 and 2006; Conradie *et al*., 2016).

In a recent paper by Chiloane *et al*. (2017), a method was developed to conduct a receptor source apportionment of equivalent black carbon (eBC, definition according to Petzold *et al.,* 2013), which was successfully employed to determine sources of eBC. This study of Chiloane *et al*. (2017) proposed that the method developed to perform source apportionment of eBC could also be applied to determine and quantify the sources of atmospheric trace gases. Therefore, considering the afore-mentioned context, the source apportionment technique developed by Chiloane *et al.* (2017) was further developed and applied in this study to enable receptor source quantification studies of trace gases. It was attempted to determine and quantify the sources of $H_2S$, $SO_2$ and $NO_2$ concentrations measured at an atmospheric measurement site, Elandsfontein, located in the highly industrialised and densely populated Mpumalanga Highveld, which is a region also classified as a pollution hotspot in South Africa and an air quality priority area. Therefore, the Elandsfontein monitoring site was considered ideal for this study, since it is impacted by several large point and regional sources, which include several coal-fired power stations, pyrometallurgical smelters, a large petrochemical plant and the Johannesburg-Pretoria megacity, without being situated in such a place that would create bias for a specific source. The comprehensive dataset utilised in this study was acquired during

the European Integrated project on Aerosol Cloud Climate and Air Quality Interactions (EUCAARI) at Elandsfontein (Laakso *et al*., 2012). Although the aim of EUCAARI was mainly focused on reducing the uncertainty associated with atmospheric aerosols on a global scale, concentrations of atmospheric gaseous species were also determined, since, as previously mentioned, these species are important precursors for atmospheric aerosols, which impact climate and air quality. South Africa was one of four developing countries outside of Europe that participated in the EUCAARI project with a successful campaign conducted during a three-year period.

## 1.2 Objectives

The general aim of this study was to conduct receptor-oriented source apportionment of ambient $H_2S$, NO, $NO_2$ and $SO_2$ measured at Elandsfontein during the EUCAARI project for the first time in South Africa with a novel method developed. The following objectives need to be met in order to reach this aim:

I.) Contextualise $H_2S$, NO, $NO_2$ and $SO_2$ concentrations measured at Elandsfontein by comparison to appropriate ambient air quality legislation and measurements conducted elsewhere, as well as assess temporal patterns of these species.

II.) Identify sources that could contribute to the inorganic trace gas concentrations at the site. This also included applying a novel method utilising satellite measurements to determine when coal dumps/seams were actively burning in the area surrounding Elandsfontein as a result of spontaneous combustion, which was one of the sources considered.

III.) Conduct source apportionment and quantification of $H_2S$, $SO_2$, $NO_2$ and NO, as well as quantification and contextualisation of the measured baseline of these species, with the novel method developed in this study.

## 1.3 Thesis outline

The thesis contains the following chapters:

Chapter 1

This chapter comprises the introduction, background and motivation, and objectives.

Chapter 2

This chapter covers a literature review on atmospheric pollutants, their origin, composition, impacts on the environment and human health. Furthermore, the Highveld Priority Area within South Africa is discussed, and finally, source apportionment techniques and how they have been applied within South Africa are provided.

Chapter 3

Descriptions of the measurement site, instrumentation, data cleaning and the main analyses methods employed in this study are presented. The identification of burning coal dumps using FRP data is also discussed, and finally, the technique applied to conduct source quantification of trace gases is presented.

Chapter 4

This chapter presents the identification of actively burning coal dumps using satellite-derived FRP data.

Chapter 5

This chapter presents the contextualisation as well as the temporal assessment of all the trace gas species used in the source apportionment study.

Chapter 6

This chapter presents numerous case studies to illustrate how different sources were identified. Furthermore, the source contributions for the different gas species are presented in this chapter.

Chapter 7

Final conclusions and the project evaluation of the successes and shortcomings are presented together with future recommendations.

# Chapter 2: Literature review

**In this chapter,** all relevant background information required for this study, with a particular focus on atmospheric pollution, sources of atmospheric pollutants, gaseous and aerosol species relevant to the study as well as their chemistry within the atmosphere will be provided. Source apportionment methods will also be discussed, including receptor and source-oriented models. Lastly, the Highveld Priority Area (HPA) and relevant source apportionment studies done within the HPA will be discussed.

## 2.1 Atmospheric pollution

The atmosphere of the earth is divided into multiple different layers (troposphere, stratosphere, mesosphere, thermosphere and exosphere), and this division is due to changes in temperature gradients with an increase in altitude (Atkinson, 2000). The closest and densest layer to the earth's surface is the troposphere; its chemical composition is 78.08% nitrogen ($N_2$), 20.95% oxygen ($O_2$), 0.93% argon (Ar), 0.036% carbon dioxide ($CO_2$) as well as varying concentrations of water vapour and trace amounts of numerous other gases. This layer also makes up approximately 80% of the atmosphere (Atkinson, 2000).

Pollution of the atmosphere is defined as a change in the natural composition of gases or aerosol particles in the atmosphere, which is deemed harmful to human and environmental health (Kampa & Castanas, 2008). Air pollution from the surface of the earth has an influence on not only the troposphere, but also the stratosphere (Atkinson, 2000). Pollution of the atmosphere also disrupts natural patterns and cycles responsible for chemical reactions and weather, which influence planetary health (Jacobson, 2002). Chemicals are distributed globally within a biogeochemical series, which is described as fluxes between reservoirs, i.e. atmosphere, oceans and terra-firma. Numerous chemical species have long resident times within the atmosphere and can therefore be transported along great distances (Swap *et al.*, 2003).

Atmospheric pollutants pose a serious health risk to the human population with each pollutant species affecting human health in different ways. Noncommunicable diseases (NCD's), which include strokes, heart diseases, lung diseases and cancer, are the leading causes of deaths globally and, after tobacco smoking, exposure to air pollution is the second largest cause of NCDs (World Health Organization, 2016). According to the World Health Organisation (WHO), it is estimated that one in every nine deaths in 2012 was related or caused by air pollution and three million deaths were solely from ambient air pollution (World Health Organisation, 2016). Furthermore, in 2016, the WHO reported that 4.2 million deaths globally were attributed to ambient air pollution and approximately 91% of these deaths occurred in low- and middle-income countries (World Health Organisation, 2019).

Not only do atmospheric pollutants threaten human health, the effects on the Earth's climate and ecosystems are also devastating. Atmospheric pollutants can disrupt the natural cycles present within the atmosphere, for example greenhouse gases (GHGs), which accelerate global warming (IPCC, 2021) or the

formation of acid rain due to chemical reactions of sulphur- and nitrogen-containing species in the atmosphere.

Because of numerous sources and transformations of emitted gases and aerosols, a multitude of different pollutants are present in the atmosphere. Pollutants can be categorised based on whether they are emitted directly into the atmosphere (primary pollutants) or formed by transformation reactions of primary pollutants and other constituents within the atmosphere (secondary pollutants) during ageing/transport (Matthias, 2004). Furthermore, these atmospheric pollutants can be split up into gaseous and aerosols/particulate matter (PM). Primary pollutants are emitted directly into the atmosphere by anthropogenic (e.g. traffic, factories, mining, chemical plants, towns/cities etc.) and natural (animals, water bodies, volcanos, field fires etc.) sources. Secondary pollutants form in the atmosphere from precursor compounds, typically via oxidation reactions or as a result of photochemical reactions.

### 2.1.1 Types of atmospheric pollutants

Within the atmosphere, a considerable amount of different pollutant species is present, and all these species have different sources, compositions, transformations, and environmental/human impacts and can mainly be classified into two major categories, i.e. aerosols (i.) and gaseous species (ii.). The impacts on the environment, climate and human health of these particles are determined by their physical and chemical properties (Engelbrecht, 2009). In this study, the focus is on gaseous pollutants.

#### *i. Aerosols*

Aerosols are very small solid or liquid particles suspended in the air, which can differ in shape, morphology, number and size (Kampa & Castanas, 2008). Aerosols are also referred to as particulate matter (PM). Primary aerosols/PM are emitted by numerous anthropogenic (e.g. household combustion, industries, mining operations, farming) and natural (e.g. sea spray, dust storms, volcanic activity) sources (Jayaratne & Verma, 2001; Ross *et al.,* 2003; Vakkari *et al.,* 2011; Laakso *et al.,* 2012). It is also common that gas phase compounds reacting in the atmosphere form secondary aerosols such as organic aerosols formed from the oxidation of VOCs, sulphuric acid ($H_2SO_4$) from $SO_2$, and the formation of nitrates ($NO_3^-$) and sulphates ($SO_4^{2-}$) from $H_2SO_4$ and nitric acid ($HNO_3$), typically accompanied by ammonia ($NH_3$) in the particle phase (Seinfeld & Pandis, 2006). VOCs play a significant role in new particle formation (e.g. Reisell *et al*., 2003; Ehn *et al*., 2014) and take part in photochemical reactions with oxides of nitrogen (NOx) to form $O_3$ (Atkinson *et al*., 2000; Seinfeld & Pandis, 2006; Monks *et al*., 2015).

#### *ii. Gaseous species*

Gaseous pollutants can be organic or inorganic in nature (Kampa & Castanas, 2008). Examples of organic species are methane ($CH_4$), volatile organic compounds (VOCs) and halogenated organic compounds (Daly & Zannetti, 2007; Kampa & Castanas, 2008). Inorganic species include sulphur dioxide ($SO_2$), hydrogen sulphide ($H_2S$), ozone ($O_3$), nitrogen oxide (NO), nitrogen dioxide ($NO_2$) and carbon monoxide (CO) (Kampa & Castanas, 2008). Many of these pollutants are primary pollutants that are emitted directly into the atmosphere, but

they also undergo intrinsic reactions to form secondary pollutants. Some examples of gas phase secondary pollutants in addition to $O_3$ are $SO_2$ formed from the oxidation of $H_2S$, $CO_2$ (carbon dioxide) through the oxidation of CO, and less volatile VOCs from more volatile VOCs (Seinfeld & Pandis, 2006). Halogenated carbons, $CO_2$, methane ($CH_4$) and nitrous oxide ($N_2O$) are regarded as greenhouse gases that have a large contribution to anthropogenic climate change (Martins, 2009; IPCC 2021).

### 2.1.2 Sources of pollutants

Atmospheric pollutants can be emitted directly into the atmosphere naturally i.) as well as anthropogenically ii.).

#### *i. Natural sources*

Typical natural sources of atmospheric pollutants are volcanic eruptions, although not of concern in South Africa, biomass burning (e.g. wildfires/forest fires), the natural decomposition of organic materials, dust that is lifted up from uncultivated land by wind, vegetation, oceanic and aqueous surfaces, and spray from sea waters. It is to be noted that biomass burning will mostly be considered as an anthropogenic source as a small fraction of the burning events is of natural occurrence (Andrea, 1991). Although these emissions are natural of origin, they can have significant air quality and climatic impacts. For instance, $SO_2$ plumes associated with volcanic eruptions from the Calbuco volcano in Chile were found to have reached South Africa through HYSPLIT forward trajectory analysis and moderate increases in $SO_2$ were observed as a result at stations in Damonsville, Mmabatho and Phola (Sangeetha *et al.*, 2018). Another study found significant cooling across southern Africa after major volcanic eruptions, namely Krakatau (1883), Santa Maria (1902), Agung (1963) and Pinatubo (1991) (Harvey & Grab, 2021).

#### *ii. Anthropogenic sources*

The combustion of fossil fuels emits numerous atmospheric pollutants, which include $SO_2$, $NO_x$, $CO_2$, CO, VOCs, PM, black carbon (BC) and numerous heavy metals (Crawford *et al.,* 2003; Scorgie *et al.,* 2004; Pretorius *et al.,* 2015). The most utilised and well-known fossil fuels are coal, natural gas and oil, and these three fuels are also the main fuels used in electricity generation providing 40%, 20% and 6% of global electricity generation, respectively (Höök, 2007). Coal-fired power plants generate most of South Africa's electricity, approximately 67% (DMRE, 2022). The combustion of coal is considered as a major source of the $CO_2$ greenhouse gas (Höök, 2007). The energy sector is the largest emitter of atmospheric $SO_2$ and NOx pollution in South Africa (Department of Environmental Affairs, 2012; Pretorius *et al.,* 2015). Furthermore, the petrochemical industry is also a major emitter of atmospheric pollutants related to fossil fuels in the area (Hakkarainen *et al*., 2023). Here, gasification of coal and other processes is used to produce fuels such as petrol, diesel, liquid petroleum gas and aviation fuel, and chemical feedstocks such as alpha olefins are produced (Pretorius *et al.,* 2007, Davis & Hower, 2017). However, due to the scale, diversity and complexity of the operation, numerous atmospheric pollutants are emitted from the operation. These include emissions of NOx, $SO_2$, $H_2S$, CO and VOCs (Pretorius *et al.,* 2007).

Another important source of atmospheric pollutants is high temperature industries such as pyrometallurgical smelters. Numerous pollutants can be released into the atmosphere through off-gas depending on the specific process used. Some of these processes make it difficult to capture the pollutant gas species due to low concentrations or intermittent production from converters, and therefore it is common practice for these gases to be discharged into the atmosphere through tall stacks in southern Africa (Jones, 2005).

Not only do these above plants emit gases, but large quantities of ash are also emitted into the atmosphere. Handling and abatement of this ash are important to minimise environmental impacts. One way to minimise ash release into the atmosphere is through the introduction of particle filters or fly ash traps that collect most of the particles. However, particles smaller in size (0.8 to 2 micron) are able to pass through the filters/traps (Linak *et al.,* 2000; Gaffney & Marley, 2009).

As the number of cars increase, congestion and vehicle emissions increase, which, in turn, degrades ambient air quality (Zhang & Batterman 2013). Vehicle emissions have become a leading atmospheric pollution source in many areas and include pollutants such as $CO_2$, CO, hydrocarbons (HCs), VOCs, NOx, PM and sulphur-containing gases such as $SO_2$ and $H_2S$ (Transportation Research Board, 2002; Supriyanto & Ansharullah, 2016). Transportation in South Africa is mostly done by road and as a result of ineffective public transport, most of the vehicles on the roads are privately owned, and this results in a very large active fleet of vehicles on the roads. Furthermore, from June 2009 to October 2023, South Africa has experienced an increase in the number of motor vehicles from ~9 million to ~12 million vehicles. Increases within Gauteng and Mpumalanga were ~3.6 million to ~4.6 million and ~600 000 to ~800 000 vehicles, respectively (RTMC, 2009; NaTIS, 2023). The road fleet in South Africa accounts for approximately 60% of the vehicles in the entire South African Development Community and within South Africa accounts for approximately 14% of the energy-related $CO_2$ emissions (Ahjum, 2020). If the road vehicle fleet has such a large contribution on the $CO_2$ emissions in South Africa, it can be assumed that this will also be a significant source of other atmospheric pollutants.

Biomass burning can be defined as the combustion of dead or living vegetation, which includes natural lightning induced combustion or human-initiated combustion (Levine, 2014). It is considered that the majority of biomass burning is of the human-initiated kind (Levine, 2014) and some estimates indicate that only about 10% of global fires occur naturally (Andrea, 1991). Therefore, biomass burning can also be classified as an anthropogenic source. Globally, most of the biomass combustion is attributed to veld fires, industrial and domestic biofuel use, tropical and boreal forest fires, and crop residue burning (Akagie *et al.,* 2011). Biomass burning contributes significantly to the atmospheric pollution budget, and it is regarded as the second largest contributor of trace gases and the largest contributor of fine carbonaceous material within the troposphere (Bond *et al.,* 2004). Approximately 90% of carbon emitted from biomass burning is oxidised to CO or $CO_2$ (Ferek *et al.,* 1998). Pollutants related to biomass burning in tropical and subtropical regions include significant amounts of NOx and other species such as aerosols, $CH_4$, CO, $CO_2$, non-methane hydrocarbons (NMHC) and $N_2O$ (Crawford *et al*., 2003). The smoke particles produced from biomass burning

consist of approximately 50 to 80% organic aerosol, 5 to 10% BC and 10 to 15% of other inorganic species (Reid *et al.,* 2005; Vakkari *et al.,* 2014). Open fires have been recognised in South Africa for the role they play in ecological function and structure (Bond & Keeley, 2005; Van Wilgen & Richardson, 1985). It was suggested by Bond and Keeley (2005) that if fires did not occur in South Africa, indigenous fynbos and grasslands would be dominated by tree species. Moritz *et al.* (2012) did a global modelling study to predict the likelihood of biomass fires occurring in the future. In this study it was found that throughout 1996 to 2007, the South African Highveld experienced high numbers of biomass fires and that there is a high likelihood that this area will experience high numbers of fires in the future.

Agricultural activities also emit atmospheric pollutants, including nitrogen containing compounds, which are mostly a product of agricultural activities such as rice cultivation, fertiliser use, manure use and burning agricultural of residues. Furthermore, $CH_4$ emissions due to enteric fermentation from livestock as well as from the handling of livestock waste (Rees & Ball, 2011) also form part of agricultural emissions. Globally, agriculture is seen as the most important contributor of anthropogenic $CH_4$ and contributes approximately 37% of the total global anthropogenic $CH_4$ emissions (Aneja *et al.,* 2009). $N_2O$ and NO are also emitted by agricultural activities, and it is mostly produced naturally within soils by microbial nitrification of ammonium and denitrification of nitrate (Smith *et al.*,1997). However, the emissions of $N_2O$ and NO can be increased by agricultural activities such as the use of organic and synthetic fertilisers, nitrogen-fixing crops, the use of livestock manure for fertilisers and the cultivation of organic soils (Smith *et al.*,1997; Aneja *et al.,* 2009). It is estimated that, in the USA, agricultural emissions of $N_2O$ account for approximately 72% of total $N_2O$ emissions (U.S. EPA, 2005). A recent study by Tongwane *et al.* (2016) on greenhouse gas (GHG) emissions related to different crop management practices in South Africa found that field crops emitted 5.2 million tonnes of $CO_2$ equivalent emissions in 2012. Another study found that cattle production in South Africa emitted 35.37 million tonnes of $CO_2$ equivalent emissions in 2019 (Tongwane & Moeletsi, 2021). $H_2S$ is also emitted through the anaerobic decomposition of sulphur containing manure by sulphur-reducing bacteria (U.S. EPA, 2001).

Spontaneous combustion of coal is prevalent in the coal mining industry and happens as coal is exposed to oxygen (Pone *et al*., 2007). This phenomenon is of global concern as these burning events contribute to global warming, and the degradation of air quality, and pose other significant environmental problems (Pone *et al.,* 2007). Many of the same pollutants are emitted by the spontaneous combustion of coal, as from coal-fired power plants (Sloss 2013). However, because there are no abatement technologies in place for these events, the emission factors are in general higher (Sloss, 2013). Greenhouse gases (GHGs) such as $CO_2$ and $CH_4$, eBC and other atmospheric pollutants such as PM, CO, mercury, NOx, SOx, $H_2S$ VOCs are typically emitted by spontaneous combustion of coal (Stracher & Taylor 2004; Pone *et al.,* 2007; Carras *et al.,* 2009; Zhen-qi *et al*., 2009; Sloss 2013).

### 2.1.3 Removal of pollutants

Removal of pollutants from the atmosphere can take place through two main mechanisms, i.e. dry deposition and wet deposition (Seinfeld & Pandis, 2006); oxidation is also a significant removal mechanism. The transport of particulate and gaseous species from the atmosphere onto the Earth's surface without precipitation is known as dry deposition (Seinfeld & Pandis, 2016). This is a slow process and is greatly affected by the chemical, physical and biological properties of the gas/particulate and surface (Wesely, 2003; Seinfeld & Pandis, 2016). Convective transport, diffusion and adhesion to the surface of the earth are processes by which dry deposition occurs (Pöscle, 2005; Engelbrecht, 2009). When the atmosphere comes in contact with the earth's surface, gas molecules can react with or dissolve within surface materials. Particles are captured by surface elements through interception or impaction (Pöscle, 2005).

Wet deposition is the removal of atmospheric pollutants with the aid of scavenging by atmospheric hydrometeors (e.g. rain, snow, cloud and fog drops), which is then deposited onto the earth's surface (Seinfeld & Pandis, 2016). Species that are rapidly removed by precipitation include but are not limited to gaseous hydrogen peroxide ($H_2O_2$), $NH_3$ and $HNO_3$. Soluble elements of cloud condensation nuclei (CCN), which include nitrates, sulphates, and sea salts, are also quickly scavenged from the atmosphere during most precipitation events (Walcek, 2003). The main sink for atmospheric aerosols is considered to be wet deposition.

### 2.1.4 Impacts of atmospheric pollutants

Atmospheric pollutants can have numerous effects/impacts on two main factors, i.e. influencing the Earth's radiative balance and air quality impacts on humans and the environment.

#### *i) Climate change*

The climate of the earth is a very complex system, ruled by interactions between the surface of the earth (e.g. land and water surfaces), atmosphere and all living organisms (IPCC, 2007b). A change in the state of the climate, which can be recognised by changes in the mean and/or variability of its properties and lasts for a long period (e.g. decades or longer) is referred to as climate change (IPCC, 2014). The climate system is subject to changes over time due to its own internal dynamics and through forcing of external factors. The external forcing can be due to natural phenomena such as solar variations, volcanic activity and natural biomass burning, or climate can be forced through anthropogenic activities that change the composition of the atmosphere. The Framework Convention on Climate Change (UNFCCC) defines climate change as "a change of climate which is attributed directly or indirectly to human activity that alters the composition of the global atmosphere and which is in addition to natural climate variability observed over comparable time periods." The fourth IPCC assessment reports an acceleration in the rate of climate change due to anthropogenic activities (IPCC, 2007b). However, although there is some interplay between pollutants and climate change, GHGs are the primary drivers of climate change. GHGs do not make up part of this study, and therefore further elaboration on the anthropogenic escalation of climate change is excluded from this review.

### *ii) Air quality*

Depending on concentration, physical properties and chemical composition, air pollutants can have serious human and environmental health implications. Numerous studies have revealed that the increase in air pollution is related to an increase in hospital admissions and mortality (Brunekreef & Holgate, 2002; Suwa *et al.,* 2002).A recent review study on the relationship between air pollution and environmental and health impacts found that inhalation of air pollutants could lead to diseases in the respiratory system such as chronic obstructive pulmonary disease, asthma, bronchiolitis, as well as lung cancer, cardiovascular incidents, central nervous system disorders, and skin conditions (Manisalidis *et al.*, 2020). Soluble gases such as $SO_2$ are absorbed in the upper airways, but gases such as $NO_2$ and $O_3$, which are less soluble, can penetrate the pulmonary region. Responses such as sneezing, rapid and shallow breathing, coughing and broncho-constriction are generally a cause of irritant gases, which stimulate the respiratory walls. Dissolved gases can be eliminated by biochemical processes or diffusion to the circulatory system (Vallero, 2008, Vallero, 2021). Due to its solubility in watery fluids, $SO_2$ is removed in the upper respiratory system. The adsorption and absorption on $SO_2$ on particles provide a transport mechanism to the pulmonary systems where $SO_2$ toxicity occurs. Therefore, particles can worsen the effect of $SO_2$ on human health. Furthermore, harmful substances such as $H_2SO_4$ can be produced by reactions of gaseous species with the moist environment found in the lungs (Godish, 2004). Human exposure to $NO_2$ at about 150ppm is fatal, either because of a pulmonary oedema or bronchiolitis obliterans with fibroses (Last *et al.,* 1994). $H_2S$ has negative human and environmental impacts. Short-term exposure to high (e.g. > 10 000 ppbv) $H_2S$ concentrations can cause health effects, including respiratory, ocular, neurological, cardiovascular, metabolic and reproductive effects and in extreme cases of exposure could result in fatalities (Rayner-Canham & Overton, 2009; WHO, 2003). $H_2S$ is also considered to be more toxic than hydrogen cyanide (Rayner-Canham & Overton, 2009).

As mentioned, atmospheric pollutants can have a detrimental effect on the environment. $SO_2$ acts as a precursor for acid rain, which acidifies water bodies, soils, and corrodes built structures. Oxides of nitrogen contribute to ozone formation and have adverse effects on aquatic and terrestrial ecosystems (Monks *et al.,* 2015). Some effects of atmospheric nitrogen oxides are acid rain and eutrophication of water bodies. Eutrophication occurs when water experiences an increase in nutrients, which results in a decrease of available oxygen in the water, making it no longer viable for fish and animal life (EPA, 2011). $O_3$ pollution also contributes greatly to the degradation of the environment, and this is evident in brown coloured lesions on leaves as well as a decrease in seed production and growth rate of plants (Scheepers *,* 2011).

## 2.1.5 Pollutant species under investigation

Although the dataset available for this study only had six gas and aerosol pollutant species, not all these pollutants will be used in the study. These species include $NO_2$, $O_3$ and $SO_2$, which have specific National Ambient Air Quality Standards (NAAQS) in South Africa and are considered to be criteria pollutants, which have major implications for air quality and climate as sources of secondary aerosols. In addition to the NAAQS

criteria pollutants, NO, $H_2S$ and BC are also part of the dataset. However, only NO, $NO_2$, $SO_2$, $H_2S$ and BC are used for the study and discussed in more detail.

*i.) Atmospheric nitrogen oxides*

Common nitrogen-containing species in the atmosphere include NO, $NO_2$, $N_2O$, $NH_3$ and $HNO_3$ (Seinfeld & Pandis, 2016). Oxides of nitrogen ($NO_x$), which are the sum of NO and $NO_2$ (Seinfeld & Pandis, 2016), make up approximately 30% of the total global nitrogen budget in the atmosphere (Monks & Leigh, 2009; Fabian & Pruchniewicz, 1977). It was estimated with $NO_x$ emission projections for coal-fired power plants in South Africa that these emissions will at best experience a 10% decline from 2015 levels and at worst experience a 40% increase up to the year 2030 (Pretorius *et al.*, 2015). Although $NO_2$ is the most prominent nitrogen-containing species, it is only emitted in small quantities together with NO through combustion activities; the bulk of $NO_2$ is formed from oxidation reactions of NO in the atmosphere (Seinfeld & Pandis, 2016). According to Lourens *et al.* (2012) and Venter *et al.* (2012), the highest $NO_2$ concentrations in South African urban areas are found in the morning and late afternoons, which coincides with an increase in traffic. Globally, an $NO_2$ hotspot is present over the South African Highveld, which is situated over the HPA where coal-fired power stations and petrochemical plants are major emitters (Toenges-Schuller *et al.*, 2006; Ghude *et al.*, 2009; Lourens *et al.,* 2011).

$NO_2$ is a key component for chemical reactions in the troposphere, as $NO_2$ is necessary for the formation of $O_3$ through photolysis (Connel, 2005). When $NO_x$ is emitted, it undergoes numerous reactions (Atkinson, 2000; Shallcross, 2009) to produce $O_3$.

$$NO + O_3 \rightarrow NO_2 + O_2 \quad (2.1)$$

$$NO_2 + hv \rightarrow NO + O(^3P) \quad (2.2)$$

$$O(^3P) + O_2 + M \rightarrow O_3 + M \ (M = N_2 \text{ or } O_2) \quad (2.3)$$

The above reactions interconvert NO, $NO_2$ and $O_3$, as is presented in Figure 2.1.

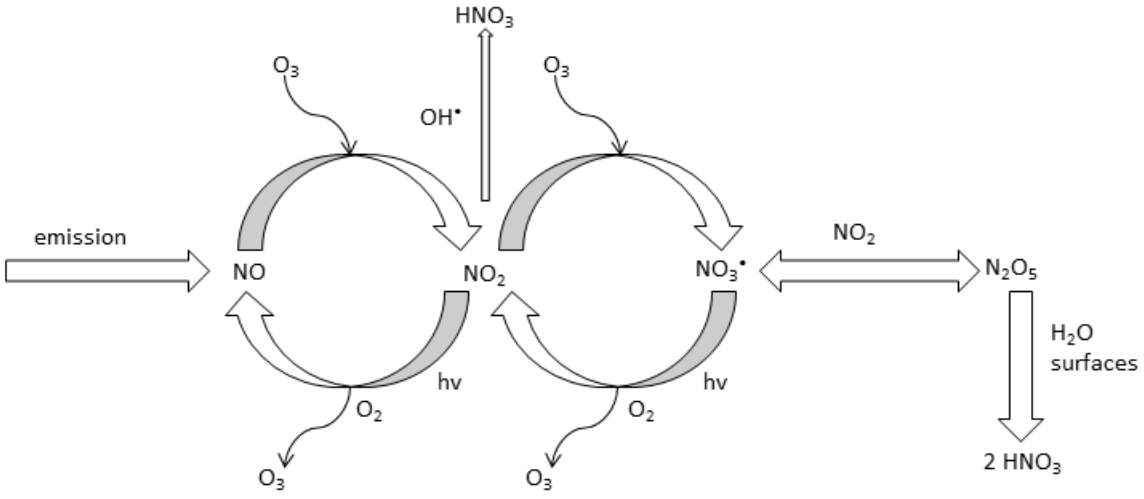


**Figure 2.1** Tropospheric NO cycle

$NO_2$ oxidation by $O_3$ can also cause the formation of nitrate radicals, $NO_3^\bullet$ by the following reaction:

$$NO_2 + O_3 \rightarrow NO_3^\bullet + O_2 \quad (2.4)$$

$NO_3^\bullet$, the hydroxyl radical (OH) and $O_3$ are responsible for most tropospheric oxidation reactions. $NO_3^\bullet$ quickly reacts (~ 5 seconds) with NO in the presence of sunlight to reform NO, as well as $NO_2$:

$$NO_3^\bullet + hv \rightarrow NO + O_2 \ (\sim 10\ \%) \quad (2.5)$$

$$NO_3^\bullet + hv \rightarrow NO_2 + O(^3P) \ (\sim 90\ \%) \quad (2.6)$$

Other important tropospheric reactions of nitrogen oxides include:

$$HO^\bullet + NO \rightarrow HONO \quad (2.7)$$

$$HO^\bullet + NO_2 \rightarrow HNO_3 \quad (2.8)$$

$$NO_3^\bullet + NO_2 \rightarrow N_2O_5 \quad (2.9)$$

$$N_2O_5 + H_2O \rightarrow 2HNO_3 \quad (2.10)$$

$$NO_2 + NO + H_2O \rightarrow 2HNO_2 \quad (2.11)$$

The rection of $NO_2$ and the OH radical is a major depleting reaction for atmospheric NOx during the day (Atkinson, 2000). From the above reactions, it is clear that NOx can also influence the acidity of aerosols and wet deposition through the production of $HNO_3$ and nitrous acid ($HNO_2$). The troposphere consists of approximately 0.03% $CO_2$, when in equilibrium with $H_2O$, which, according to Henry's law, will result in precipitation with a pH of about 5.7 (Connell, 2005). Further acidity within precipitation is usually because of the presence of inorganic acids such as $H_2SO_4$, HCl and HNO3 (Connell, 2005). $H_2SO_4$ generally dominates in contribution to acidity with less contribution from $HNO_3$ and low concentrations of HCl (Connell, 2005). A study by Mphepya *et al*. (2004) at a rural site in Louis Trichardt and an industrial site in Amersfoort, both in South Africa, found the average pH of precipitation was 4.4 and 4.9, respectively. In this study, 901 rain samples were retrieved and analysed from July 1986 to June 1999 (Mpehpya *et al*., 2004). Another study found that 94% of rain events at four South African IGAC DEBITS Africa sites had a pH below 5.6 (Conradie *et al*., 2016).

### *ii.) Atmospheric sulphur*

In the 2001 IPCC report, the global sulphur emission trend from 1850 to 2000 is presented. It is noticeable that sulphur emissions presented a rapid increase since the late eighteenth century, which coincides with the start of the industrial revolution. However, global awareness of air quality in the latter parts of the twentieth century forced industries and governments to take action. Recently, ambient sulphur concentrations started to decrease in first world countries, which can mainly be attributed to the use of low sulphur content fuel as well as the desulphurisation of stack emissions (IPCC, 2007b; Aas *et al*., 2019).

Sulphur is mostly present in gaseous form in the atmosphere as sulphides (e.g. $H_2S$, carbonyl sulphide, carbon disulphide and dimethyl sulphide) and oxides (e.g. sulphur di/trioxide) (Calvert *et al.,* 1978; Pienaar & Helas, 1996; Warneck, 1988; Seinfeld & Pandis, 1998; Herrmann *et al.,* 2000; Hewitt, 2000; Shallcross, 2009; Williams & Baltensperger, 2009). Significant amounts of these sulphur compounds are observed in the South African Highveld and South Africa is among the top ten sulphur emitting countries globally (Stern, 2006). This is of international interest, but it also leads to adverse regional impacts. It was reported that $SO_4^{2-}$ was the dominating ionic species in wet deposition at industrial areas as well the regional background within the interior of South Africa; furthermore, it was found that the pH of wet deposition in South Africa is very low (i.e. pH 4.32 to 4.89) because of the fractional contribution of $H_2SO_4$ (Conradie *et al.,* 2016). $H_2SO_4$ and/or $SO_4^{2-}$ also play an important part in new particle formation (NPF) events and succeeding particle growth in the region (Vakkari *et al.,* 2015). South African interior sites have shown the highest measured annual median NPF frequencies and annual median growth rates (Nieminen *et al.,* 2018). Furthermore, $SO_4^{2-}$ and particulate organic matter (POM) have been reported as dominant species in particles smaller than one micron ($PM_1$) in the interior of South Africa (Tiitta *et al.,* 2014; Aurela *et al.,* 2016; Venter *et al.,* 2018). The most commonly found sulphur species in the South African Highveld are $H_2S$ and $SO_2$ (Held *et al.,* 1993), especially during winter when emission loads increase as a result of space heating practices.

### *a.) Sulphur dioxide*

$SO_2$ is anthropogenically emitted into the atmosphere through the combustion of fossil fuels and smelting of sulphur-rich mineral ores (EPA, 2015; Shallcross, 2009), as mentioned in previous sections. Large natural sources of $SO_2$ include wildfires and volcanic activity/eruptions (EPA, 2009; Shallcross, 2009); however, volcanic activity is not relevant to the study area. It has a choking and suffocating odour (O'Niel, 2013; PubChem) with an odour threshold of 0.67 to 4.75 ppm (National Research Council, 2010) and may also irritate mucous membranes (Sullivan & Krieger, 1999). Brief time exposures to small quantities of $SO_2$ may cause death or permanent injuries; 1000 ppm causes death in 10 minutes to several hours due to respiratory depression and it is also an eye and respiratory tract irritant (EPA, 1998).

$SO_2$ oxidation acts as a precursor for the formation of $H_2SO_4$ aerosols within the atmosphere (Shallcross, 2009). The process starts when $SO_2$ reacts with $O_2$ to produce $SO_3$ (Seinfeld & Pandis, 2006):

$$2SO_2 + O_2 \rightarrow 2SO_3 \qquad (2.12)$$

The reaction rate of $SO_2$ and $O_2$ is quite slow under atmospheric conditions. This allows for $SO_3$ to be more readily produced through the radical abstraction reaction with $OH^\bullet$ (Seinfeld & Pandis, 2006):

$$OH^\bullet + SO_2 + A \rightarrow HOSO_2^\bullet + A \qquad (2.13)$$

$$HOSO_2^\bullet + O_2 \rightarrow HO_2^\bullet + SO_3 \qquad (2.14)$$

Finally, $SO_3$ reacts with $H_2O$, which then produces sulphuric acid (Seinfeld & Pandis, 2006):

$SO_3 + H_2O + A \rightarrow H_2SO_4 + A$ (2.15)

(A = vibrational exchange of species)

Many sulphur-containing species can also produce atmospheric $SO_2$. $H_2S$ reacts with the $OH^{\bullet}$-radical to produce an $SH^{\bullet}$-radical and a sequence of other reactions to produce $SO_2$ (Seinfeld & Pandis, 2006):

$H_2S + OH^{\bullet} \rightarrow SH^{\bullet} + H_2O \rightarrow SO_2$ (2.16)

$CH_3SCH_3$ also reacts with the $OH^{\bullet}$-radical to produce $SO_2$ (Seinfeld & Pandis, 2006):

$CH_3SCH_3 + HO^{\bullet} \rightarrow CH_3SCH_2O_2^{\bullet}$ (2.17)

$CH_3SCH_2O_2^{\bullet} \rightarrow CH_3S^{\bullet} + HCHO \rightarrow SO_2 + CH_3$ (2.18)

*b.) Hydrogen sulphide*

$H_2S$ is a flammable, colourless gas with a distinct odour of rotten eggs at very low concentrations. The human detection threshold of $H_2S$ is approximately 0.48 ppbv (WHO, 2003) – this is the concentration at which 50% of the human population can detect $H_2S$ gas. Currently, there is no South African national ambient air quality standard (NAAQS) for $H_2S$ (DEA, 2010).

$H_2S$ is a key compound in the global sulphur cycle, of which a simplified flow chart is depicted in Figure 2.2. The anaerobic breakdown of sulphur by sulphur-reducing bacteria produces $H_2S$ in the environment (Reaction 2.19). Approximately 90% of $H_2S$ emitted are of natural origin through the anaerobic breakdown of sulphur-containing material and other natural sources (e.g. volcanic gases, sulphur deposits and sulphur springs) (EPA, 1993).

$H_2SO_4 + 2CH_2O \rightarrow 2CO_2 + 2H_2O + H_2S$ (2.19)

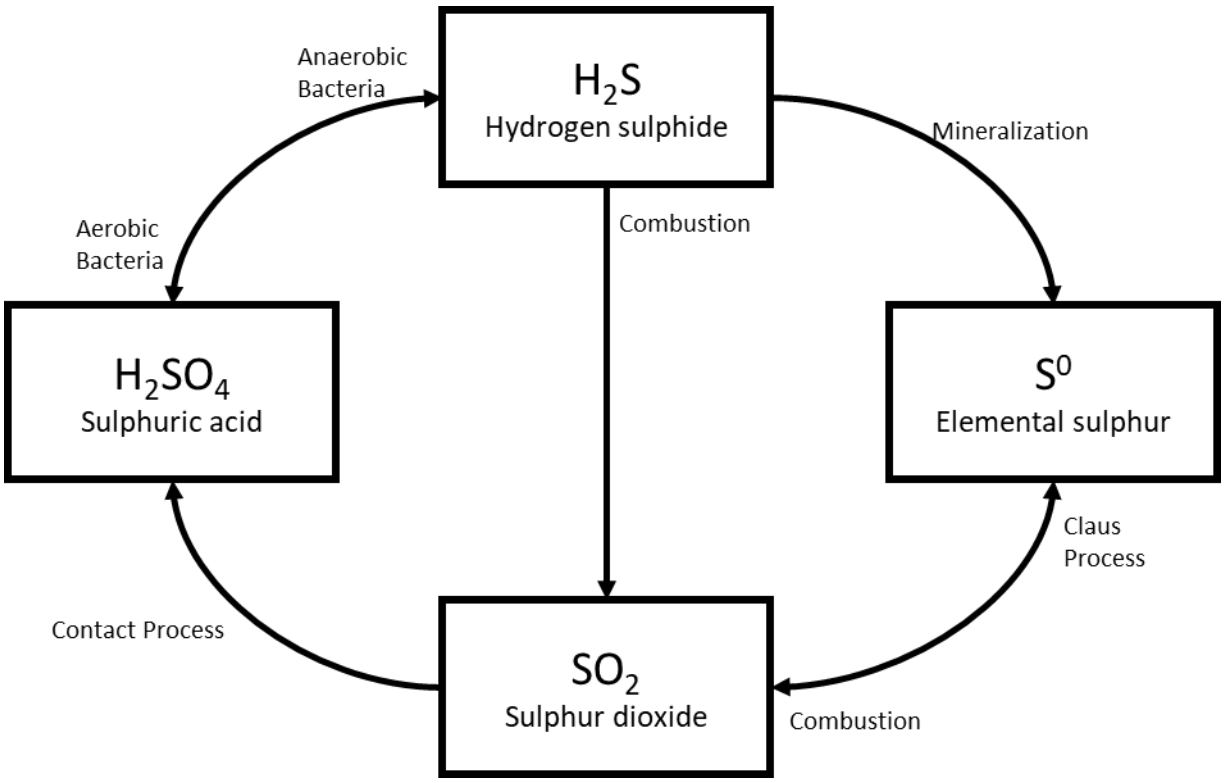


**Figure 2.2** The participation of $H_2S$ in the global sulphur cycle (Rubright *et al.,* 2017)

Anthropogenic $H_2S$ emissions occur by way of a variety of industrial processes (Rayner-Canham & Overton, 2009; Camacho, 2009; Rubright *et al.,* 2017) such as in the petrochemical (extraction and refining of natural gas and oil) and pyrometallurgical industries (if a reducing environment is present), and from the paper manufacturing industry. Other anthropogenic sources include sewage plants, tanneries, pyrometallurgical coke oven plants and manure-handling facilities (Chou *et al*., 2016).

Furthermore, $H_2S$ undergoes numerous intrinsic reactions to produce different sulphur-containing compounds such as sulphuric acid ($H_2SO_4$), elemental sulphur ($S^0$) and $SO_2$. A typical reaction of this kind is anoxygenic photosynthesis, where bacteria use light energy as energy source for the bonding of inorganic carbons onto organic materials, with $H_2S$ acting as an electron donor to produce $S^0$ and $H_2SO_4$ (Camacho, 2009). Reactions 2.20 and 2.21 depict how $H_2SO_4$ and $S^0$ are formed in this manner.

$$2H_2S + CO_2 \rightarrow CH_2O + H_2O + 2S^0 \quad (2.20)$$

$$H_2S + 2CO_2 + 2H_2O \rightarrow 2CH_2O + H_2SO_4 \quad (2.21)$$

Chemotrophic sulphur oxidation is yet another bacterial reaction where prokaryotes (uni- or multicellular organisms that lack a membrane-bound nucleus or mitochondria) use $H_2S$ as an energy source for their metabolism. A characteristic reaction used by these chemolithotrophic bacteria is the aerobic oxidation of $H_2S$ with oxygen ($O_2$), as seen in Reaction 2.22 (Camacho, 2009).

$$H_2S + ½O_2 \rightarrow S^0 + H_2O \quad (2.22)$$

In the atmosphere, $H_2S$ acts as a precursor for $SO_2$ when it reacts with the hydroxyl radical ($OH^\bullet$) to form an $HS^\bullet$-radical, whereafter the radical undergoes numerous reactions to form $SO_2$ (Seinfeld & Pandis, 2006; Rubright *et al.,* 2017):

$$H_2S + OH^\bullet \rightarrow HS^\bullet + H_2O \quad (2.23)$$

$$HS^\bullet + O_2 \rightarrow HO^\bullet + SO \quad (2.24)$$

$$SO + O_2 \rightarrow SO_2 + O \quad (2.25)$$

Atmospheric ozonation of $H_2S$ (the oxidation of $H_2S$ with $O_3$) can also occur to produce $SO_2$ (Hales *et al.,* 1973):

$$H_2S + O_3 \rightarrow SO_2 + H_2O \quad (2.26)$$

$H_2S$ undergoes combustion reactions in air to produce $SO_2$ (Reaction 2.27) or elemental sulphur (Reaction 2.10) (Rayner-Canham & Overton, 2009; Rubright *et al.,* 2017):

$$2H_2S + 3O_2 \rightarrow 2H_2O + 2SO_2 \quad (2.27)$$

$$2H_2S + O_2 \rightarrow 2H_2O + 2S \quad (2.27)$$

In industrial processes, $H_2S$ is converted to elemental sulphur by way of the Claus process to limit $H_2S$ emissions. Firstly, the $H_2S$ is burned with oxygen present to produce $SO_2$ (Reaction 2.28), with the remaining $H_2S$ then reacted with $SO_2$ to produce elemental sulphur (Reaction 2.29) (Goar *et al.,* 1986; Scott, 1992).

$$2H_2S + 3O_2 \rightarrow 2SO_2 + 2H_2O + \text{heat} \quad (2.28)$$

$$2H_2S + SO_2 \rightarrow 3S + 2H_2O + \text{heat} \quad (2.29)$$

The Claus process is not 100% effective in removing $H_2S$ gas from off-gas emissions (Goar *et al.,* 1986; Scott 1992). Therefore, even if industries use the Claus process to eliminate $H_2S$ emissions, a small fraction of the produced $H_2S$ will still be emitted. As an example, it has been reported that the petrochemical operation near Secunda in the HPA does have methods in place to remove $H_2S$ from the off-gas, but, according to an atmospheric impact report, a fraction of $H_2S$ is still emitted (Airshed Planning Professionals, 2017).

### *iii.) Ozone*

Tropospheric $O_3$ is a secondary pollutant that is formed through photochemical reactions of $NO_2$, VOCs and CO. These serve as precursors for the formation of intermediates that lead to the formation of tropospheric ozone (Jacob, 2000; Jain, 2009; Monks, 2015). It was found on numerous occasions that the interior of South Africa has high levels of $O_3$ that are promoted by elevated levels of $O_3$ precursor emissions; furthermore, an abundance of sunlight and recirculation of air seen in the interior of South Africa allow aging and photochemistry to take place (Laakso *et al.,* 2008; Josipovic *et al.,* 2010; Lourens *et al.,* 2011; Venter *et al.,* 2012; Thompson *et al.,* 2014).

The tropospheric production of $O_3$ can be described as a HOx-catalysed chain oxidation of CO and hydrocarbons in the presence of NOx. Photolysis of $O_3$ at wavelengths < 319 nm produces ground state (O)

and excited singlet ($O(^1D)$) oxygen atoms, the ground state O then rapidly combines with $O_2$ to produce $O_3$ (Seinfeld & Pandis, 2006).

*iv.) Black carbon*

eBC is a black sooty compound that is emitted from coal-fired power stations, gas/diesel engines and other sources and covers a significant percentage of particulate matter (PM) pollution (EPA, 2020). eBC is produced by partial combustion of carbonaceous material; however, it is not limited to this formation process (Petzhold, 2013), it has also been found as a product through pyrolysis of carbonaceous materials (Chow *et al.,* 2004; Schwartz & Lewis, 2012).

## 2.2 The Mpumalanga Highveld and HPA

Globally, the South African Highveld is known for its various anthropogenic activities (e.g. power generation, agriculture, mining operations, metallurgical operations, petrochemical operations and transportation) (Freiman *et al*., 2002; DEA, 2010; Lourens *et al*., 2011). From an industrial standpoint, the coal- and mineral-rich Highveld region is of great importance. Many of these industrial activities are situated within a single region of the South African Highveld, namely the Highveld Priority Area (HPA). This area was declared a priority area with regard to air quality because of the regular recorded exceedances of air quality standards for criteria pollutants (DEA, 2007). In Figure 2.3, the locality of this area is depicted through the blue polygon on the map. The geographical extent of the HPA mostly comprises areas within the Mpumalanga Highveld (e.g. Delmas, Dipaleseng, Emalahleni, Govan Mbeki, Lekwa, Steve Thswete, Msukaligwa and Pixley ka Seme), but also includes two municipal areas of Gauteng (e.g. Ekurhuleni and Lesedi) (DEA, 2007).

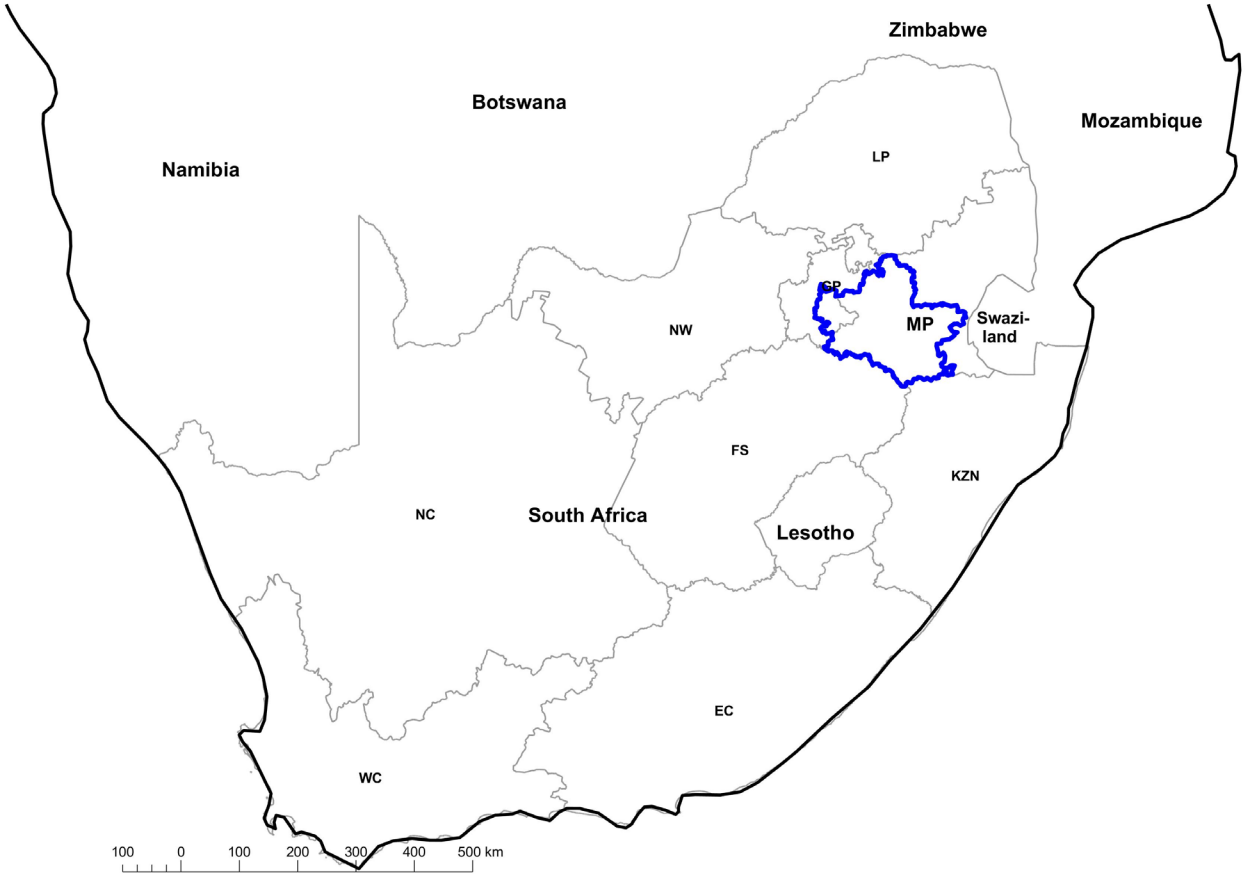


**Figure 2.3** Map representing the Highveld Priority Area (HPA) within the South African context. The blue polygon indicates the position of the HPA.

The Mpumalanga Highveld and HPA is situated on a plateau approximately 1600 m above mean sea level (AMSL). Regionally, the topography has a gradual downward slope towards the south and west. The Drakensberg escarpment lies to the east and the Vaal basin (1400 m AMSL) to the south, which have a tendency to channel cold air from the adjacent high plain of the Gauteng Province (Held *et al.*, 1996). The HPA is a hub for South Africa's industry with significant sources of $NO_2$, $SO_2$, $CO_2$ and $O_3$ (Laakso *et al*., 2012). Furthermore, there is a mixture of both regional and industrial emissions with intense solar radiation (Swap *et al*., 2003), which makes the HPA a complex area to study with regard to receptor source apportionment.

The major atmospheric pollutant sources in the HPA are mining, coal-fired power stations, as well as the metallurgical and petrochemical industries (Lourens *et al.,* 2011; Adesina *et al.,* 2022) from which common pollutants are $SO_2$, $NO_x$, VOCs, PM and $H_2S$, of which the latter is commonly associated with the petrochemical industry (Cardoso *et al.,* 1997). Furthermore, a significant fraction of coal mining activities take place within the HPA. Coal mining activities typically include open-cast mines, coal refuse disposal areas and open-cast mining operations above old board-and-pillar mining operations. The latter is known for the spontaneous combustion of coal as old board-and-pillar workings are re-mined and exposed to oxygen (Bell

*et al.,* 2001; Pone *et al*., 2007), which could further contribute to the anthropogenic emissions of pollutants in the HPA.

### 2.2.1 Meteorology and climatology of the Mpumalanga Highveld

What happens to air pollutants after they are emitted into the atmosphere is largely dependent on the meteorological conditions present during emission: pollution concentrations vary as a result of the changing nature of atmospheric stability, variations in mixing depth and to the effect of meso- and microscale wind systems present during transport/dispersion of pollutants (Preston-Whyte & Tyson, 1993). The Mpumalanga Highveld is dominated by generally dry conditions with low annual precipitation, generally during summer months, during summer north-westerly winds dominate, and during wintertime westerly winds prevails. Transport of air masses predominantly occurs by means of anticyclonic circulations over southern Africa (Tyson *et al.,* 1976). The sub-tropical high-pressure belt is situated over South Africa, which causes general circulation of air to be anticyclonic above 700 hPa in most cases. In summertime, when pressure reaches 850 hPa, cyclonic circulations occur as troughs develop in the central Highveld plateau of South Africa (Tyson & Preston-Whyte, 2000). In wintertime, this effect is more pronounced, which results in low-level stability in the atmosphere (Anselm, 2007). Circulation at the eastern regions of the South African Highveld remains under the influence of anticyclonic circulation during most times. Anticyclonic circulation frequency and related atmospheric subsidence reach a peak in winter to early spring from July to September (Held *et al.,* 1996). This subsidence is favourable for the creation of elevated temperature inversions with base heights varying from 2000 to 3000 m AGL in summertime and 1700 m AGL in wintertime (Held *et al.*, 1996). In wintertime, temperature inversions have a very high frequency over the Highveld. During summer months, these temperature inversions still occur during night times, but they are not as strong as in the winter (Pretorius *et al.,* 1986).

Moist, unstable conditions and precipitation are almost solely limited to summertime when the anticyclonic belt is situated further south (Tyson & Preston-Whyte, 2000). Furthermore, increased ambient temperature and solar radiation in the summer are ideal conditions for the formation of secondary pollutants and new particle formation (NPF) (Holmes, 2007). In wintertime, the drier and more stable atmospheric conditions are ideal for the accumulation of atmospheric pollutants (Anselm, 2007). When atmospheric pollutants diffuse into a greater volume of the atmosphere, the concentration of those pollutants is reduced, which happens most often under free convection conditions when the mixing layer is deep. These unstable conditions are mostly present in summertime during the day.

#### *i.) Surface inversions and planetary boundary layer over the Mpumalanga Highveld*

Atmospheric boundary layers have an important influence on air quality, weather and climate (Gierens *et al.,* 2018). Boundary layer is defined as the lowest part of the atmosphere that is influenced by the earth's surface (Stull, 1988; Garrat, 1994). Boundary layer has a distinct diurnal variation and is characterised by a stable layer at night, residual layer on top of the stable layer and a mixing layer during daytime (Stull, 1988). During

night-time, when radiative cooling of the ground surface regularly leads to surface air that is cooler than the air above, inversions near ground level occur and are known as radiation or surface inversions (Seinfeld & Pandis, 2006). This produces a stable boundary layer in approximately the lower 100 m of the atmosphere, which prevents ventilation of emissions during the night (Seinfeld & Pandis, 2006). Therefore, pollutants emitted during this time inside these shallow layers get trapped and can reach relatively high concentrations (Seinfeld & Pandis, 2006). When the sun starts to rise, temperature of the ground and adjacent air increases. The increase in temperature produces a profile corresponding to an unstable atmosphere, which typically takes a couple of hours and results in the break-up of the stable boundary layer (Seinfeld & Pandis, 2006), thereby allowing vertical mixing of the atmospheric constituents to occur. These atmospheric stability changes throughout the day can have significant impacts on pollutant concentrations within the atmosphere.

Within the context of the South African Highveld, surface inversions are observed regularly. These inversions are present between 80 and 90% of the time during winter nights and early mornings over the Highveld (Held *et al.*, 1996). Diurnal variations of these stable layers are often clear, with 50% of layer depths during the day being between 1 and 3 km and 80% of night-time layers' depth a few hundred meters (Gierens *et al.,* 2018). Winter surface inversions during early mornings over the Highveld region fluctuate from 3 to 11°C, with extreme occurrences reaching 15°C in strength with depth between 100 and 400 m AGL. In the Mpumalanga Highveld region, inversions larger than 10°C normally occur during 25 to 30% of all winter nights and can last up to approximately 16 hours (Held *et al.*, 1996). This is important as high-stack sources typically emit pollutants above these temperature inversions, which allows for the pollutants to be dispersed over a larger area and are therefore less concentrated. Because of this, pollutants of high-stack origin will typically be observed during day times when the temperature inversions are less pronounced or have broken up, which allows for downward mixing (Garstang *et al.,* 1996; Korhonen *et al.,* 2014; Gierens *et al.,* 2018).

### *ii.) Precipitation over the Mpumalanga Highveld*

South Africa is generally considered to be a semi-arid country, and is characterised by extremely variable climate and sparse water supplies (Botai *et al.,* 2018). South Africa has an annual rainfall of approximately 450 mm/year, which is approximately half of the worlds annual average of 860 mm/year (Botai *et al.,* 2018). The eastern Highveld, which includes the Mpumalanga Highveld, receives between 500 and 900 mm per annum, occasionally exceeding 2000 mm/year (Botai *et al.,* 2018), which is considerably more than the South African average. Most of this rainfall is predominantly during summertime (December, January and February) as South Africa is mostly dominated by summer rains, except for the south and south-western regions (Botai *et al.,* 2018).

### *iii.) Mechanisms of transport over the Mpumalanga Highveld region*

Mean daytime surface winds in the Mpumalanga Highveld predominantly consist of north to north-westerly winds and the next most present winds are easterly. As a result of the increased cyclonic occurrences associated with westerly weather disturbances in wintertime, the frequency of south-westerly winds

increases (Held *et al.*, 1996). At night-time, a greater frequency of north-easterly winds occurs than north-westerly winds. However, significant surges of light, topographically-induced winds occur from the east and southerly sectors during the night. Annually, the surface wind speeds fluctuate between 2 and 4 m/s with extremes occurring between late winter and spring (e.g. August to October) (Held *et al.*, 1996).

As temperature inversions occur after sunset, a decrease in frictional drag and the development of nocturnal low-level jet are caused. A low-level jet is a speeding ribbon of air in the lower levels of the atmosphere and can rapidly transport air. Nocturnal jets are strongest during early morning hours and decreases in strength as the day progresses due to a reverse in the temperature gradient (Jury & Tosen, 1989). Low-level jets over various regions of southern Africa have also been observed because of a thermal gradient established over slightly sloping terrain that spread outside the nocturnal temperature inversions. Winds reaching 10 m/s in the jet core at about 200 m AGL (Zunckel *et al.*, 1996) have been detected, and therefore contributions from low-level jets in regional wind systems may be somewhat accountable for the night-time transport of pollutants.

As a result of the expansion of the south Indian Ocean anticyclone over the cooler Mpumalanga interior during wintertime, the Highveld is dominated by anticyclonic circulation. The *winter mode* 800 hPa wind circulation at about 350 meters above ground level (MAGL) implies that boundary layer winds are subject to the Indian Ocean anticyclone, which spreads inland over the Northern Province (Tosen & Jury, 1988). Because of this wintertime northerly movement of the anticyclonic pressure belts, the Mpumalanga Highveld is subject to west-north-westerly and westerly winds. However, in summertime, these pressure belts move southwards and circulation is distinguished by the occurrence of northerly winds. These winds gradually change direction towards the north-north-west later in summer and the inverse occurs at the onset of autumn, where winds change to westerly (Held *et al.*, 1996).

## 2.3 Source apportionment

To design and implement air quality policies, it is essential to have information on pollution sources (Belis *et al*., 2014). Therefore, identifying the different sources of atmospheric pollutants and quantifying their contribution to ambient air pollution, i.e. source apportionment (Belis *et al*., 2014) are important information gathering processes. Mainly two different approaches to conduct source apportionment are currently applied, i.e. i) source-oriented models and ii) receptor-oriented models (Belis *et al*., 2014; Viana *et al*., 2008). In Figure 2.4, a schematic representation of these two approaches is presented, as well as some common techniques used within these methods to conduct source apportionment. These two approaches and their associated techniques will be discussed in more detail in the following two paragraphs.

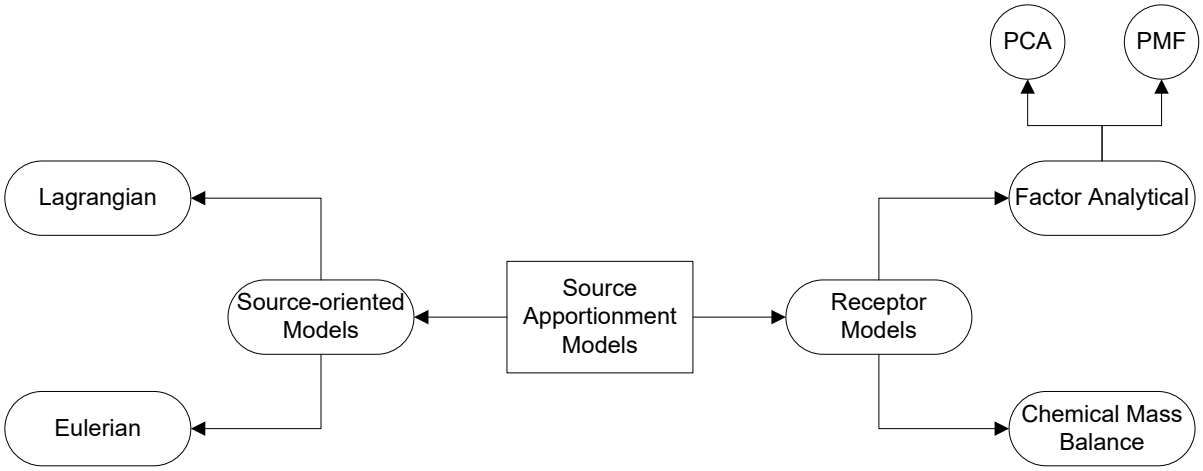


**Figure 2.4** Schematic representation of the two main approaches used to conduct source apportionment and the common techniques used therein

### 2.3.1 Source-oriented models

Source-oriented techniques do source apportionment by using emission inventories to simulate the processes of emission, transport, physical and chemical alterations, and the deposition of atmospheric pollutants (Doraiswamy *et al*., 1995; Eldering & Cass, 1996; Visser *et al*., 2001; Viana *et al*., 2008). However, these techniques are highly reliant on accurate emission inventories – databases that indicate the number of pollutants emitted into the atmosphere per time unit at either the discrete location of sources, or sources allocated within grid cells, to get the correct spatial coverage (EPA, 2018). However, using these models has been challenging, as there are no regional-specific comprehensive peer-reviewed inventories available in the public domain for South Africa. However, there are global inventories that cover similar sources. According to South African environmental legislation, significant emitters must supply atmospheric emission data to government (DFFE, 1998). However, this data is supplied with some legal safeguards, which have thus far prevented a comprehensive peer-reviewed emission inventory becoming available in the public domain. Interested and affected parties can use the Promotion of Access to Information Act 2 of 2000 (PAIA) (http://www.dirco.gov.za/department/paia.pdf, accessed 4 March 2019) to attempt to obtain such information, but this process is lengthy and costly, and does not always yield all the required information. In addition, emissions from area sources of which the spatial coverage and emission factors do not stay constant (e.g. open biomass burning), and sources such as household combustion in semi- and informal settlements that are difficult to regulate, complicate the South African situation further. Therefore, the vast majority of source-oriented atmospheric modelling studies undertaken for this region have used global emission inventory databases (e.g. Tummon *et al*., 2010; Laakso *et al*., 2013; Kuik *et al.,* 2015; Lourens *et al.,* 2016), which do not always contain enough region-specific information. Typical source-oriented methods apply the a) Eulerian and b) Lagrangian techniques.

i.) Lagrangian techniques

In these models, a moving framework of reference is used to describe the trajectories of, for instance, particles or aerosols as they move through the atmosphere. This can be done for single- or multiple particles (Belis *et al.,* 2014). For example, Bhave *et al*. (2001) used a source-oriented Lagrangian trajectory model to generate synthetic datasets of source-segregated single particles, with the model including aerosol processes such as emission, transportation, deposition, gas-phase transformations and fog chemistry (Bhave *et al.,* 2001).

Various South African source-oriented studies have used Lagrangian models. For instance, a Lagrangian kinematic model was used by Freiman and Piketh (2002) to model air transport in the industrial Highveld of South Africa. It was discovered that 43% of air reaching the Highveld was clean marine air and that 25% of all air transported to the Highveld region is loaded with aerosols from subtropical Africa (Freiman & Piketh, 2002). Bruwer and Kornelius (2017) used a CALPUFF dispersion model to simulate the deposition rates for nitrogen- and sulphur-containing species. To determine the impact of biogenic emissions of $NO_x$ on the Highveld, the model was applied with and without biogenic emissions of $NO_x$ (Bruwer & Kornelius, 2017). The results indicated that biogenic $NO_x$ made up a total of 3.96%, 4.14% and 3.34% of total NOx emitted for 2001, 2003 and 2010, respectively (Bruwer & Kornelius, 2017).

ii.) Eulerian techniques

Eulerian models incorporate chemical and physical (motion and other physical processes/transformations) equations that are solved at selected points on a three-dimensional grid (Belis *et al.,* 2014). These models are better suited for secondary pollutants, as they account for the chemical interactions between sources (Yarwood *et al.,* 2007). As an example, Kleeman (2001) developed a three-dimensional source-oriented model for externally mixed aerosols to conduct source apportionment in the South Coast Air Basin surrounding Los Angeles. The model simultaneously tracked fine/inhalable particle concentrations, ozone and other gaseous species (Kleeman *et al.,* 2001).

Wang *et al*. (2021) used potential source contribution function (PCMF), HYSPLIT and emission trends from 2014 to 2020 to model potential source regions and their impact on $SO_2$ and $NO_2$ concentrations within the Jiangsu Province in China. It was established that the Jiangsu province was mainly impacted by local anthropogenic sources, with some contributions from the neighbouring countries (Whang *et al*., 2021). Transport and the deposition of sulphur over South Africa were modelled by Zunckel *et al*. (2000) with the MATCH Eulerian model. Modelled wet deposition rates of sulphur for the Highveld were between 1 and 5 kg S $ha^{-1}$ $a^{-1}$ (Zunckel *et al*., 2000). Laakso *et al*. (2013) used the GLOMAP model, which is an extension of the TOMCAT 3-D Eulerian model, to simulate particle growth in South Africa. However, they found that the model did not reproduce the particle growth characteristics of observations (Laakso *et al*., 2013). Recently, de Lange *et al.* (2021) used an Advanced Research Weather Research and Forecasting (WRF-ARW) model to simulate pollution levels over the Highveld of South Africa and to compare the modelled results with ground-based

observations to determine which planetary boundary layer (PBL) schemes should be used when running numerical weather prediction models (NWP). It was discovered that there was statistically relevant differences between different PBL schemes depending on seasonality and type of pollutant. Furthermore, one of the local schemes (MYNN) modelled higher $SO_2$ surface concentrations against what was measured on site (de Lange *et al*., 2021). Maseko *et al*. (2021) conducted a source contribution study on $NO_x$ produced from lightning strikes by using data from the South African Lightning Detection Network and the emission factor of 11.5 kg $NO_2$/flash. In this study, it was found that lightning produced $NO_x$ accounted for 14% of the total $NO_x$ budget in South Africa and that the South African highveld is the largest contributor to lightning produced $NO_x$ (Maseko *et al*., 2021).

### 2.3.2 Receptor models

Receptor models apply multivariate statistical techniques to identify and quantify air pollutants to their sources (Hopke, 2008; 2011; 2016). These models are based on the fundamental principle that mass conservation takes place between the emission site and receptor site. A mass balance analysis is used by most receptor modelling techniques for the identification and apportionment of PM/aerosols (Cooper & Watson, 1980; Hopke, 2008; 2011; 2016). An equation is written to account for all *m* chemical species in the *n* samples as contributions from *p* independent sources (mass balance equation, Equation 2.1).

$$x_{ij} = \sum_{p=0}^{p} g_{ip} f_{pj} + e_{ij} \quad (2.1)$$

with $x_{ij}$ equal to the measured concentration of the $j_{th}$ species in the $i_{th}$ sample, $f_{pj}$ is the concentration of the $j_{th}$ species in material emitted by source p, $g_{ip}$ is the contribution of the $p_{th}$ source to the $i_{th}$ sample and $e_{ij}$ is the portion of the measurement that cannot be fitted by the model.

Naturally, any model developed for the identification and apportionment of atmospheric pollutants will have some physical constraints (Henry, 1991). It is therefore important to consider these limitations/difficulties before developing any model. For receptor modelling, the fundamental constraints that need to be adhered to are (Hopke *et al.,* 2008):

- The model must reproduce the original data and explain the observations;
- non-negative source compositions must be predicted; a negative concentration cannot be obtained by a source as it is then a sink;
- the sum of the predicted source contributions must be less or equal to the total measured mass/concentrations of each element.

Typical receptor models are i) chemical mass balance models (CMB) and ii) factor analytical (FA) methods such as a) principal component analysis (PCA) and b) positive matrix factorisation (PMF), with all of these methods taking different routes to solve the mass balance equation (Equation 2.1).

*i.) Chemical mass balance*

In CMB models, the sources of pollutants must be known to conduct the analysis (Hopke *et al.,* 2008). These models solve the mass balance equation (Equation 2.1) by using effective variance least squares. To solve this equation, the number (p) and composition of sources ($f_{pj}$) must be known, which leaves only the contribution ($g_{ip}$) unknown (Hopke *et al.,* 2008; Belis *et al.,* 2014). CMB software can be readily obtained from the U.S. EPA (Environmental Protection Agency) at www.epa.gov/SCRAM. Although CMB is an effective receptor modelling technique for primary PM, it is not able to effectively deal with secondary PM (Hopke *et al.,* 2008).

Source contributions to mean ambient concentrations of CO, $SO_x$ and $NO_x$ have been determined through CMB analysis in the Southeastern United States. Although the study had a key focus on PM, it did show that source apportionments of trace gases is possible using CMB and trusted emission inventories (Blanchard *et al*., 2012). CMB source apportionment has been applied within the South African context. For instance, in a study by Maenhaut *et al*. (1996), CMB was done after PCA was first applied to identify the possible sources. As previously stated, CMB is more appropriate if the major sources are already known (Maenhaut *et al*., 1996). It was discovered that, in the Highveld, mineral dust and sea salt contributed to a ratio of 99 to 1 to the coarse PM fraction and the pyrogenic component was the dominant contributor in the fine PM fraction (Maenhaut *et al*., 1996). Engelbrecht *et al*. (2002) used a CMB model to compare source contributions from residential coal and low-smoke fuels in the Qalabotjha township. The study confirmed that the greatest source of PM in the township was residential combustion of coal, followed by biomass burning (Engelbrecht *et al*., 2002).

*ii.) Factor analytical techniques*

FA methods (e.g. PCA and PMF) are multivariate techniques that aim to solve the mass balance equation (Equation 2.1). These methods do not require information about the number and composition of the sources under investigation for input (Hopke *et al.,* 2008; Belis *et al.,* 2014). However, detailed source knowledge is required from the user to relate modelled source profiles to specific sources (Viana *et al*., 2008). These methods gain information on source contributions by the variability of different elements in large datasets (Cooper, 1980; Hopke *et al.,* 2008). It has been suggested that factor analytical methods tend to retrieve more information from atmospheric data than there actually is (Henry, 1987). Regardless of this, these methods are often used for source apportionment, as software packages to do the studies are widely available and no prior information of sources and emission profiles is required (Viana *et al.,* 2008).

*a.) Principal component analysis*

PCA is a multivariate data analytical technique used to correlate a large number of variables into a smaller number of variables known as principal components (Wold *et al.,* 1987; Adbi & Williams, 2010). The principal components are uncorrelated with each other and orthogonal (Pires *et al.,* 2007). The components are linear combinations of the original variables in a way that the first component represents the largest portion of the

data variability, the second component represents a lesser portion than the first and so forth (Abdul-Wahab *et al.,* 2005; Sousa *et al.,* 2007; Wang & Xiao, 2004). The influence of each original variable on the different components is determined by running a rotational algorithm (e.g. Varimax rotation), which calculates the rotated factor loadings and represents each variable's contribution to the principal components (Pires *et al.,* 2007). Pires *et al.* (2007; 2008), for example, used PCA to classify atmospheric monitoring sites and sort them into classes according to their pollution behaviours in terms of $SO_2$ and PM, as well as $NO_2$, CO and $O_3$.

As previously stated, Maenhaut *et al*. (1996) used PCA to first determine the main sources (components) of aerosols before applying CMB. Components for the course PM fraction were mineral dust and sea salt, while four components were identified in the fine fraction, i.e. sea salt, sulphate, mineral dust and biomass burning (Maenhaut *et al*., 1996). Conradie *et al*. (2016) used PCA as an exploratory tool to determine sources influencing wet deposition at four sites in South Africa, i.e. Amersfoort, Vaal Triangle, Louis Trichardt and Skukuza. For Amersfoort, crustal combustion of fossil fuel and marine- and agricultural components were identified as possible sources (Conradie *et al*., 2016). Identifying sources in the Vaal Triangle proved more difficult, since it is a complex site surrounded by numerous industries and anthropogenic sources. The sources for Skukuza and Louis Trichardt were divided into two components: i) species associated with crustal and marine sources, and ii) species associated with agricultural- and fossil fuel combustion sources (Conradie *et al.,* 2016).

*b.) Positive matrix factorisation*

PMF is a specific type of factor analytical method that uses the experimental uncertainty for scaling matrix elements and coerces factor elements to be non-negative (Belis *et al.,* 2014). The most significant problem in PMF is to determine the identity and contribution of different components in an unfamiliar mixture (Malinowski *et al.,* 2002; Reff, 2007). The most common PMF model is a bilinear model where observations of PM species are expressed as the sum of contributions from several different time-invariant source profiles (Reff, 2007). The model deconstructs the data into two matrices, i.e. factor profiles and factor contributions, with the aim to classify the specified quantity of factors, which are viewed as sources (Jaars *et al.,* 2018). Contini *et al*. (2016) used PMF to determine the contribution of a large coal-fired power station to $PM_{10}$ concentrations in Italy. The contributions of the power station were approximately 2% of primary PM in the study area (Contini *et al*., 2016).

Recently, Jaars *et al*. (2018) used PMF to conduct a source apportionment study on VOCs measured at a regional background site in the interior of South Africa. They differentiated ten meaningful factors for VOCs. Five of these factors were associated with biogenic emissions and the other five were from anthropogenic sources (Jaars *et al*., 2018). From the biogenic factors, three factors could be characterised by specific species (i.e. limonene, isoprene and 2-methyl-3-buten-2-ol) and the other factors were made up of biogenic mixtures and tracer species (Jaars *et al*., 2017). Muyemeki *et al.* (2021) recently used a PMF receptor model to identify sources of $PM_{10-2.5}$ within in the Vaal Triangle Airshed Priority Area (VTAPA). Major sources of $PM_{10-2.5}$ were

identified to be related to dust and secondary aerosol formation. Further significant sources of $PM_{2.5}$ were identified as coal burning, biomass and wood burning, and industry (Muyemeki *et al.,* 2021). PMF was also applied to conduct source apportionment of PM in Pretoria, South Africa, from April 2017 to April 2018 (Adeyemi *et al*., 2021). Sources identified in this study were soil dust, fossil fuel combustion, vehicle emissions, traffic, coal burning and pyrometallurgical industries, of which coal burning and secondary sulphur accounted for 50% of the $PM_{2.5}$ sources during winter time (Adeyemi *et al*., 2021). Alpheus *et al*. (2023) recently conducted dispersion-normalised PMF source apportionment on $PM_{2.5}$ in Cape Town, South Africa. The respective contribution of the sources were 21.8 % for sea salt, 16.8% for 2-stroke vehicles, 15.7% traffic, 15.7 heating/cooking/biomass burning, 12.3% soil/road dust and 3.6% sulphates (Alfeus *et al*., 2023).

Source apportionment techniques are not limited to the above methods; numerous other less well-known methods exist and are in use. However, these mentioned above are the most well-known and frequently used models.

### 2.3.3 Source apportionment in South Africa

To date, numerous source apportionment studies have been conducted within the context of South Africa, which included source and receptor-oriented methods. It was found in a recent review study on source apportionment of air particulate matter in South Africa, a total of 35 source apportionment studies were done. The majority of these studies focused on urban areas (60%), followed by rural areas (22.9%) and industrial areas (17.1%) (Mathuthu *et al.,* 2019). In the review, it was discovered that between 1990 and 2016, most source apportionment studies were done on aerosols with 56.5%. $PM_{2.5}$ and $_{10}$ and NOx studies accounted for 30.4% of studies done combined. The least number of studies was conducted on trace metals, $PM_1$ and carbon monoxide (CO) with a combined percentage of 13.1% (Mathuthu *et al.,* 2019). It was also found that trajectory models were the most commonly used method to conduct source apportionment followed by using mass concentrations of air particulate species consisting of 12 and 10 studies, respectively. Chiloane *et al.* (2017) recently used continuous ambient measurements and co-incidental increases of trace gas and eBC together with HYSPLIT back-trajectories to identify sources of eBC at Elandsfontein. Detailed analysis at Elandsfontein identified major sources including coal-fired power stations, pyrometallurgical smelters, traffic, household combustion, and savannah/grassland fires (Chiloane *et al.,* 2017). Despite the focus on industrial pollution, household combustion and savannah/grassland fires emerged as dominant sources, particularly in colder months, while other sources contribute year-round (Chiloane *et al.,* 2017). Aerosol optical characteristics and PCA each had four studies and CMB studies only had two. Finally, tracer methods, PMF and multivariate analysis each only had one study (Mathuthu *et al.,* 2019).

It is clear from the review study (Mathuthu *et al.,* 2019) as well as from the examples listed with the different source apportionment methods that there are very little source apportionment studies on trace gas species such as $H_2S$, $SO_2$, NO and $NO_2$ with most of the studies focused on PM and aerosols, thereby highlighting the

need for source apportionment studies on trace gases within South Africa by improving the method as presented by Chiloane *et al,* (2017) to be suitable for trace gas source apportionment.

## 2.4 Conclusion of literature review

It is well known that the HPA is one of the most polluted areas within South Africa regarding air quality. Furthermore, HPA is considered as a NOx and $SO_2$ hotspot globally. The HPA is a relatively small area that contains most of South Africa's large industrial activities (e.g. coal mining, power generation, petrochemical operations, pyrometallurgical smelter, etc.). This, together with the recirculation of air and strong inversions over the South African Highveld, creates the ideal environment for entrapping and concentration of air pollution, especially during the colder months of the year. Considering the effects of atmospheric pollution on climate change, air quality and human/environmental health, it is of great importance to further our understanding of said pollutants.

From the literature survey, it is evident that there is a need for source apportionment studies on $NO_x$ and gas phase sulphur species ($SO_2$ and $H_2S$) to better understand what makes the Highveld a global $NO_x$ and $SO_2$ hotspot, as the majority of source apportionment studies have been undertaken on PM and aerosols. The little that has been done on NOx and $SO_2$ are source-oriented models that model the contribution of a specific source over a region based on emissions rates/factors and meteorological conditions (e.g. Maseke *et al*., 2021; de Lange *et al*., 2021). Also, to better the current studies being done, South African-specific emission inventories need to be available in the public domain. Although it is possible to use other emission inventories that are not specific to South Africa, it is advised to use region-specific emission inventories as source profiles could differ. It was also evident that there were not many South African-specific receptor source apportionment studies on trace gases available in the peer-reviewed domain, as seen from Mathuthu *et al.* (2019) and the literature review. The literature survey therefore supports the objectives set in section 1.2. To achieve the objectives set out, a novel receptor-oriented source quantification method, recently presented by Chiloane *et al.* (2017), was improved and applied to four trace gas species.

# Chapter 3: Methodology

**In this chapter,** the methodologies used and developed in this study are presented. In section 3.1, a site description of the Elandsfontein monitoring station where atmospheric measurements relevant to this study were conducted is presented. Detailed description of instrumentation used to perform atmospheric measurements and to obtain ancillary data are discussed in section 3.2. The Lagrangian particle dispersion model, FLEXPART, used to compile air mass back trajectories, is discussed in section 3.3, while data cleaning, as well as data quality control/assurance procedures are discussed in section 3.4. In section 3.5, the methodology applied to identify burning coal dumps is discussed, while the novel method developed in this study to conduct source apportionment of atmospheric gaseous species is presented in section 3.6. These novel methods, i.e. identification of coal dumps and source apportionment of gaseous species were also presented in the research papers "The use of fire radiative power observations to determine spontaneous combustion event activities associated with coal mining on the Mpumalanga Highveld", published in Clean Air Journal (Cogho *et al*., 2022), and "Concentration contextualisation, temporal patterns and sources of hydrogen sulphide at a site on the South African Highveld", published in Atmospheric Environment (Cogho *et al*., 2023), respectively.

## 3.1 Site description

Measurements were conducted from 1 February 2009 to 31 January 2011 during the South African measurement campaign, which was part of the European Integrated Project on Cloud Climate, Aerosols and Air Quality (EUCAARI) (Kulmala *et al*., 2011; Laakso *et al*., 2012) and conducted at the Elandsfontein measurement station (26° 14'43 S, 29° 25'30 E, 1750 m AMSL). As indicated in Figure 3.1, this site was centrally situated with regard to most of the large point sources within the Mpumalanga Highveld, which, depending on the prevailing winds, limits bias to a specific source(s).

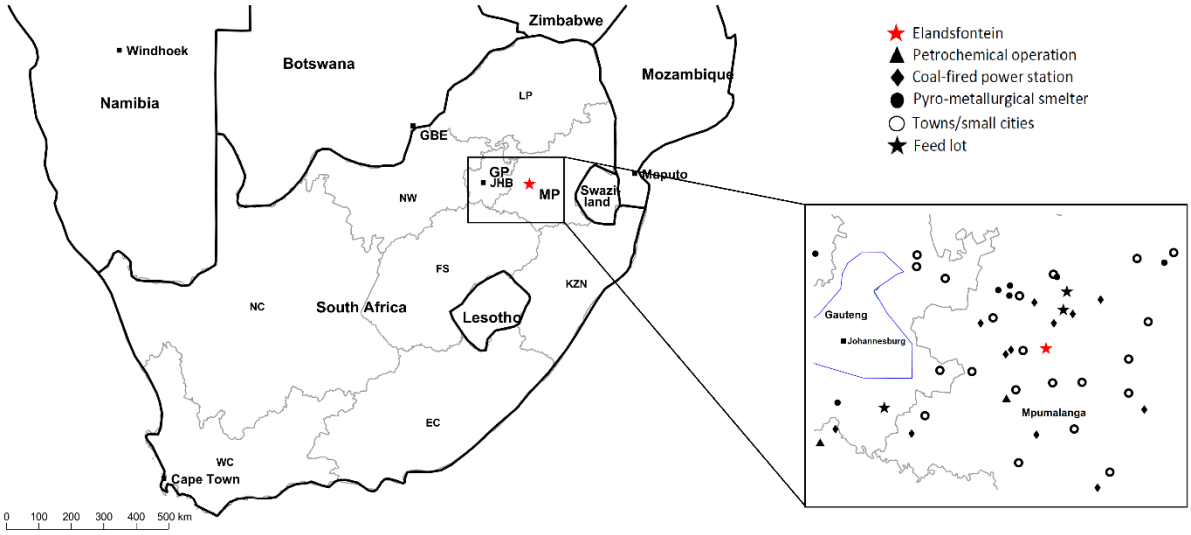


**Figure 3.1:** Map indicating the position of the Elandsfontein measurement site within a southern African context. The blue polygon in the zoomed-in map indicates the Johannesburg-Pretoria megacity, while markers indicate the locations of various anthropogenic sources. The following abbreviations for the South African provinces were used: MP (Mpumalanga), GP (Gauteng), LP (Limpopo), NW (North West), FS (Free State), KZN (KwaZulu-Natal), NC (Northern Cape), EC (Eastern Cape) and WC (Western Cape).

The immediate surroundings of the Elandsfontein site are mainly grazed grassland (Mucina & Rutherford, 2006), as clearly evident in the Google Earth image in Figure 3.2, as well as cultivated land that is not evident from the Google Earth image. No large point sources occur within an approximate 15 km radius of the station. However, within a 100 km radius, numerous pyrometallurgical smelters, several coal-fired power stations and a large petrochemical operation are located (Collett *et al.,* 2010; Laakso *et al.,* 2012). In addition, there are also multiple other sources such as towns, landfills, burning coal dumps, large feedlots (> 20 000 animals), traffic, open biomass burning, domestic fuel burning, waste burning, as well as marshlands and still standing water reservoirs. Another large source area is the Johannesburg-Pretoria (Jhb-Pta) megacity with approximately 10 million inhabitants (Department of Cooperative Governance and Traditional Affairs, 2020), which is an area with many air quality issues (Scorgie, 2012; Lourens *et al.,* 2012; 2016). From the afore-mentioned description, it is evident that the region has a high density and diversity of atmospheric pollution sources, which makes it a complex area for a trace gas receptor-oriented source identification and quantification study.


**Figure 3.2:** Google Earth image of the Elandsfontein measurement station and its immediate surrounding environment. The red line on the image indicates a ruler of 100m (for scaling purposes)

## 3.2 Instrumentation

$H_2S$, ozone ($O_3$), nitrogen oxides ($NO_x$) and $SO_2$ were measured using a Thermo Electron 43A with a Thermo Electron 340 converter, a Monitor Europe ML9810B $O_3$ analyser, Thermo Electron 42i NOx analyser and a Thermo Electron 43C $SO_2$ analyser, respectively. Equivalent black carbon (eBC) (definitions according to Petzold *et al.,* 2013) was measured with a Thermo Scientific model 5012 multi-angle absorption photometer (MAAP), for which eBC concentrations were corrected according to the algorithm presented by Hyvärinen *et al.* (2013). Meteorological measurements were taken with a Vaisala WXT510 meteorological station fitted on the roof of the measurement building at approximately 3.5 m above ground level and solar radiation with a photo-active radiation (PAR) sensor (Laakso *et al.,* 2012). All measurements were taken at 1-min. resolution, from which 15-min. averages were calculated, if at least two thirds of the data in the 15-min period were available. Data cleaning and quality assurance, as well as site maintenance procedures have previously been presented and applied to the dataset (e.g. Laakso *et al.,* 2012; Beukes *et al.,* 2015) and are therefore not repeated here. All instruments were housed in two small airconditioned huts, with an additional structure to house the pumps (Laakso *et al*., 2012).

Elandsfontein is an ESKOM-operated ambient air quality measurement station (Collett *et al*., 2010), for which the instrument measurement set was significantly augmented during the EUCAARI project, e.g. scanning mobility particle sizer (SMPS) (Wiedensohler *et al.,* 2011), optical particle counter (OPC), 3-wavelength particle soot absorption photometer (PSAP) (Backman *et al.,* 2014), 3-wavelength Nephelometer (Venter *et*

*al.,* 2020), Cimel multichannel sunphotometer (https://aeronet.gsfc.nasa.gov/index.html, accessed 18 February 2020), dichotomous aerosol sampler with off line PM analyses (Venter *et al.,* 2016) and a multi-wavelength Raman lidar (Giannakaki *et al.,* 2015). However, these measurements were not considered in this paper and are therefore not discussed further. The dataset from the EUCAARI campaign was specifically used as, during this time, the station was extensively monitored by staff, thereby resulting in a trusted dataset.

### 3.2.1 Trace gas and eBC measurements

Similar to Chiloane *et al.* (2017), concurrent trace gas and eBC measurements were considered to identify coincidental concentration peaks during the receptor-oriented technique applied for this study. Therefore, these measurements and instruments are considered in greater detail.

a) $NO_x$

Operation of the Thermo Electron 42i $NO_x$ analyser is based on the reaction of NO with $O_3$ to produce characteristic luminescence, which is directly proportional to the concentration of NO present. When $NO_2$ molecules decay to lower energy levels or states, infrared light is emitted (Thermo Fischer Scientific, 2007); the reaction thereof follows:

$$NO + O_3 \rightarrow NO_2 + O_2 + h\nu \quad (3.1)$$

To measure the $NO_2$ concentration, a molybdenum $NO_2$-to-NO converter must first convert $NO_2$ to NO heated to 325°C, to then be measured by the chemiluminescence reaction as explained for NO (Thermo Fischer Scientific, 2007). This converter may also convert other reactive nitrogen species to NO, but their contribution to $NO_2$ is expected to be very little at Elandsfontein. The result of this is a total $NO_x$ concentration; to determine the $NO_2$ concentration, the initial NO concentration is subtracted from the total $NO_x$ concentration.

b) $SO_2$

The operation of the Thermo Electron 43C $SO_2$ analyser is based on the fluorescence of $SO_2$ when it absorbs ultraviolet (UV) light (EPA, 2009). $SO_2$ is bombarded by UV light between wavelengths of 190 and 230 nm; the $SO_2$ then absorbs this UV light and becomes electronically excited. As a result of this, it emits a unique decay radiation, which is measured with a photo multiplier tube (PMT) through light energy striking the PMT. This energy converted to a voltage, which is then directly analysed (EPA, 2009).

c) $H_2S$

$H_2S$ was converted to $SO_2$ by the Thermo Electron 340 converter and then analysed by the Thermo Electron 43A $SO_2$ analyser. This analyser operates in the same manner as the Thermo Electron 43C $SO_2$ analyser by measuring the decay radiation after the absorption of UV light by $SO_2$, resulting in a total sulphur measurement (EPA, 2009). By bypassing the converter, the analyser measures only non-converted $SO_2$ and not the $SO_2$ converted from $H_2S$. The $H_2S$ concentration is calculated by subtracting the latter from the total sulphur concentration.

d) eBC

A Thermo Scientific model 5012 multi-angle absorption photometer (MAAP) was used to measure the eBC concentration, and, afterwards, the 1-minute eBC concentrations were corrected according to an algorithm presented by Hyvärinen *et al.* (2013). The MAAP measures the absorption of light and then uses the mass absorption efficiency of 6.6 $m^2g^{-1}$ to compute eBC concentrations (Laakso *et al.,* 2012). Air is drawn in through an inlet, which then deposits particles on glass-fibre filter tape. The particles accumulate on the tape where a 670 nm light source is aimed at the aggregate of particles. Photo detectors measure both reflected and diffused light. Thereafter, real-time concentration data is calculated by constant integration of numerous reflection intensities, decrease of light transmission and air sample volume over time (Thermo Fischer Scientific, 2007). MAAP was operated with a $PM_{10}$ inlet and relative humidity (RH) was kept below 35% (Laakso *et al.,* 2012).

### 3.2.2 Ancillary measurements

In addition to the above measurements of atmospheric species, meteorological parameters were also determined. A Vaisala WXT510 meteorological station (Vaisala, 2010) that was fitted on the roof of the measurement station building, approximately 3.5 m above ground level, was deployed at Elandsfontein. Meteorological measurements included wind speed and -direction, rain intensity, temperature and relative humidity. Solar radiation was measured with a PAR sensor and the potential temperature gradient with two Rotonic temperature-RH sensors placed at 2 and 4 m above the ground (Laakso *et al*., 2012).

## 3.3 FLEXPART sensitivity analysis

The Lagrangian particle dispersion model FLEXPART (FLEXible PARTicle dispersion model) version 10.4 (Seibert & Frank, 2004; Stohl *et al.,* 2005, Pisso *et al.,* 2019) was used to calculate air mass histories to determine potential sources at the receptor site. According to Stohl *et al.* (2018), FLEXPART can be used backward in time to determine possible source contributions at receptor sites (Pisso *et al.,* 2019). The European Centre for Medium-Range Weather Forecasts' (ECMWF) ERA5 reanalysis was used as inputs for FLEXPART. The resolution of the input data was 0.28125° over the 15°S to 40°S and 10°E to 45°E area. The temporal resolution of the ERA5 was 1 h, while the vertical resolution was 137 model levels. Hourly arriving FLEXPART emission sensitivities were calculated for at least 48 hours backwards, as this is estimated to be the approximate atmospheric lifetime of $H_2S$ (Seinfeld & Pandis, 2006). FLEXPART emission sensitivities can be described as simulated particles that are modelled to be released backwards in time from a receptor site and their residence time within the output grid cells determines the sensitivity (Pisso *et al.,* 2019).

## 3.4 Data cleaning and quality control/assurance procedures

During the two-year sampling period, measurements were only interrupted during regular maintenance checks and calibrations, while unscheduled power cuts also contributed to off-times (Laakso *et al.,* 2012). Regular maintenance occurred at least once every ten days or whenever required. General maintenance of the instruments mainly comprised inspection and adjustment of instrument flows, and cleaning of inlets, as

well as other ancillary procedures if necessary. In addition, an electronic diary was kept during these visits. Typical diary entries comprised the arrival and departure times of each site visit, as well as the names of personnel visiting the site. The latter was also important since a record of personnel visiting the site to perform maintenance, which was conducted by several people, assisted with solving measurement problems or any abnormalities in the collected data. All activities with corresponding time stamps were noted in the diary, which even included routine and mundane checks. In addition, *ad hoc* maintenance procedures, abnormal observations, or any events of interest, e.g. nearby open biomass burning events were also logged, which greatly assisted with processing of data and explaining anomalies. Furthermore, the diary could also be used as a manual on how to address future problems (Laakso *et al.,* 2012; Beukes *et al.*, 2015).

He calibration of gas instruments was performed monthly or whenever necessary. More comprehensive maintenance of the monitoring station was conducted every three months, which included more complex procedures such as cleaning of measurement instrumentation cells.

The diary, together with all measurement data, was transferred daily to a central server in order to prevent loss of any information. Data downloaded onto the server also underwent visual checks throughout the week for any irregularities. If any irregularities were found, an additional site visit was scheduled to resolve the issue(s) as soon as possible (Laakso *et al.,* 2012; Beukes *et al.*, 2015).

Fit-for-purpose MATLAB scripts were used to visualise raw measurement data (one-minute resolution) and to make corrections, as explained by Laakso *et al.* (2012) and Beukes *et al.* (2015). All data collected during site visits (as logged in the electronic diary), as well as any unusual measurements, e.g. spikes after power cuts, were removed from the dataset. The data was also corrected according to zero and span measurements, as well as flow checks. Multiple species were also visualised simultaneously with the aforementioned fit-for-purpose MATLAB scripts to enable manual detection of errors and/or suspicious data. For example, if NO and eBC peaked simultaneously, it indicated the measurement of a fresh combustion plume. However, if a spike is observed for only one of the measured species, this suspicious data points(s) would be further inspected through a review of the electronic diary, other measured species/parameters and air mass histories. If no evidence was found to validate the suspicious data, it was removed from the dataset.

After all data corrections were made, the data was averaged over 15-minute periods to provide a smaller dataset easier to handle in data analyses (Laakso *et al.,* 2012; Beukes *et al.,* 2015). 15-minute averages were only calculated if at least two thirds of the one-minute resolution data points were available for the entire 15-minute period.

## 3.5 Identification of burning coal dumps

The method presented by Beukes *et al.* (2018) was used to identify the location and temporal activity of burning coal dumps in the area. Here, fire radiative power (FRP) data obtained by the Moderate Resolution Imaging Spectro-radiometer (MODIS) instruments onboard the Terra and Aqua satellites to determine the

availabilities of pyrometallurgical smelters was used (Beukes *et al.,* 2018). This was performed by Beukes *et al*., (2018) by identifying and tracking the activity patterns of false positive fires (sources that emitted radiative power signals, similar to open biomass burning), which were attributed to, for example, off-gas flaring and metal/slag tapping at pyrometallurgical smelters (Beukes *et al.,* 2018). In the current study, the same method was used to determine the location and temporal activity of burning coal dumps within the study area.

FRP data was obtained from the MODIS instruments aboard the Terra and Aqua satellites for the period January 2001 to December 2019 (Kaufman *et al.,* 1998; Justice *et al.,* 2002). The MODIS collection 6 FRP data was downloaded from the Fire Information for Resource Management System archives (https://firms.modaps.eosdis.nasa.gov/download/). MODIS FRP data (MOD14A1/MYD14A1) indicates the locations of fires with substantial thermal emissions at times when the satellites pass over the area, overpasses were usually around 08:00, 12:00 and 23:00. These thermal emissions are usually from open biomass burning events (grassland, savannah and forest fires), but certain point sources with substantial thermal emissions (e.g. metal/slag tapping or off-gas flaring from pyrometallurgical smelters) are also detected as thermal anomalies (Beukes *et al*. 2018). Considering the thermal emissions from spontaneous coal combustion, these burning events could also be captured in the FRP data, depending on the fire size ($m^2$) and temperature (°C). MODIS easily detects smouldering and flaming landscape fires of a 1000 $m^2$ in size. However, if conditions are favourable, fires as small as 50 $m^2$ can be detected (Giglio *et al.,* 2016). On the other hand, false alarms are possible but rare, especially for southern Africa (Giglio *et al.,* 2016). In our application, where we are looking for sites with continuous combustion for weeks or more, occasional false positive FRP observations are not an issue.

In Figure 3.3, an example of the FRP data is depicted, with red dots indicating fires recorded for February and March 2016. Each red dot represents a burning activity recorded in a 1 $km^2$ cell. A Google Earth image of the encircled area indicated in Figure 3.3 is also presented. Numerous detected fires can be seen in Figure 3.3, as well as thermal anomalies at industrial facilities. Within the encircled area in Figure 3.3, 6 pixels (at 1 km resolution) indicate continuous combustion for two consecutive months and three more pixels indicate combustion for a part of the time. It is obviously impossible for the same vegetation to be actively burning constantly for months on end, as the fuel required for combustion will mostly be consumed after one burning event. Additionally, the timing of the fires (i.e. in February and March) does not coincide with the South African interior's open biomass burning season. The green polygon seen in the Google Earth image in Figure 3.3, which is located within the encircled area, indicates the location of an open-cast coal mine. Considering the timing (within the rainy season), reoccurring nature of the fires and that there are no clear visible signs of burnt vegetation, it is evident that the coal combustion is responsible for the observed FRP.

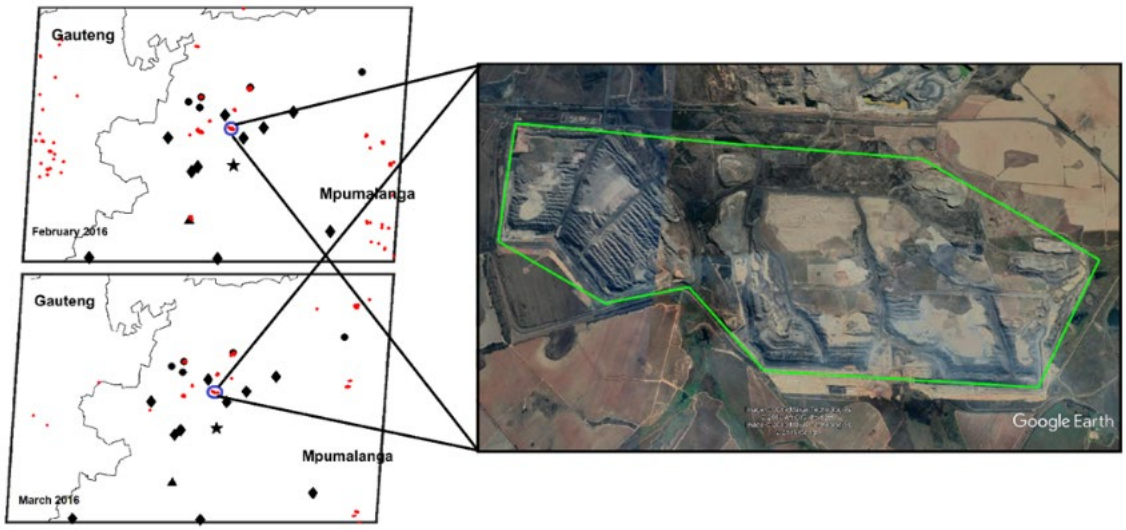


**Figure 3.3:** Maps depicting active fires (red dots) for February and March 2016 in the Mpumalanga Highveld. The blue circle represents the area presented by the green polygon in the Google Earth image

To investigate whether there was active burning at coal mining sites, circles with radii between 1 and 5 km (depending on size of mining activity, determined by analyses of the above-ground visible mined area on Google Earth) were drawn around the coordinates of each of the mining locations and the monthly fire counts within these polygons were tallied. If reoccurring fires for consecutive months were observed, such a site was classified as having had actively burning coal. A MATLAB script was used to pick-up and count all the fires that occurred in the drawn circles.

## 3.6 Identification and quantification of source contributions

A novel receptor-oriented technique to identify sources of atmospheric trace gases and quantify their relative contributions to above baseline concentrations was developed in which a dataset comprising concurrently and continuously measured eBC and trace gasses was used. This was done by modifying and improving a method presented by Chiloane *et al.* (2017). Although the aforementioned paper focused on eBC, this method developed indicated the potential of being modified and applied to trace gases (Chiloane *et al.,* 2017). In order to explain this technique, the algorithm developed is presented in Figure 3.4. This algorithm has been programmed as a MATLAB script, but any similar programming language (e.g. R, Python) could be used.

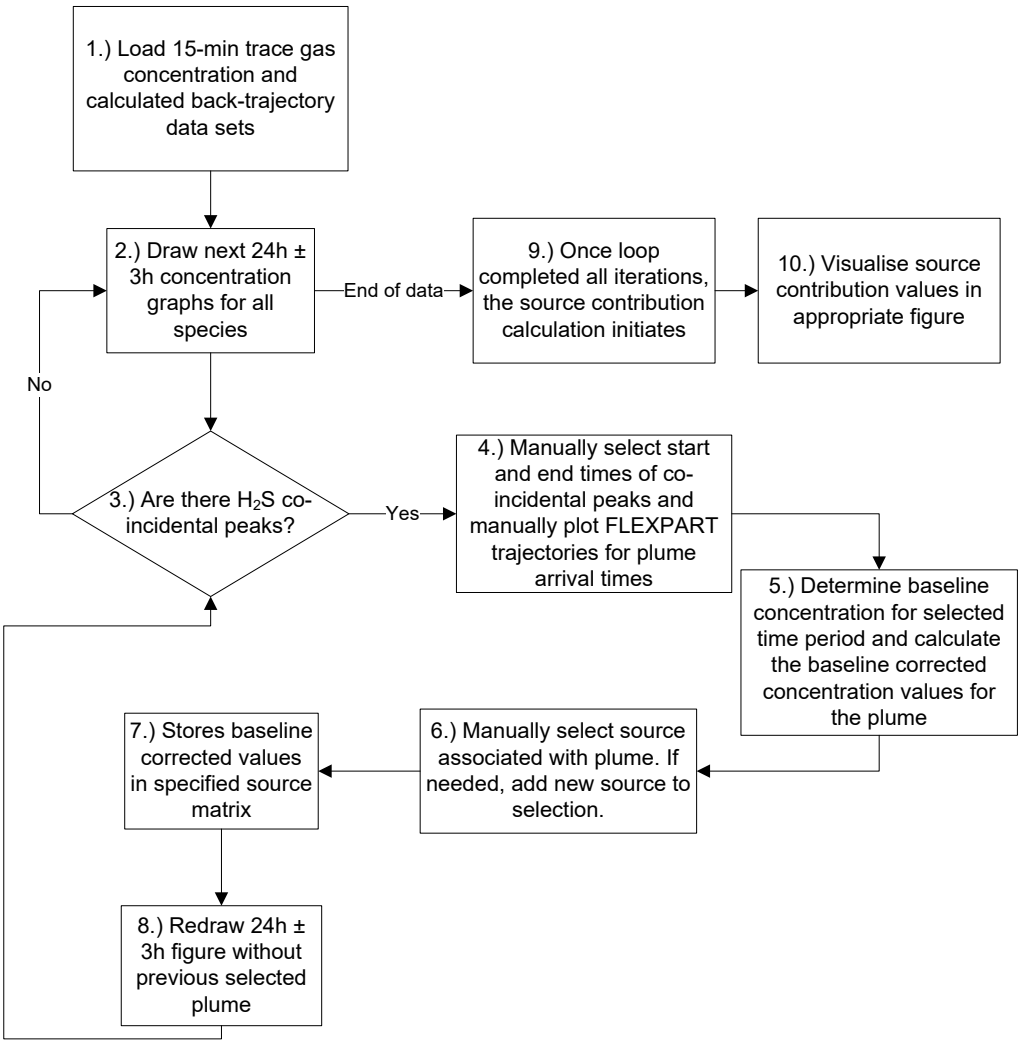


**Figure 3.4:** Algorithm (flow diagram) for the novel source quantification method developed

The steps indicated in the algorithm (Figure 3.4) are discussed in more detail below.

1) In the first step, the relevant datasets are loaded. In this case the 15-minute resolution Elandsfontein trace gases and eBC measurement data set, acquired during the EUCAARI project (Laakso *et al.,* 2012), as well as hourly arriving FLEXPART back trajectories calculated for the entire measurement period, were loaded. Both datasets were in local time.
2) In the next step, 24hr ± 3hr time series concentration graphs for all the relevant species considered are plotted for visual inspection of gaseous plumes. 24hr ± 3hr time series graphs indicating increased concentrations of nitrogen oxide (NO), nitrogen dioxide ($NO_2$), $SO_2$, $H_2S$ and eBC are presented in Figure 3.5 as examples. The developed receptor-oriented technique is based on the identification of co-incidental concentration peaks. Therefore, to ensure that a peak that extends over two consecutive

days is correctly identified as a single peak, the ± 3hr periods are drawn to account for any overlapping peaks from the previous day or the next day with the specific 24hr period considered.

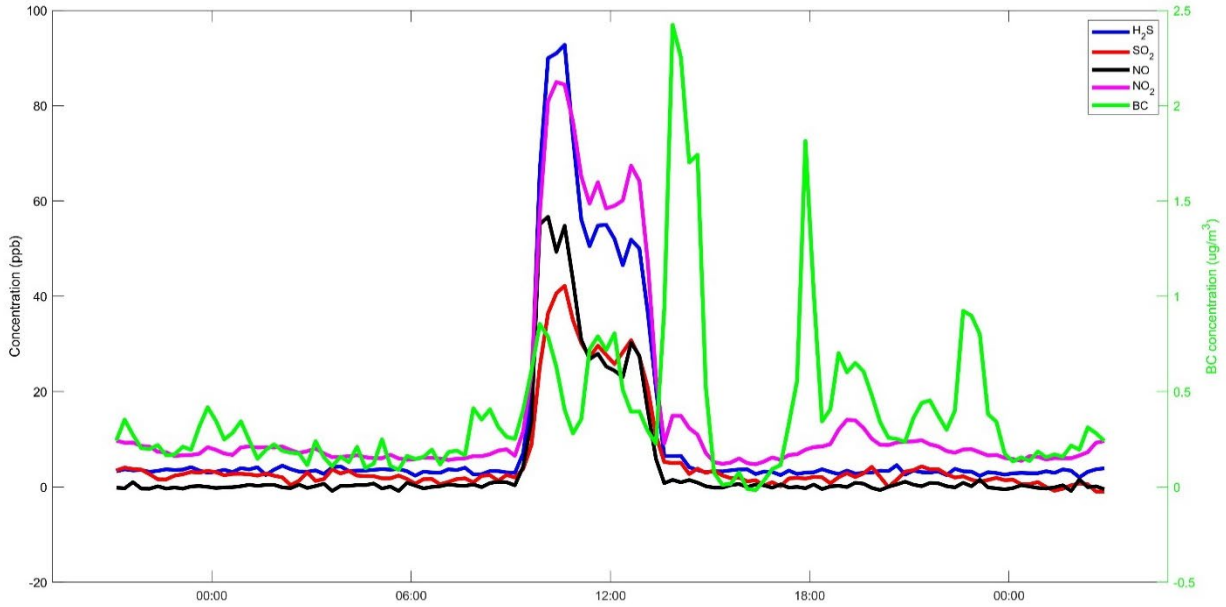


**Figure 3.5:** Examples of 24hr ± 3hr concentration *vs*. time graphs for $H_2S$, $SO_2$, NO, $NO_2$ and eBC on 1 June 2009

3) If visual inspection shows a peak in $H_2S$ that can clearly be identified from the measurement noise and baseline concentration, we proceed to step 4. Otherwise, we move forward to the next day (i.e. step 2).

4) The user must now select the start and end times of the observed peak. If more than one such peak occurred, the most prominent one should be selected first. As is evident from the example presented in Figure 3.5, there was a well-defined co-incidental peak from 09:07:30 to 13:35:30 (format HH:MM:SS), where $H_2S$ peaked at the same time as NO, $NO_2$ and $SO_2$. Furthermore, to help the user classify/attribute the plume to the correct source or identify a source that was not initially included for selection, the user must now manually plot the FLEXPART air mass emission sensitivities for each hour during the selected plume period (Figure 3.6). The brighter yellow the emission sensitivities are, the more time the air parcels spent in that specific gridded cell will be.

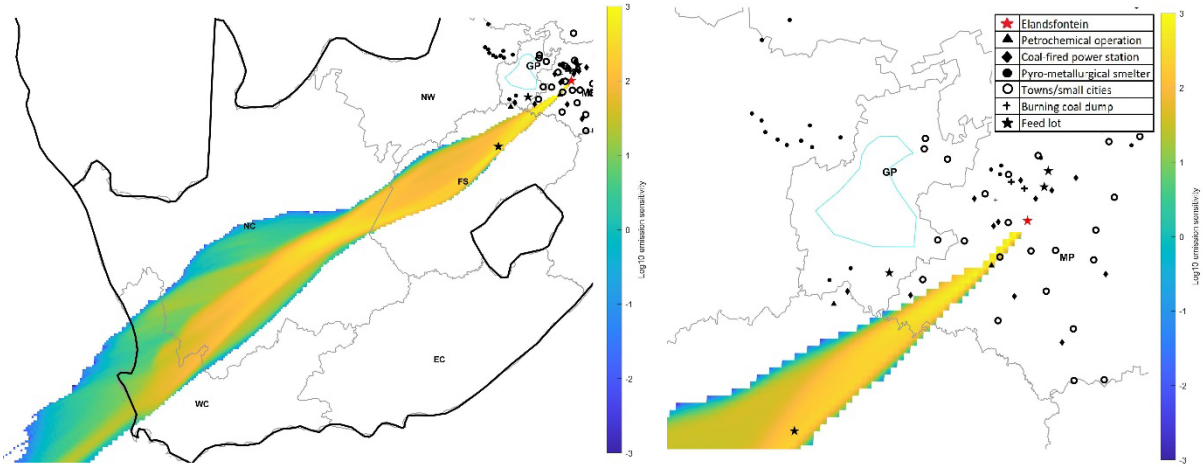


**Figure 3.6:** Summed up FLEXPART air mass emission sensitivities for the example co-incidental $H_2S$ plume depicted in Figure 3.5. The markers indicate the location of sources, as defined in Figure 3.1. On the left is the zoomed out FLEXPART emission sensitivities and the right side depicts a zoomed in version which helps to identify possible sources.

5) For the indicated plume period, the baseline trace gas concentrations and baseline corrected plume concentrations are calculated. The baseline value is calculated as the average between the start and end gas concentrations of the plume, while the plume baseline corrected concentrations are calculated by subtraction of the baseline value from each 15-min average concentration during the selected plume period.

6) The potential sources of the identified $H_2S$ plume are considered. Sources were grouped into the following categories: petrochemical operation near Secunda, coal-fired power stations, pyrometallurgical smelters, the Jhb-Pta megacity, feedlots, the paper mill near Nelspruit, emissions associated with towns/small cities/in- and semiformal settlements (which include wastewater treatment facilities, landfills, household combustion emissions, small industries, as well as vehicle emissions, especially from older diesel engines) and mixed/undefined sources. This categorisation is performed by considering all the relevant information available for each plume. For instance, co-incidental increases in certain species can be expected from certain sources and different sources might have different plume amplitude strengths. For the specific plume example presented in Figures 3.5 and 3.6, four complementary pieces of evidence indicated that the measured $H_2S$ plume originated from the petrochemical operation near Secunda with very high probability. Firstly, the plume amplitude was relatively large, which is not expected for regional sources. Secondly, the increase in $H_2S$ concentration coincide with increased NO, $NO_2$ and $SO_2$ levels, but not with eBC (Figure 3.5). The petrochemical operation generates a significant fraction of its own electricity, and therefore NO, $NO_2$ and $SO_2$ emissions will coincide with $H_2S$. Additionally, Chiloane *et al*. (2017) showed that the specific petrochemical operation considered here did not significantly contribute to eBC measured at

Elandsfontein, and therefore the negligible increase thereof in this plume is expected. Thirdly, the timing of the identified plume corresponds to a typical high-stack emission that mixes down to surface after the breakup of the low-level inversion layer(s), which typically occurs between 08:00 and 10:00 local time as the depth of the planetary boundary layer (PBL) starts to increase at Elandsfontein (Korhonen *et al.,* 2014), as well as on the Highveld in general (Gierens *et al.,* 2018). Lastly (4$^{th}$), the source assumption was also supported by considering the corresponding air mass history information (Figure 3.6), since the calculated FLEXPART emission sensitivity during the plume period passed very close to the petrochemical operation. In addition to the petrochemical associated plume example considered here (Figures 3.5 and 3.6), more examples in the form of case studies are presented in section 6.1 and criteria for the different source categories are summarised in Table 3.1 below.

**Table 3.1:** Criteria for selection of possible sources based on type of pollutants, meteorological conditions, plume characteristics and plume timings.

| Source | $H_2S$ | NOx | $SO_2$ | BC | Plume characteristics | Timing | FLEXPART |
|---|---|---|---|---|---|---|---|
| **Petrochemical** | Present | Present, ratios of NO and $NO_2$ differ depending on plume age | Present | Absent | Strong well defined plumes, very high concentrations | Typically, during daytime after the break-up of inversions and PBL's | Finally for all occasions FLEXPART emission sensitivity analysis is used as a last filter to determine if the source identification was correct |
| **Power stations** | Rarely present and concentration much lower than other co-incidental species | Present, ratios of NO and $NO_2$ differ depending on plume age | Present | Present | Strong well defined plumes, very high concentrations except for $H_2S$ | Typically, during daytime after the break-up of inversions and PBL's | |
| **Pyrometallurgical smelters** | Present | Present, ratios of NO and $NO_2$ differ depending on plume age | Present and typically higher than other co-incidental species | Present and typically higher than in other combustion sources | Strong well defined plumes | Are seen throughout the day as stacks emit below PBL's | |
| **Urban** | Present | Present, ratios of NO and $NO_2$ differ depending on plume age | Present | Present | Plume amplitude typically not large, but the duration of plumes are usually long | Typically, during night time and early mornings as PBL depth is shallow and low level emissions are common | |
| **Jhb/Pta** | Present | Present, ratios of NO and $NO_2$ differ depending on plume age | Present | Present | Plume amplitude typically not large, but the duration of plumes are usually long | Typically, during night time and early mornings as PBL depth is shallow and low level emissions | |

| Source | $H_2S$ | NOx | $SO_2$ | BC | Plume characteristics | Timing | FLEXPART |
|---|---|---|---|---|---|---|---|
| | | | | | | are common | |
| **Burning coal dumps** | Present | Present, ratios of NO and $NO_2$ differ depending on plume age | Present | Present | Weak plume amplitudes and strength compared to other sources | Typically, during night time and early mornings as PBL depth is shallow and low level emissions are common | |
| **Feedlots** | Present | Present, ratios of NO and $NO_2$ differ depending on plume age | Sometimes, probably due to fractional oxidation of $H_2S$ to $SO_2$ | Absent as there are rarely any combustion activities at the feedlots | Weak plume amplitudes and strength compared to other sources | Typically, during night time and early mornings as PBL depth is shallow and low level emissions are common | |

7) Once the source category has been identified, the plume baseline corrected concentration values of the trace gases are stored in the data matrix for that particular source. For the example plume considered here in Figure 3.5, 19 plume baseline corrected 15-min average $H_2S$ concentration values (09:07:30 ≤ period ≤ 13:35:30) were stored in the source matrix of the petrochemical operations together with the concentration values of the other gases.

8) In this step, the program redraws the considered 24h ± 3h time series concentration graphs for further visual inspection, as indicated in Figure 3.7, and the process continues by going back to step 4 (Figure 3.4). However, in these graphs, the previously attributed plume concentrations are replaced with the baseline corrected value calculated in step 7 and the y-axes of the graphs (species concentrations) are automatically rescaled to enable easier identification of possible smaller (lower concentration) co-incidental peaks.

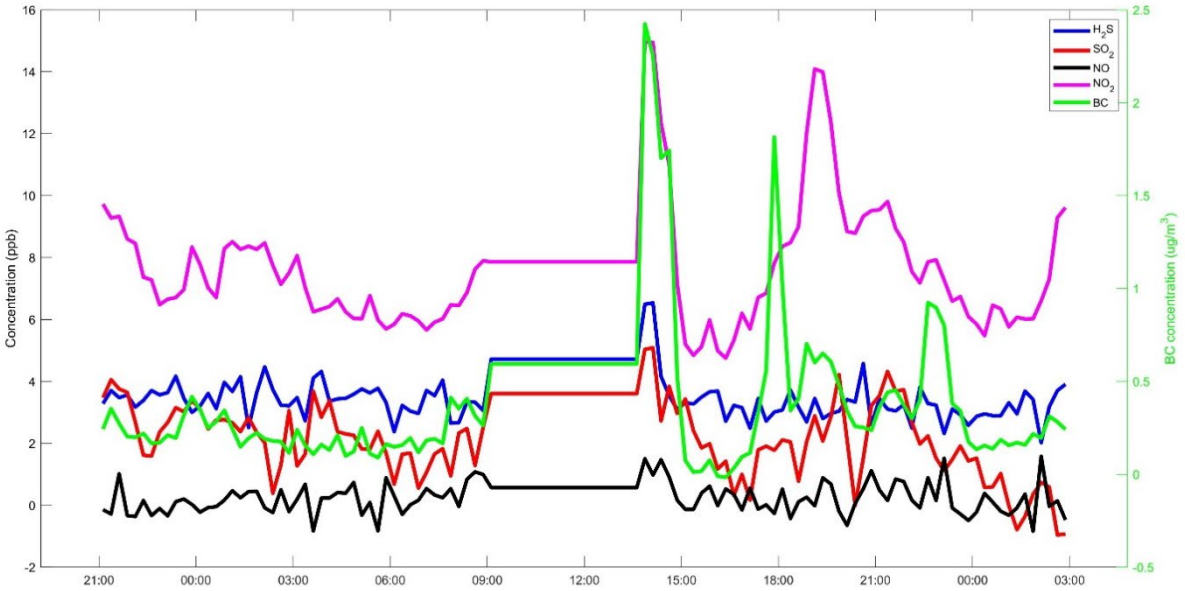


**Figure 3.7:** Example 24hr ± 3hr concentration *vs*. time graphs for $H_2S$, $SO_2$, NO, $NO_2$ and eBC on 1 June 2009, with the previously selected $H_2S$ and other co-incidental peaks (identified in Fig. 3) replaced by the baseline value

9) Once the analysis of full dataset has been completed, the source contribution calculation initiates (step 10). In this calculation, Equation (1) is applied to each of the source matrices. This equation calculates the percentage contributions to $H_2S$ measured above the baseline concentrations for each of the identified sources.

$$\%\ Source\ contribution = \frac{Cs}{Tc} \text{ x } 100 \qquad (1)$$

Where $C_s$ is the sum of all the plume baseline concentration corrected values that were attributed to the specific source; and $T_c$ is the sum of all the plume baseline corrected concentrations that were attributed to all the source matrices. Additionally, the baseline $H_2S$ concentration for the entire measurement period is also calculated from the average concentrations remaining after all attributed plume concentrations have been replaced by the plume-specific baseline values.

10) Finally, an appropriate figure (and table with actual values) is drawn to visualise the trace gas source quantifications in terms of the species under investigation (e.g. $H_2S$, $SO_2$, NO or $NO_2$) above the baseline concentrations, as well as provide ratios of baseline corrected gas concentrations divided by baseline corrected concentrations of the other species relevant to each source type. Since South Africa lacks peer-reviewed South African-specific emission inventories in the public domain, such ratios can be used in future modelling studies to approximate emissions if only emission(s) of other species are known.

# Chapter 4: Spontaneous combustion activities associated with coal mining on the Mpumalanga Highveld

**In this chapter**, spontaneous coal combustion activity within the Mpumalanga Highveld is discussed (section 4.1), as determined by the method presented in section 3.5. In section 4.2, a case study of emissions of pollutants associated with a burning coal seam is presented and the chapter is concluded in section 4.3. The work presented in this chapter has been published in the *Clean Air Journal* (Cogho *et al.,* 2022). The complete article as published is attached in the addendum.

## 4.1 Burning coal dump activities

Considering the aforementioned in Chapter 2, it is of utmost importance to determine where spontaneous combustion of coal is taking place, for how long these activities take place and to estimate the contribution of these burning emissions to air quality. However, doing this is problematic as many of these combustion events occur in remote areas and some even go by unnoticed.

Therefore, the fire radiative power (FRP) data obtained from the Moderate Resolution Imaging Spectroradiometer (MODIS) onboard the Terra and Aqua satellites (Kaufman *et al.,* 1998; Justice *et al.,* 2002) was used to determine the location and number of burning events from January 2001 to December 2019 within the Mpumalanga Highveld region. A similar method was used by Beukes *et al.* (2018) to identify and determine the activities of pyro-metallurgical smelters within South Africa. In Figure 4.1, the region in South Africa, more specifically the Mpumalanga Highveld, under investigation is presented with a Google Earth map. Within this area, the locations of open-cast coal mining operations, as well as mine refuse dumps, were derived from rigorous visual inspection of Google Earth images and are presented in the Google Earth map.

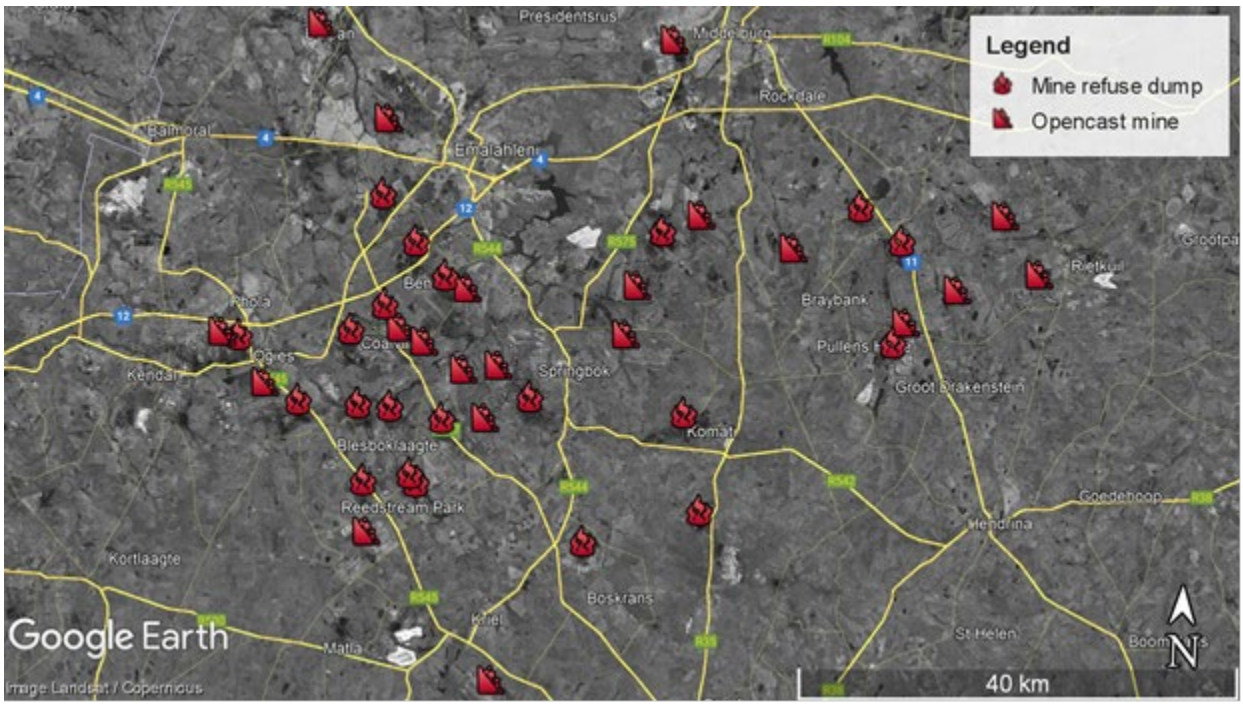


**Figure 4.1:** Google Earth image of the possible burning coal dump locations identified using FRP observations over the Mpumalanga Highveld. As seen in the legend, the "fire" icon indicates mine refuse dumps and the "rockfall" icon represents opencast mines.

Five out of the possible sites depicted in Figure 4.1 recorded long-lasting and reoccurring anomalous thermal values in the FRP time series, indicating significant spontaneous combustion events. However, it is possible that sites, where combustion occurs at smaller quantities and FRP remains below MODIS detection limits, could be missed. On the other hand, emissions scale with FRP (e.g. Sofiev *et al.,* 2009) and so we consider the five sites identified here as the most important ones from air quality perspective. The locations of these sites are presented in Figure 4.2. All of these mines are opencast mines, which are situated above old board-and-pillar mines from the 1900s. Once the roofs of these underground board and pillars are opened, an influx of oxygen can cause the old unmined coal pillars to spontaneously combust (Bell *et al.,* 2001; Pone *et al.,* 2007).

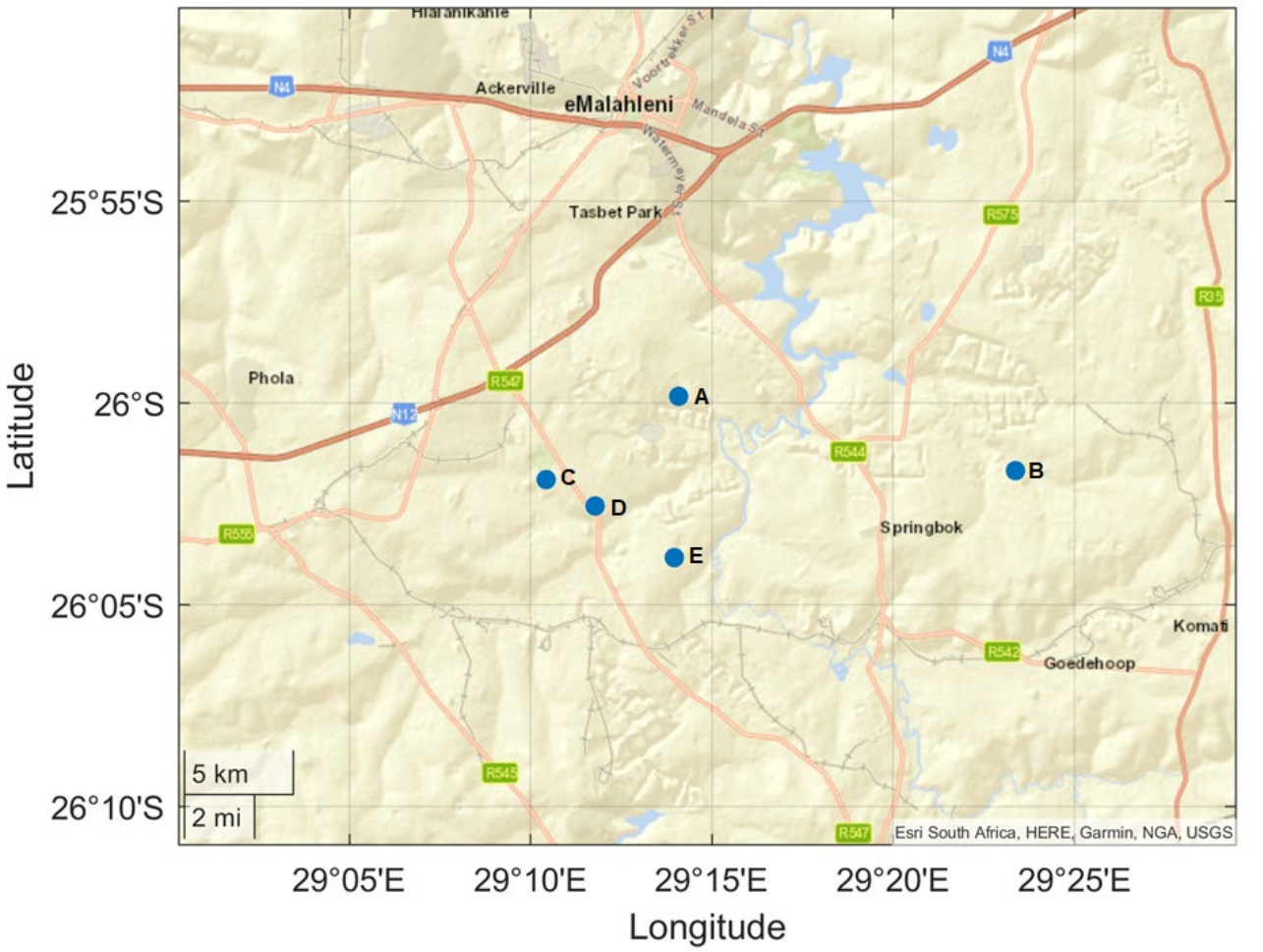


**Figure 4.2:** Map indicating the positions of the five mines that exhibit the most spontaneous combustion events

The algorithm developed by Beukes *et al.* (2018) was applied to the repetitive fires to establish when the sites were actively burning. Three-month moving averages of the fire pixels were calculated for each of the sites to account for possible data gaps, which were then divided by the 75$^{th}$ percentile for that specific site (Beukes *et al.,* 2018). These values were converted to percentages and grouped into five ranges as follows (Beukes *et al.,* 2018):

a) ≤ 10% represented zero calculated spontaneous combustion

b) 10% > ≤ 25% represented 5 to 25% calculated spontaneous combustion

c) 25% > ≤ 50% represented 25 to 50% calculated spontaneous combustion

d) 50% > ≤ 75% represented 50 to 75% calculated spontaneous combustion

e) 75% > ≤ 100% represented 75 to 100% calculated spontaneous combustion

The algorithm was adjusted to address the volatility of the data by incorporating three-month moving averages instead of relying on individual monthly counts of repetitive fire observed FRP. Additionally, the division by the 75th percentile, rather than the highest monthly active fire count, and the categorisation of smelter availabilities into ranges, rather than the monthly figures, were introduced (Beukes *et al*., 2018). These modifications were made to accommodate the erratic nature of the repetitive fire data. This erratic

behaviour stems not from sensor limitations but from the inherent challenges of capturing all high-radiation events during daily satellite overpasses (Beukes *et al*., 2018). Geostationary satellite observations would offer a solution, but they are presently unavailable for southern Africa. Consequently, there are significant constraints on the accuracy of the data and the ability to calculate coal dump burning activities from it. In Figure 4.3, the calculated percentage spontaneous combustion ranges for the five mining locations are presented. It is evident that spontaneous combustion at these five sites is prevalent throughout the 19-year period with locations A and B being the most active. Burning at sites A and B continued for several consecutive months, over many years. From this figure a possible season cycle also becomes evident, but this (the season cycle) will be considered in greater detail later.

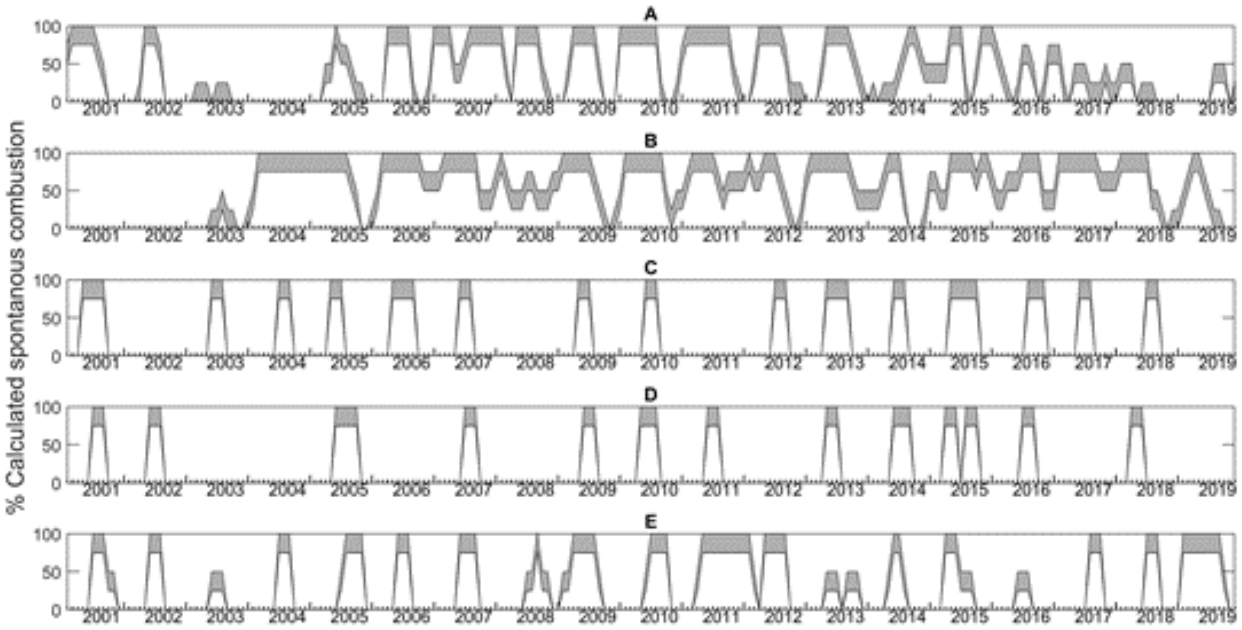


**Figure 4.3:** The calculated percentage ranges of spontaneous combustion events for the January 2001 to December 2019 for each of the five sites

In Table 4.1, the percentage of months with at least one active fire pixel is presented for each of the five mining sites considered. Site B was by far the most active, as on 86 % of all months there was at least one active fire within the area defined for this specific site, over the 19-year period. However, no fires were recorded during the years 2001 and 2002. Site A had the second highest percentage with 59 %. Thereafter, sites E, C and D had percentages of 22%, 9% and 7 %. Although smaller percentages were calculated for sites E, C and D, it is evident from Figure 4.2 that burning at these sites occurred for a few months continuously.

**Table 4.1:** Calculated percentage of months with at least one active fire pixel for each of the five mining sites considered

| Site | Percentage months with at least one burning pixel | Maximum number of active pixels per month |
|---|---|---|
| A | 59 % | 28 |
| B | 86 % | 83 |
| C | 9 % | 3 |
| D | 7 % | 3 |
| E | 22 % | 36 |

In Figure 4.4, the active fire counts for site A and B are presented in a monthly box plot. From the figure it is evident that there is a well-defined seasonal pattern in recorded burning activities, with burning more prevalent during the colder and drier months. Although this pattern largely coincides with the open biomass burning season in the South African Highveld (e.g. Maritz *et al.,* 2019), open biomass burning is unlikely the cause for significant increases in burning for the specific coal mining sites considered, as it is impossible for the same natural area (savannah/grassland) to burn multiple times in one month and for consecutive months. A possible cause for this observed seasonal variation could be the moisture content present in the coal. It has been found that the moisture content of coal could increase or decrease the probability for coal to self-heat and spontaneously combust (Bhat & Agarwal 1996; Xu *et al.,* 2013). If the coal is saturated with moisture, a negligible rate of oxidation occurs and self-heating of the coal is not possible (Bhat & Agarwal 1996). However, when the coal dries during the drier months, the condensation of moisture releases latent heat associated with vaporisation, which raises the heat of the coal particles and increases the potential for spontaneous combustion (Bhat & Agarwal 1996), and therefore the coal will be more likely to self-heat and spontaneously combust during the drier months as little to no rainfall will occur.

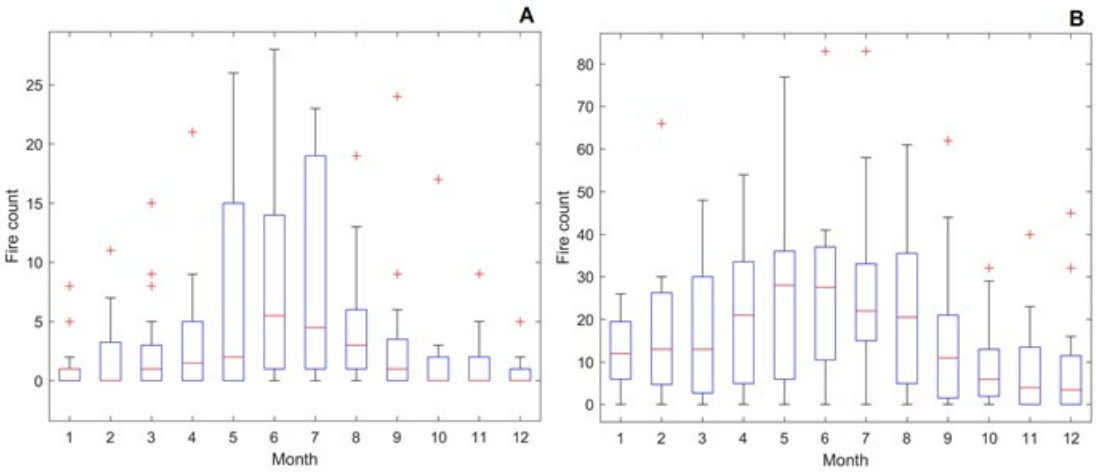


**Figure 4.4:** Box plots for coal mining sites A and B, which were the most prominent regarding spontaneous combustion of coal. The red line indicates the median, the top and bottom edges of the box the 25% and 75% percentiles and the black whiskers 1.5 times the interquartile range from the bottom or top of the box.

## 4.2 Case study of emissions originating from a spontaneous combustion event

Considering the extended time and repetitive nature of the spontaneous coal combustion fires considered in this paper, these events will emit substantial amounts of atmospheric pollutants. To illustrate this, a case study is presented of a plume originating from one such spontaneous combustion event, which was measured at the Elandsfontein measurement station in the Mpumalanga Highveld. In Figure 4.5, active fire pixels for the burning activity under investigation are presented. On 22 to 23 April 2009, a total of three fires were recorded within the blue circle in Figure 4.5; the blue circle is representative of the opencast coal mine used in this case study.

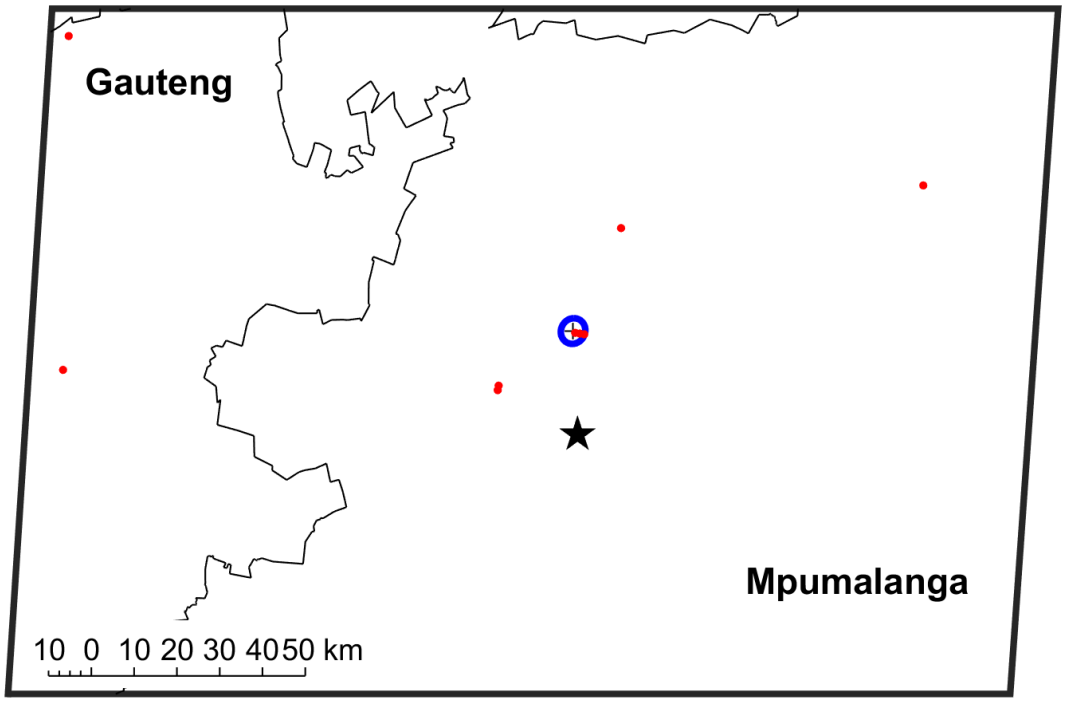


**Figure 4.5:** Active fire pixels (red dots) plotted from MODIS FRP data for the 22nd to the 23rd of April 2009. The blue circle represents an opencast coal mine, and the black star is the Elandsfontein station

In Figure 4.6, a HYSPLIT dispersion calculation (Stein *et al.,* 2015; Rolph *et al.,* 2017) is presented for mining site B on 23 April 2009. The model was set to run from 22 April at 23:00 for 24 hours with parameters displayed in Table 4.2.

**Table 4.2:** Parameters used for HYSPLIT dispersion calculation

| | |
|---|---|
| Pollutant | Unspecified |
| Release quantity | 1 mass unit |
| Release frequency | Continuous |
| Meteorology | GDAS1 |

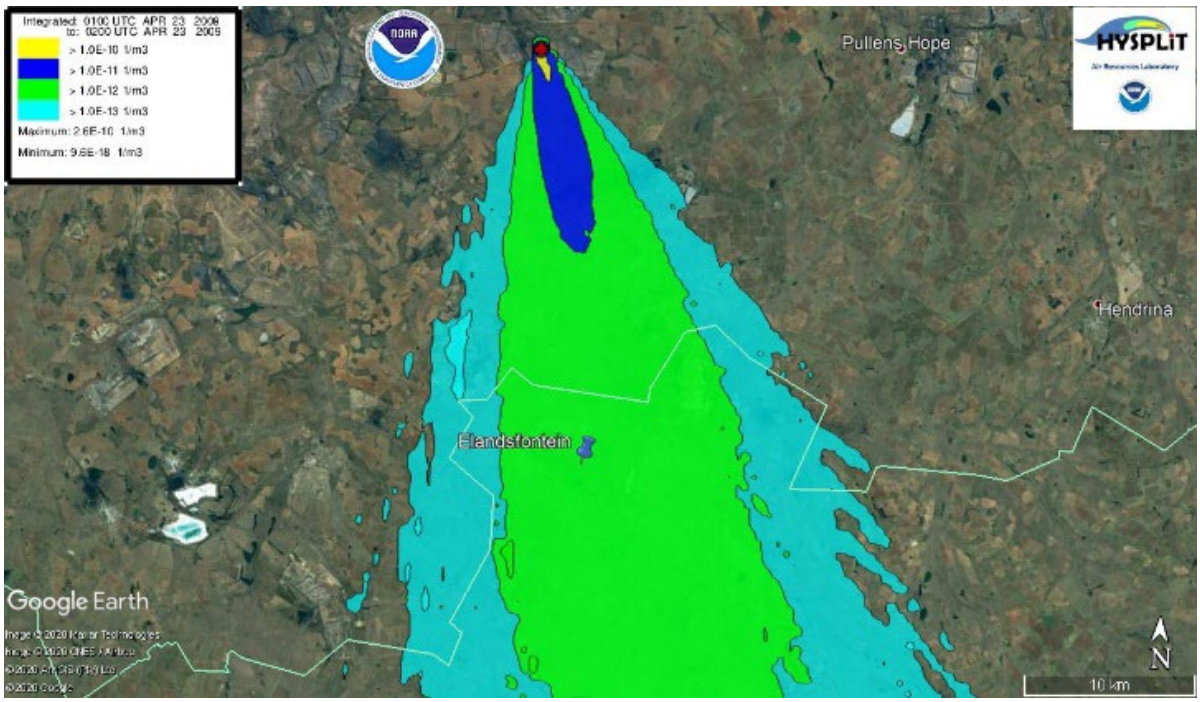


**Figure 4.6:** HYSPLIT dispersion calculation displayed on a Google Earth map for spontaneous combustion site B for the 23rd of April 2009 (01:00-02:00)

As is evident from the dispersion calculation in Figure 4.6, pollutants released by the case study spontaneous coal combustion event passed over the Elandsfontein atmospheric measurement site at 01:00 to 02:00. Figure 4.7 represents the hourly concentrations of trace gases (NO, $NO_2$, $SO_2$ and $H_2S$), as well as eBC measured on 23 April 2009. As is apparent, an increase in all species except NO is observed from 00:00, which reaches a peak at about 02:30 and decreases until 05:00. The increases in ambient trace gas and eBC concentrations are observed at the same time as the HYSPLIT dispersion calculations determined that the polluted air parcel from the spontaneous coal combustion source would reach the measurement station. Other peaks, after 05:00 in Figure 4.7, are also evident, but these are not discussed here. Considering Figures 4.5 to 4.7, it is clear that substantial amounts of $NO_2$, $SO_2$, $H_2S$ and eBC were released by the spontaneous coal combustion event, as $H_2S$ and $SO_2$ were in excess of 10 ppbv, approximately 23 km downwind of the source.

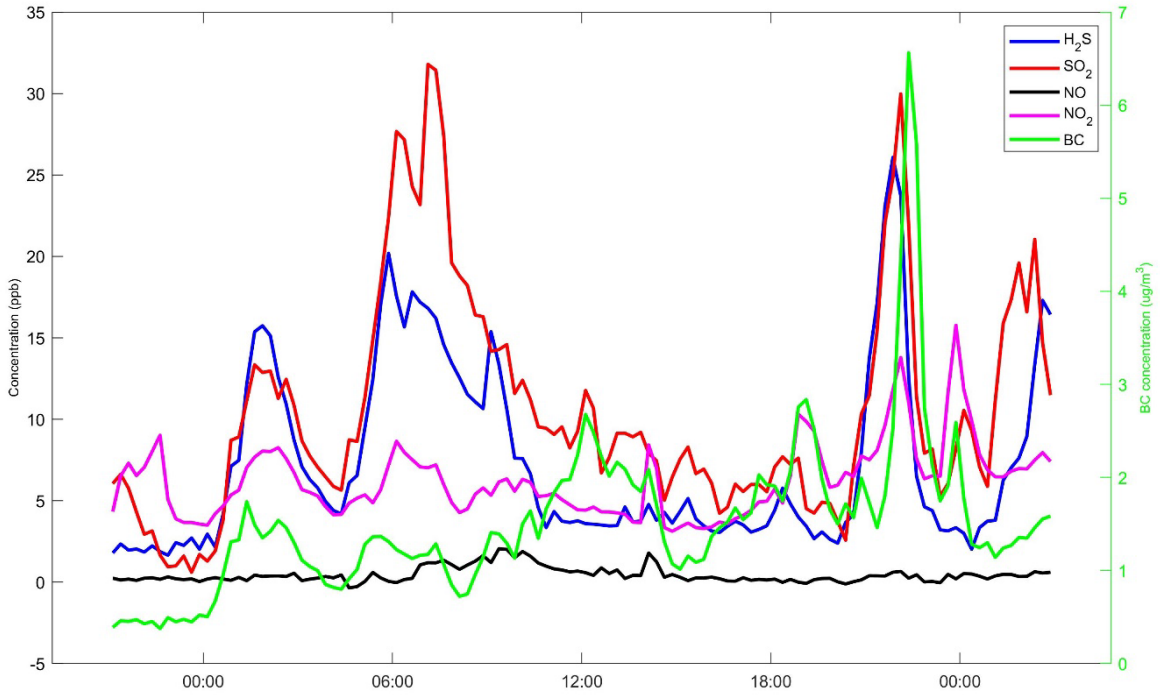


**Figure 4.7:** Hourly concentration of trace gases and eBC measured at the Elandsfontein measurement station on the 23rd of April 2009

## 4.3 Chapter 4: Conclusion

It is evident that spontaneous combustion of coal in the Mpumalanga Highveld can have a large environmental impact, especially on air quality. Through the use of FRP data it was found that five mining sites were prone to spontaneous combustions over a period of 19 years. These sites were all opencast mines, situated on top of old board-and-pillar mines. Of these five sites, two (A and B) were actively burning almost continually for the whole study period. A relatively well-defined seasonal pattern was observed for the spontaneous combustion activities, which could be attributed to the suppression of such events during the rainy season. A case study pollution plume originating from a spontaneous coal combustion event, captured at the Elandsfontein measurement site, recorded high concentrations of $NO_2$, $SO_2$, $H_2S$ and eBC originating from location B.

The FRP-based method we used here demonstrates that remote sensing observations can be utilised to determine when there is spontaneous coal combustion at a site and can be applied throughout the world if the locations of mining activities are known. Furthermore, it offers a way to incorporate the emissions in air quality models (see e.g. Sofiev *et al.,* 2009), once the emission factors have been quantified. However, the resolution of the MODIS instrumentation and frequency the satellite passes over (twice daily) an area might be limiting in detecting smaller combustion events. The method used here to determine when coal dumps were actively burning in the area is of great importance to the applied source apportionment method as it allows the user to determine whether spontaneous combustion of coal could have been a possible source for a plume under investigation.

# Chapter 5: Air quality in the rural Mpumalanga Highveld

**In this chapter**, the general meteorology at Elandsfontein is discussed in section 5.1, while section 5.2 presents the data coverage for the sampling period. Temporal patterns of all trace gaseous species relevant to this study ($H_2S$, $SO_2$, NO and $NO_2$) are presented in section 5.3, and the concentrations of these species are also contextualised. The temporal patterns and contextualisation of $H_2S$ presented in this chapter have been included in the research paper *Concentration contextualisation, temporal patterns and sources of hydrogen sulphide at a site on the South African Highveld* published in *Atmospheric Environment* (Cogho *et al.,* 2023). The main findings and conclusions of this chapter are presented in section 5.4.

## 5.1 General meteorology at the Elandsfontein site

Meteorological parameters measured at Elandsfontein are presented in Figures 5.1 (a-e), which include temperature, wind direction and -speed, relative humidity, global radiation and precipitation. As previously mentioned (section 2.2.1), this part of the South African interior is characterised by a distinct wet season in the warmer months, i.e. from mid-October to mid-May and a dry season from late autumn to mid-spring. Seasons can also be classified as spring (Sep, Oct and Nov), summer (Dec, Jan and Feb), autumn (Mar, Apr, May) and winter (Aug, Jun and Jul). These seasonal patterns are reflected in the meteorological patterns presented in Figure 5.1, with precipitation measurements at Elandsfontein, in particular, corresponding with the wet and dry seasons (Figure 5.1e). Annual rainfall in 2009 was below the annual rainfall average for this region, while rainfall depth in 2010 was similar than the annual rainfall average. The lowest temperatures were recorded in June and July, while lower relative humidity measurements coincided with the dry season. The lowest relative humidity determined in September could be attributed to higher temperatures compared to the other colder months during the dry season. Wind predominantly arrived from the northwestern and eastern sectors (as discussed in section 2.2.1), with wind speeds generally ranging between 2 and 10 m/s (Figure 5.1c). Diurnal patterns of global radiation were similar during all four seasons and peaked at midday as expected. Slightly higher global radiation levels were measured during spring, which can be attributed to the atmosphere being less saturated with water vapour resulting in decreased absorption of radiation.

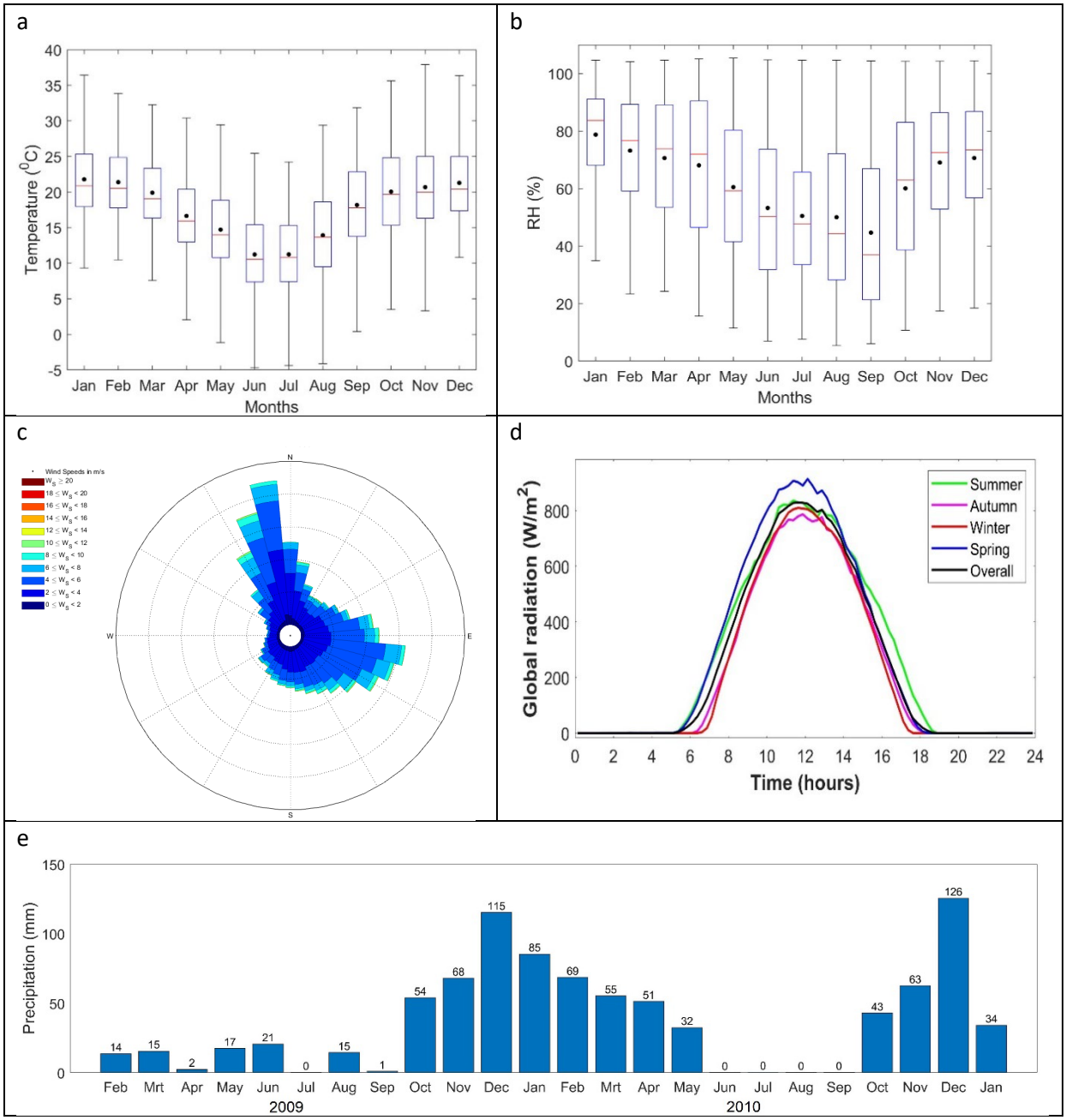


**Figure 5.1:** Meteorological parameters measured at Elandsfontein for Feb 2009 to Jan 2011, i.e. a) temperature, b) relative humidity, c) wind direction and -speed, d) global radiation, and e) monthly precipitation. The red line in the box-and-whisker plots indicates the median, the top and bottom edges of the box the 25% and 75% percentiles and the black whiskers 1.5 times the interquartile range from the bottom or top of the box.

## 5.2 Data coverage

The data coverages for $SO_2$, NO, $NO_2$ and $H_2S$ during the measurement period were 82%, 85%, 83% and 75%, respectively after data cleaning. Most of the data gaps were due to electrical power outages, since South Africa was in an energy crisis at the time (Pretorius *et al.,* 2015). Additionally, questionable and/or uncertain data points were removed to ensure a high-quality dataset, as per the previously published quality control procedures (Laakso *et al.,* 2012; Beukes *et al.,* 2015). Considering that most of the data gaps were associated

with power outages and that the dataset was subjected to thorough quality procedures, these data coverages for these atmospheric species can be considered relatively good. Additionally, gaps in data occurred throughout the entire measurement period and were not associated with specific periods, which therefore avoid seasonal bias.

## 5.3 Contextualisation and temporal patterns of gaseous species

### 5.3.1 $H_2S$

In Table 5.1, the mean and median, as well as 5$^{th}$, 25$^{th}$, 75$^{th}$ and 95$^{th}$ percentile $H_2S$ concentration values for the entire study period are presented. The mean $H_2S$ concentration of 3.1 ppbv was significantly higher than mean concentrations reported for background sites such as over the northern equatorial Atlantic Ocean and rural regions of France where mean $H_2S$ concentrations of 5 to 50 ppt (0.005 to 0.05 ppbv) and 0.055 ppbv were respectively recorded (Slatt *et al.,* 1978; Delmas *et al.,* 1980). The mean of 3.1 ppbv was similar to the mean concentration of 5.55 ppbv reported for the city of Thessaloniki, Greece (Kourtidis *et al.,* 2007), as well as to a residential area in Arkansas, USA in proximity of gas processing plants where mean concentrations of 2.4 and 3.4 ppbv were recorded for May to July and October to December 1998, respectively (Skrtic, 2006). However, the mean $H_2S$ concentration at Elandsfontein was significantly lower than the mean levels reported for heavily $H_2S$ polluted sites such as Whakarewarewa Village in the city of Rotorua in New Zealand for which a mean ranging between 66 to 100 ppbv was recorded (Hinz, 2011; Bates *et al.,* 2013), which was attributed to the proximity of an active geothermal field.

**Table 5.1** Mean and median, as well as the 5$^{th}$, 25$^{th}$, 75$^{th}$ and 95$^{th}$ percentile concentration values for $H_2S$ over the entire measurement period

| Description | Value (ppbv) |
|---|---|
| Mean | 3.1 |
| Median | 1.8 |
| 5$^{th}$ Percentile | 0.4 |
| 25$^{th}$ Percentile | 1.1 |
| 75$^{th}$ Percentile | 3.2 |
| 95$^{th}$ Percentile | 11.1 |

Currently there is no South African National Ambient Air Quality Standard (NAAQS) limit value for ambient $H_2S$. However, the South African Department of Environmental Affairs (DEA) stipulates that if a one-hourly average $H_2S$ concentration exceeds 29 ppbv on any specific day, this day is regarded as a high $H_2S$ day (DEA, 2009). The calculated hourly average $H_2S$ levels exceeded this 29 ppbv "standard limit" 47 times on 13 days. In Table 5.2, the timestamp, concentration and potential source associated with each of these exceedances are presented. The potential sources in Table 5.2 have been determined through back-trajectory analysis and

are only potential sources based on this. Therefore, 13 "high $H_2S$ days" were recorded at Elandsfontein during the two-year measurement period. Considering the average $SO_2$ concentration of 11.5 ppbv (section 5.2.2) determined at Elandsfontein (Laakso *et al.,* 2012), it appears that > 20% of gas phase sulphur is in the form of $H_2S$, as the mean $H_2S$ concentration was measured at 3.1 ppbv.

**Table 5.2:** Hourly exceedances of 29 ppbv $H_2S$ high day threshold value and the respective sources.

| Date and Time | Source | Hourly average concentration (ppbv) | Date and Time | Source | Hourly average concentration (ppbv) |
|---|---|---|---|---|---|
| 2009/04/18 03:00 | Urban | 34.9 | 2009/09/18 11:00 | Jhb/Pta | 48.6 |
| 2009/04/24 06:00 | Pyrometallurgical smelter | 36.7 | 2009/12/18 05:00 | Jhb/Pta | 46.8 |
| 2009/04/24 07:00 | Pyrometallurgical smelter | 30.9 | 2009/12/23 02:00 | Coal Dump | 36. |
| 2009/04/24 08:00 | Pyrometallurgical smelter | 33.3 | 2009/12/23 03:00 | Coal Dump | 30.3 |
| 2009/04/25 02:00 | Pyrometallurgical smelter | 31.8 | 2010/05/24 03:00 | Urban | 33.4 |
| 2009/05/16 05:00 | Coal-fired Power station | 31.3 | 2010/05/24 15:00 | Petrochemical | 32.0 |
| 2009/05/19 14:00 | Coal-fired Power station | 34.9 | 2010/05/24 16:00 | Petrochemical | 42.3 |
| 2009/05/19 15:00 | Coal-fired Powerstation | 33.9 | 2010/05/24 17:00 | Petrochemical | 38.6 |
| 2009/06/01 10:00 | Petrochemical | 66.7 | 2010/06/05 15:00 | Petrochemical | 52.3 |
| 2009/06/01 11:00 | Petrochemical | 68.2 | 2010/06/05 16:00 | Petrochemical | 60.8 |
| 2009/06/01 12:00 | Petrochemical | 52.1 | 2010/06/05 17:00 | Petrochemical | 44.7 |
| 2009/06/01 13:00 | Petrochemical | 39.8 | 2010/06/05 18:00 | Petrochemical | 32.2 |
| 2009/06/03 01:00 | Jhb/Pta | 34.4 | 2010/06/06 16:00 | Urban | 33. |
| 2009/06/28 10:00 | Petrochemical | 37.4 | 2010/06/06 17:00 | Urban | 33.6 |
| 2009/06/28 11:00 | Petrochemical | 74.6 | 2010/06/08 06:00 | Urban | 71.6 |
| 2009/06/28 14:00 | Petrochemical | 41.0 | 2010/06/21 21:00 | Combination | 30.8 |
| 2009/06/28 15:00 | Petrochemical | 32.2 | 2010/06/21 22:00 | Combination | 31.3 |
| 2009/07/02 02:00 | Coal dump | 29.8 | 2010/06/23 01:00 | Jhb/Pta | 36.4 |
| 2009/07/03 03:00 | Coal dump | 38.7 | 2010/06/23 04:00 | Jhb/Pta | 33.5 |
| 2009/07/09 13:00 | Petrochemical | 29.5 | 2010/07/16 10:00 | Petrochemical | 30.0 |
| 2009/07/10 20:00 | Urban | 37.4 | 2010/08/14 12:00 | Petrochemical | 32.8 |
| 2009/07/12 00:00 | Urban | 42.0 | 2010/09/27 10:00 | Urban | 31.4 |
| 2009/08/20 10:00 | Petrochemical | 42.1 | 2010/11/20 11:00 | Jhb/Pta | 53.5 |

| Date and Time | Source | Hourly average concentration (ppbv) | Date and Time | Source | Hourly average concentration (ppbv) |
|---|---|---|---|---|---|
| 2009/09/15 23:00 | Urban | 32.4 | | | |

Statistical distribution of monthly $H_2S$ concentrations measured at Elandsfontein are presented in Figure 5.2 It is evident from Figure 5.2 that $H_2S$ concentrations were generally higher in the colder (May to August) and/or dryer (May to mid-October) months, and lower in the wetter (mid-October to April) and/or warmer (September to April) months (seasonal classification according to Venter *et al.,* 2020). This could be that low-level emission sources likely make a significant contribution to ambient $H_2S$ measured at Elandsfontein, since these emissions are trapped and concentrated by low-level thermal inversion layers and/or a shallow PBL depth. Such conditions are particularly common over the South African Highveld during night-time and early mornings during the colder months (Garstang *et al.,* 1996; Korhonen *et al.,* 2014; Gierens *et al.,* 2018), which reduce vertical mixing in the troposphere.

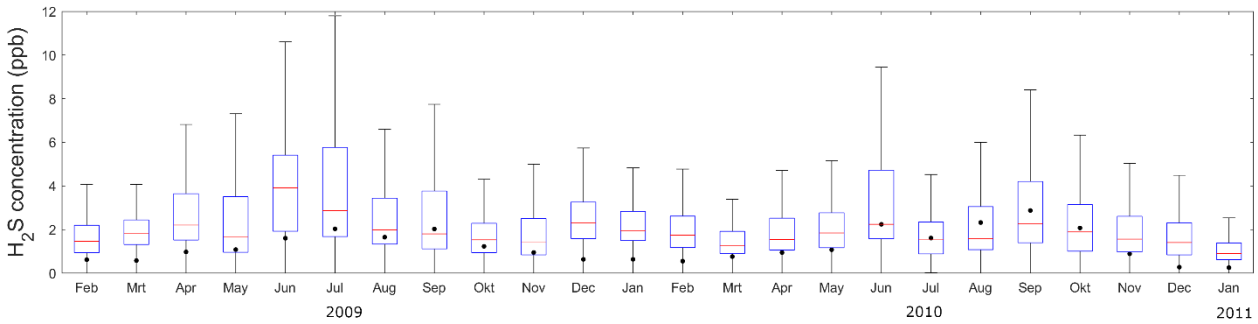


**Figure 5.2:** Box-and-whisker plots of the measured $H_2S$ concentrations for each month during the study period. The red line represents the median, the black dot the mean, the box the 25$^{th}$ and 75$^{th}$ percentiles and the whiskers are equal to 1.5 times the interquartile range.

In Figure 5.3, the overall diurnal pattern (for the entire measurement period), as well as diurnal patterns for the different seasons are depicted. It is evident that $H_2S$ concentrations were highest in winter (red line), which agrees with the seasonal analysis considered in Figure 5.2. In general, the diurnal patterns are characterised by bimodal peaks, occurring in the early morning (between approximately 04:00 and 08:00) and evening (after approximately 19:00), which also correspond with low-level emissions being trapped by a low-level inversion layer(s) and/or a shallow PBL depth (Garstang *et al.,* 1996; Korhonen et al., 2014; Gierens *et al.,* 2018). Additionally, lower $O_3$ and hydroxyl radical ($OH^{\bullet}$) concentrations during night-time (Laban *et al.,* 2018; Gierens *et al.,* 2014), with associated less oxidation of $H_2S$, could contribute to the higher $H_2S$ levels during night-time. An $H_2S$ peak is also observed between 9:00 and 13:00 in all the diurnal patterns, which is indicative of downward mixing of high stack emissions after the break-up of the aforementioned inversion layer(s) and growth of the PBL (Garstang *et al.,* 1996; Korhonen *et al.,* 2014; Gierens *et al.,* 2018). This peak is particularly prominent in winter due to more frequent and pronounced thermal inversion layers, as well as

a lower PBL depth over the South African Highveld during this time of the year (Garstang *et al.,* 1996; Korhonen *et al.,* 2014; Gierens *et al.,* 2018).

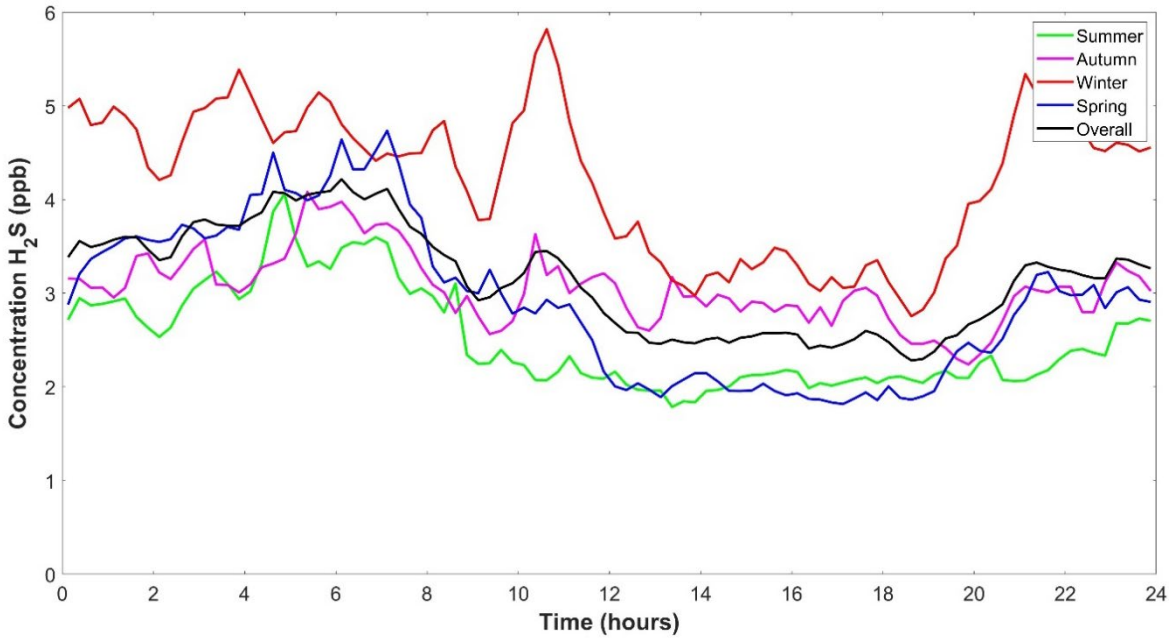


**Figure 5.3:** Diurnal patterns based on average 15 min data of $H_2S$ for the entire measurement period, as well as separate average patterns for each season (Summer = December, January and February; Autumn = March, April and May; Winter = June, July and August; Spring = September, October and November).

Although an in-depth source apportionment of $H_2S$ (and other gaseous species) was conducted with the novel method developed in this study (section 3.6) and presented in the subsequent chapter, potentials sources of $H_2S$ (and other gaseous species) were explored by compiling pollution and frequency roses. In Figure 5.4, pollution and frequency roses are presented for hourly $H_2S$ concentrations exceeding the annual mean (3.1 ppbv) and 95$^{th}$ percentile (11.1 ppbv) levels. The frequency plot was compiled by dividing the number of wind directions associated with these higher $H_2S$ concentrations with the wind directions measured during the entire sampling period, i.e. wind rose presented in Fig. 5.1 (c). It is evident from the pollution rose that $H_sS$ levels exceeding 3.1 ppbv corresponded mostly with winds from the northwest to northeastern sector with the highest $H_2S$ concentrations (95$^{th}$ percentile) associated with winds from the north-north-west to north-north-eastern sector from Elandsfontein. On the other hand, in Figure 5.4 it is observed that high $H_2S$ concentrations are approximately as frequent in both the north and southwest directions. These higher $H_2S$ concentrations associated with northerly winds are somewhat unexpected, since the main sources of atmospheric pollutants in this region are high-stack emissions from coal-fired power plants, which are not typically associated with $H_2S$ since the boiler ovens burn too hot to produce $H_2S$. There are, however, other potential sources of atmospheric $H_2S$ in this region, e.g. pyrometallurgical smelters. A possible source of atmospheric $H_2S$ in the southwestern region is a petrochemical plant located in this area. As mentioned above, comprehensive source apportionment will be conducted in Chapter 6.

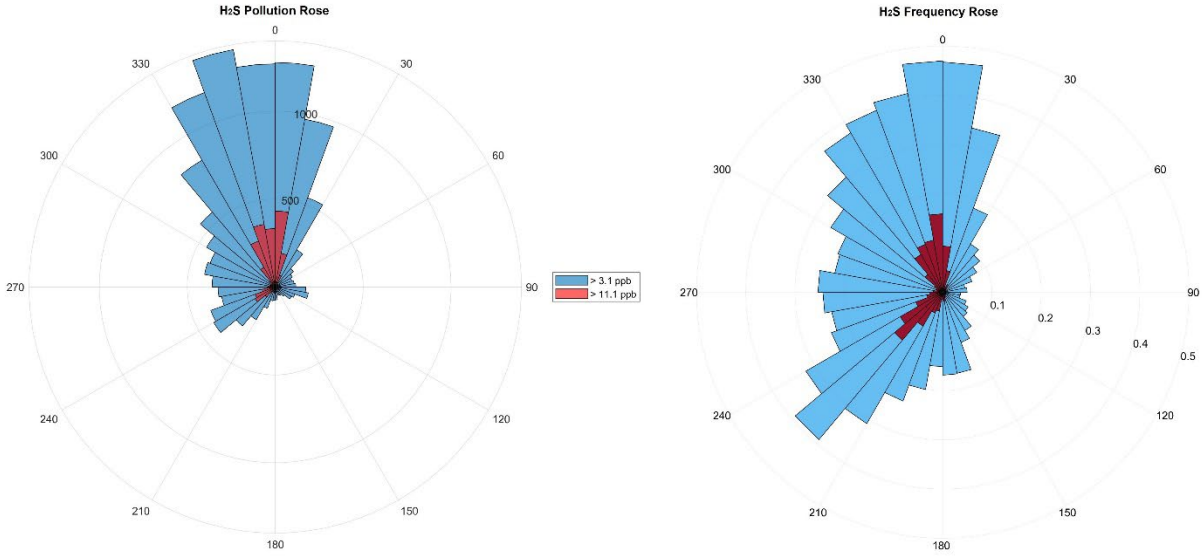


**Figure 5.4:** Pollution (left) and frequency roses (right) associated with $H_2S$ concentrations (15-min averages) measured at Elandsfontein. Indicated in blue are wind directions corresponding with $H_2S$ concentrations exceeding 3.1 ppbv (annual mean concentration), while red represents wind directions associated with $H_2S$ levels exceeding the 95$^{th}$ percentile (11.1 ppbv).

### 5.3.2 $SO_2$

In Table 5.3, the mean and median, as well as 5$^{th}$, 25$^{th}$, 75$^{th}$ and 95$^{th}$ percentiles of $SO_2$ concentration values for the entire study period are presented. Over the two-year period, $SO_2$ had an hourly mean concentration of 11.5 ppbv, which is significantly higher than the average $SO_2$ concentration of 1.77 ppbv determined at a regional site in the South African interior (Welgegund) from and a regional background site (Shangdianzi station) in Northern China (2.2 ppbv) (Meng *et al.,* 2009). This is also higher than the concentration measured at Marikana in South Africa by Venter *et al.* (2012), where an average of 3.8 ppbv was measured. However, the $SO_2$ levels were similar to $SO_2$ concentrations measured at throughout ground-based measurement stations in China of 8.8 ppbv (Wei *et al.,* 2023). The value of 11.5 ppbv is comparable to yearly averages for monitoring stations in the Highveld area from 2008 to 2013, where annual averages between 8.31 ppbv and 12.38 were measured (Sangeetha & Sivakumar, 2019). Feig *et al*. (2019) found a similar annual mean concentration in Ermelo with 10.7 ppbv in 2016. However, the 2014 annual average $SO_2$ concentration in Witbank was 19.3 ppbv, which is significantly higher than the value at Elandsfontein (Feig *et al*., 2019).

**Table 5.3** Mean and median, as well as the 5th, 25th, 75th and 95th percentile concentration values for $SO_2$ over the entire measurement period

| Description | Value (ppbv) |
|---|---|
| Mean | 11.5 |
| Median | 7.4 |
| 5th Percentile | 1.2 |
| 25th Percentile | 4.1 |
| 75th Percentile | 13.3 |
| 95th Percentile | 36 |

In Table 5.4, the South African NAAQS (DEA, 2009) limit values and the European air quality standards for atmospheric $SO_2$ are listed and compared with data collected at Elandsfontein. The number of times these standard limits were exceeded per year during the sampling period are also indicated. $SO_2$ had a mean 10-min average concentration of 3.8 ppbv during the sampling period with a maximum $SO_2$ 10-min concentration of 213 ppbv determined during the sampling period. The South African 10-min standard (191 ppbv) was exceeded twice per year, which is much lower than the 526 tolerable exceedances. The 1-h average concentration for $SO_2$ at Elandsfontein had a maximum level of 158 ppbv. This 1-h South African and European standard of 134 ppbv was exceeded six times, which was well below the respective 88 and 24 tolerable exceedances allowed. The maximum 24-h average concentration of 11.34 ppbv was below the South African and European 24-h standard of 48 ppbv, while the mean annual concentration of 3.8 ppbv was also well below the South African standard limit of 19 ppbv. Therefore, although the average ambient $SO_2$ concentration was significantly higher than recorded averages at background sites in South Africa and China, $SO_2$ concentrations did not exceed standard limit values like in Witbank, where Feig *et al*. (2019) found that Witbank exceeded the one-year average NAAQS value, with an average value of 19.3 ppbv in 2014. Furthermore, Adesina *et al*. (2022) found that SO2 in the HPA exceeded the 24-hour NAAQS and WHO standards 45 times from March 2007 to February 2018.

**Table 5.4** Comparison of $SO_2$ and $NO_2$ data collected at Elandsfontein with South African NAAQS limits and the European air quality standards

| Pollutant | Averaging Period | Air quality standards | | | | Observed | |
|---|---|---|---|---|---|---|---|
| | | South African standards | | European standards | | Exceedances per year | |
| | | Concentration ppbv (µg/m³) | Number of tolerable exceedances per year | Concentration ppbv (µg/m³) | Number of tolerable exceedances per year | South African standards | European standards |
| $SO_2$ | 10 minutes | 191 (500) | 526 | n/a | n/a | 2 | 2 |
| | 1 hour | 134 (350) | 88 | 134 (350) | 24 | 6 | 6 |
| | 24 hours | 48 (125) | 4 | 48 (125) | 3 | 0 | 0 |
| | 1 year | 19 (50) | 0 | n/a | n/a | 0 | 0 |
| $NO_2$ | 1 hour | 106 (200) | 88 | 106 (200) | 18 | 8 | 8 |
| | 1 year | 21 (40) | 0 | 21 (40) | n/a | 0 | 0 |

Statistical distributions of monthly $SO_2$ concentrations measured at Elandsfontein are presented in Figure 5.5. It is evident that ambient $SO_2$ concentrations also peaked during the colder and/or dryer months, which is typical for this part of South Africa. This seasonal pattern is attributed to more pronounced low-level inversion layers trapping these species near the surface that, together with decreased rainfall, result in pollutant build-up (e.g. Swartz *et al.,* 2020). In addition, depending on the type of fuel, increased domestic burning for space heating during winter can also contribute to increased $SO_2$ (Adesina *et al*., 2022). However, the predominant source of $SO_2$ in the north-eastern interior is high-stack emissions associated with industrial activities, e.g. coal-fired power stations and pyrometallurgical activities, which will be further explored in Chapter 6.

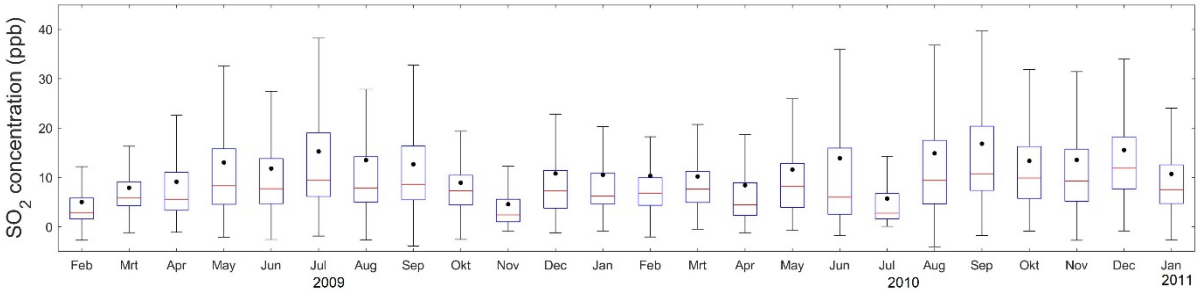


**Figure 5.5:** Box and whisker plots of the measured $SO_2$ concentrations for each month during the study period. The red line represents the median, the black dot the mean, the box the 25$^{th}$ and 75$^{th}$ percentiles and the whiskers are equal to 1.5 times the interquartile range.

The overall and seasonal diurnal patterns for $SO_2$ are presented in Figure 5.6, which also reflect higher $SO_2$ concentrations during the colder and dryer months, i.e. winter and spring, as indicated by the seasonal analysis (Figure 5.5). $SO_2$ diurnal patterns exhibit a single peak with $SO_2$ increasing just after 08:00 and reaching a maximum between 10:00 and 12:00, depending on the season. This single, relatively late morning $SO_2$ peak corresponds with the break-up of inversion layers and an increase in PBL height, which is indicative of high-stack emissions mixing downwards after the break-up of the lowest inversion layer (Garstang *et al.,* 1996; Korhonen *et al.,* 2014; Gierens *et al.,* 2018). A similar diurnal $SO_2$ peak was observed by Sangeetha and Sivakumar (2019) for the Mpumalanga power stations group in their study. Therefore, as mentioned above, high-stack emissions can be considered the main source of $SO_2$ measured at Elandsfontein. The influence of high-stack emissions on $SO_2$ concentrations at Elandsfontein is also substantiated by the $SO_2$ peak in winter occurring later than the other seasons, which is ascribed to more frequent and persistent inversion layers during winter, as well as lower PBL depth (Garstang *et al.,* 1996; Korhonen *et al.,* 2014; Gierens *et al.,* 2018). A similar diurnal pattern was observed at site in the highly industrialised and densely populates western Bushveld Complex, where high-stack emissions associated with pyrometallurgical smelters were considered the major sources of atmospheric $SO_2$ (Venter *et al.,* 2012). However, also evident in Figure 5.6, are small bimodal peaks during night-time and early mornings in winter and spring, which can be attributed to the influence of low-level emissions, e.g. increased

household combustion during winter. Similar bi-modal peaks were observed in the HPA during March 2017 to February 2018 (Adesina *et al.*, 2022).

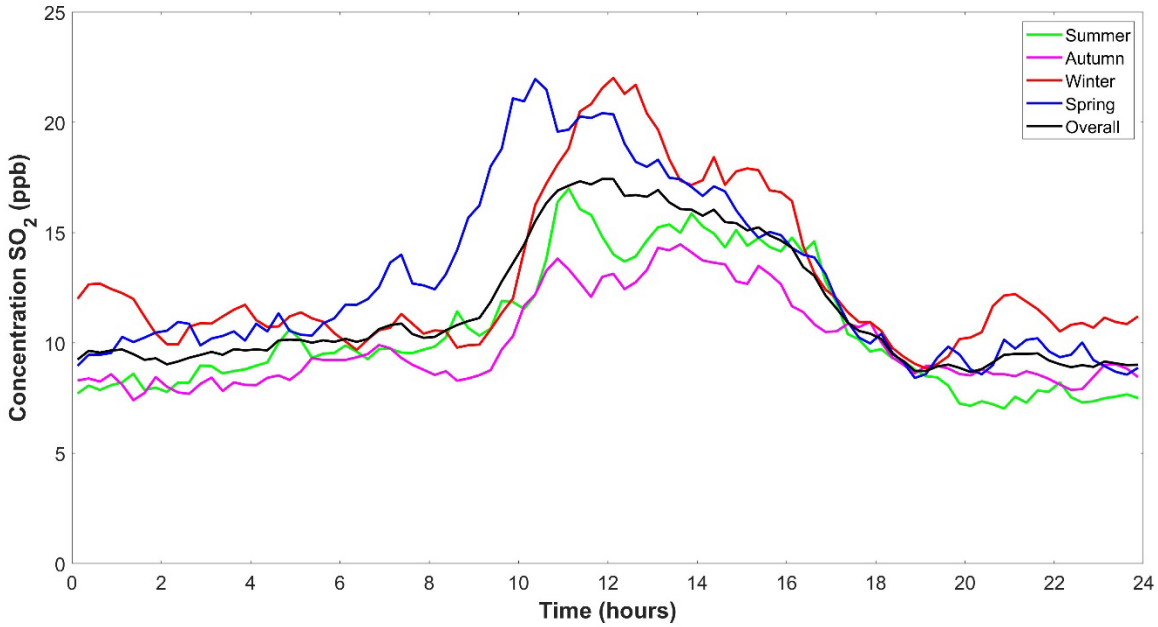


**Figure 5.6:** Diurnal patterns based on average 15 min data of $SO_2$ for the entire measurement period, as well as separate average patterns for each season (Summer = December, January and February; Autumn = March, April and May; Winter = June, July and August; Spring = September, October and November).

Possible sources of $SO_2$ at Elandsfontein were also explored through pollution and frequency roses compiled for $SO_2$ levels higher than the annual mean of 11.5 ppbv and the 95$^{th}$ percentile of 36 ppbv, which are presented in Figure 5.7. Higher $SO_2$ concentrations were associated with winds predominantly from the west to north-north-eastern sector. However, $SO_2$ levels exceeding the annual mean were from a larger fetch region (west-south-west to east-south-east) according to these plots. As mentioned previously and indicated by the diurnal $SO_2$ concentration patterns (Figure 5.6), the main sources $SO_2$ in this region are considered to be high-stack emissions. In-depth source apportionment analysis of $SO_2$ was also conducted with the novel technique developed in this study and presented in Chapter 6.

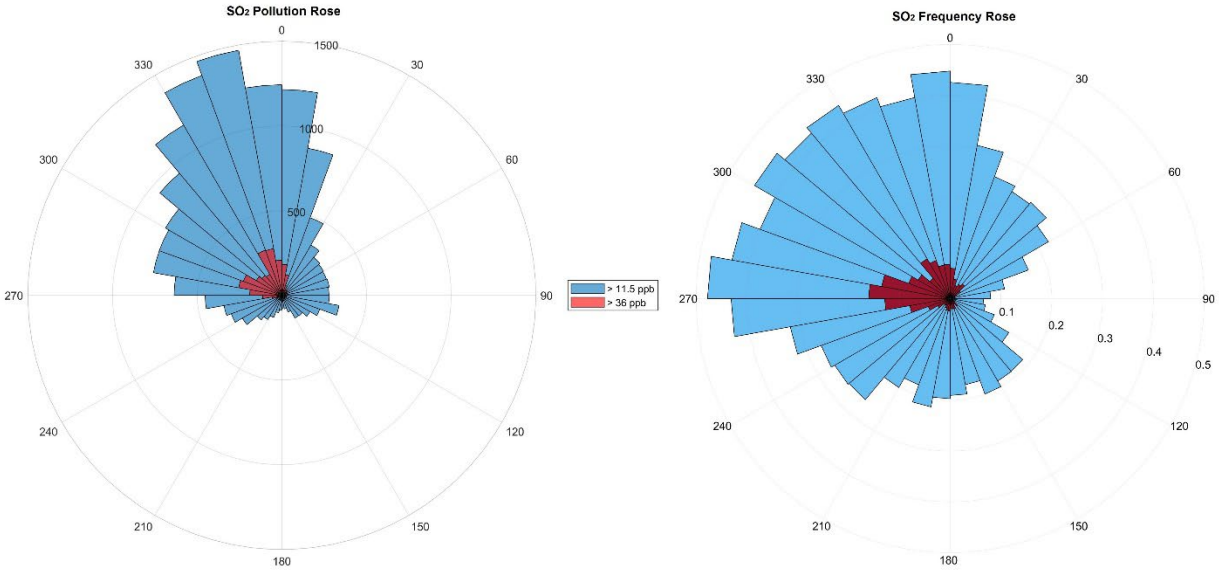


**Figure 5.7:** Pollution (left) and frequency roses (right) associated with $SO_2$ concentrations (15-min averages) measured at Elandsfontein. Indicated in blue are wind directions corresponding with $SO_2$ concentrations exceeding 11.5 ppbv (annual mean concentration), while red represents wind directions associated with $SO_2$ levels exceeding the 95$^{th}$ percentile (36 ppbv).

### 5.3.3 NO

Although NO is not considered a criteria pollutant from a legislative perspective, it is an important precursor for atmospheric $NO_2$ and also plays a role in tropospheric $O_3$ chemistry. Furthermore, NO is usually associated with fresher pollution plumes. The mean and median, as well as 5$^{th}$, 25$^{th}$, 75$^{th}$ and 95$^{th}$ percentile NO concentrations determined during the sampling period are presented in Table 5.5. The 2.7 ppbv mean average concentrations determined for NO during the sampling period were lower than NO concentrations measured in a recent study in nine cities in the Jilin province in China from 2016 to 2018 (Wang *et al*., 2020). In the study of Wang *et al.* (2020), NO concentrations ranged between 3.6 and 14.96 ppbv with higher NO concentrations associated with coal-fired power station and densely populated regions. Furthermore, Venter *et al*. (2021) found NO concentrations at the Sasol Secunda monitoring station networks for January to June 2020 to be between ~ 1 ppbv and ~ 24 ppbv, which was done as part of a study to determine how ambient air quality was affected during the COVID-19 lockdown period. Similarly, Collett *et al*. (2010) observed NO monthly mean concentrations at the Elandsfontein measurement station ranging from ~ 1 ppbv to ~5.7 ppbv, which is similar to what was observed at Elandsfontein during this study.

**Table 5.5** Mean and median, as well as the 5th, 25th, 75th and 95th percentile concentration values for NO over the entire measurement period

| Description | Value (ppbv) |
|---|---|
| Mean | 2.7 |
| Median | 0.8 |
| 5th Percentile | 0.2 |
| 25th Percentile | 0.4 |
| 75th Percentile | 1.8 |
| 95th Percentile | 9.9 |

In Figure 5.8, the monthly statistical distribution of NO concentrations measured at Elandsfontein are presented, while the overall and seasonal diurnal patterns for NO are presented in Figure 5.9. Although monthly variability is evident in Figure 5.8, no distinct seasonal pattern is evident. However, it seems that higher NO levels were determined in June, July, October and November. Collet *et al*. (2010) observed a similar trend at Elandsfontein, with NO concentration peaking during the winter, however the high NO concentrations in spring were not observed. Increased NO concentrations in the spring months (October and November) can be attributed to the onset of the rain season, while elevated NO levels in the dry winter months (June and July) can be ascribed to pollutant build-up and increased household combustion for space heating. Since NO is associated with fresher plumes, sources of these species would most likely be within proximity of Elandsfontein. The box-and-whisker plot for NO also indicates no distinct seasonal pattern with slightly higher NO concentrations determined during winter as similarly observed by Collett *et al*. (2010). The NO diurnal trends also have a single peak, i.e. NO concentrations increasing after 06:00 and, similar to $SO_2$, peaking between 10:00 and 12:00 for the different seasons. This same observation was seen previously for the Elandsfontein monitoring station (Collett *et al*., 2010). Therefore, it also seems that high-stack emissions mixing downwards with the break-up of inversion layers and elevation of the PBL are the major source of NO measured at Elandsfontein. In addition, no early morning and late afternoon/evening peaks are evident, which indicates that low-level emissions (e.g. household combustion) are not a significant source of NO measured at this site. Further evidence for high-stack emissions being the major NO source, is NO levels peaking later in winter compared to the other seasons (as also seen for $SO_2$).

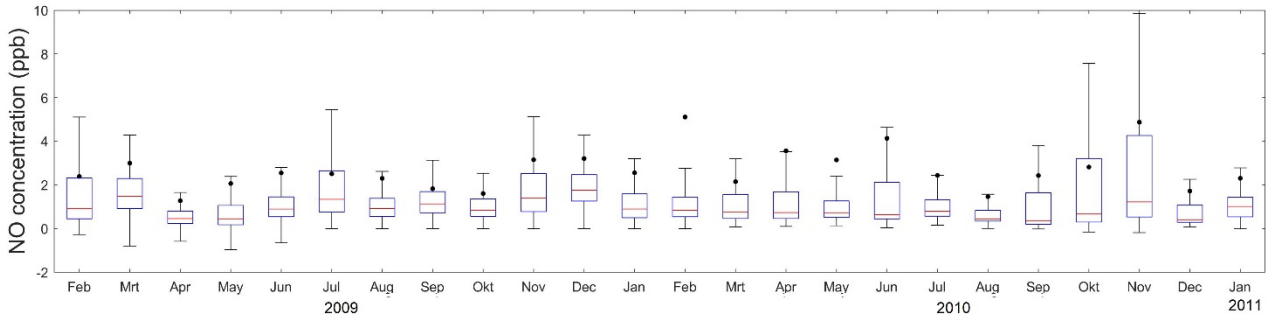


**Figure 5.8:** Box and whisker plots of the measured NO concentrations for each month during the study period. The red line represents the median, the black dot the mean, the box the 25$^{th}$ and 75$^{th}$ percentiles and the whiskers are equal to 1.5 times the interquartile range.

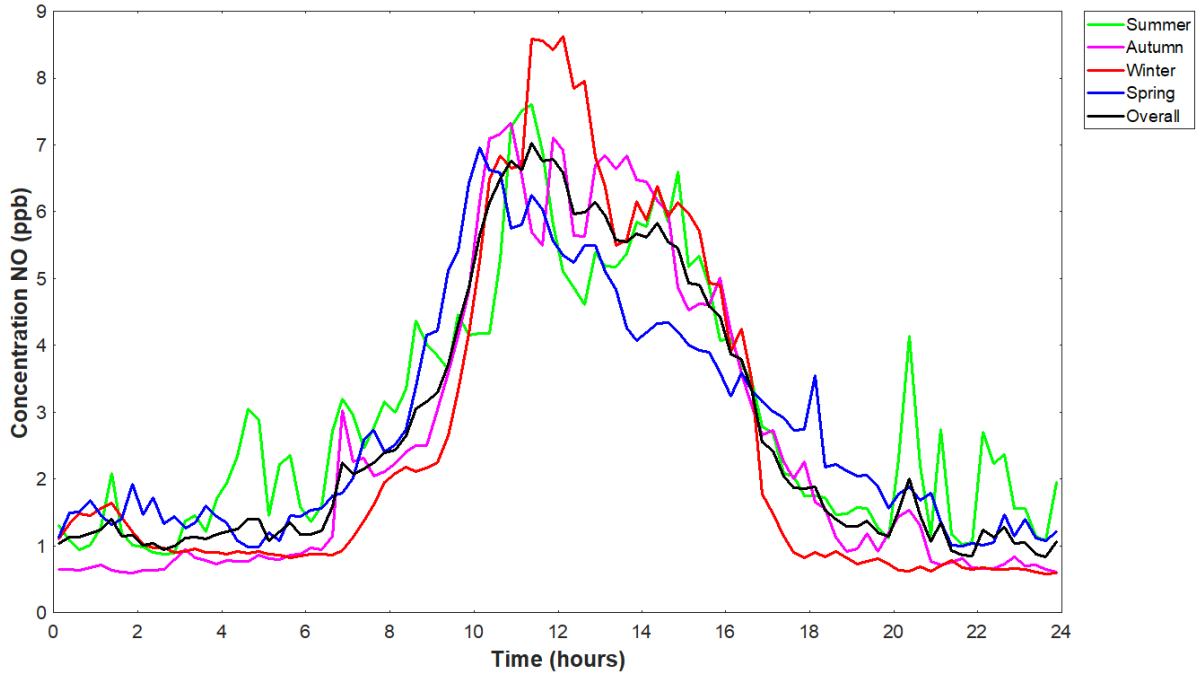


**Figure 5.9:** Diurnal patterns based on average 15 min data of NO for the entire measurement period, as well as separate average patterns for each season (Summer = December, January and February; Autumn = March, April and May; Winter = June, July and August; Spring = September, October and November).

Pollution and frequency roses were also compiled for winds associated with NO levels higher than the annual mean (2.7 ppbv) and the 95$^{th}$ percentile (9.9 ppbv), which are presented in Figure 5.10. NO levels exceeding the annual mean and the 95$^{th}$ percentile were generally related to winds from the west to northern sector. However, with the exception of southerly winds, increased NO concentrations corresponded with most of the wind directions, which is indicative of several possible sources in this region with high-stack emissions associated with coal-fired power stations being the predominant source (as indicated by the temporal patterns).

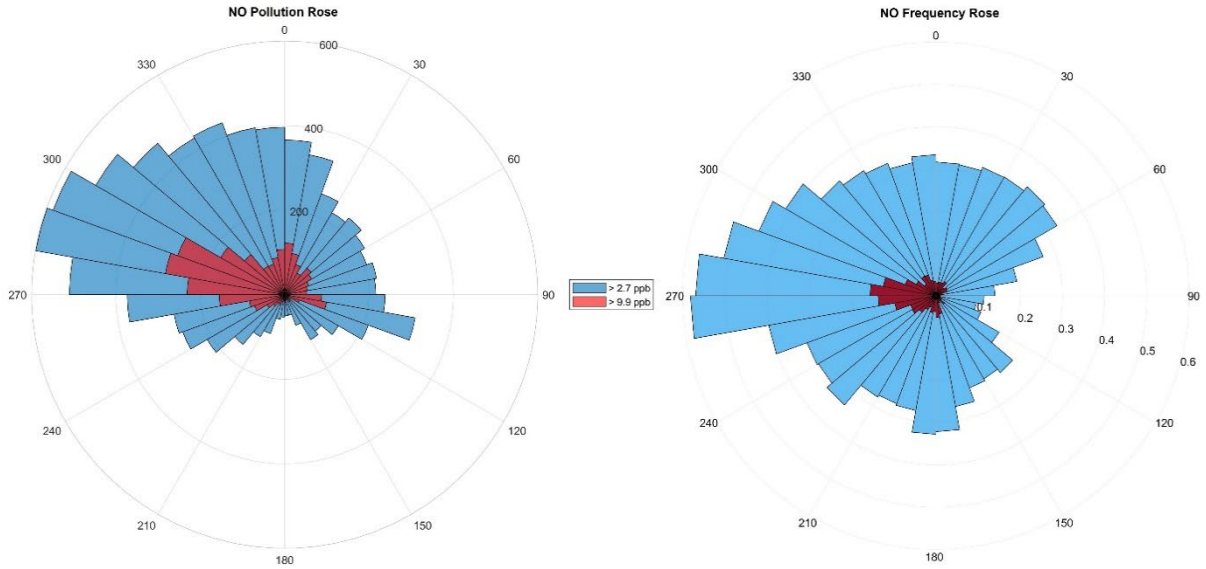


**Figure 5.10:** Pollution (left) and frequency roses (right) associated with NO concentrations (15-min averages) measured at Elandsfontein. Indicated in blue are wind directions corresponding with $SO_2$ concentrations exceeding 2.7 ppbv (annual mean concentration), while red represents wind directions associated with $SO_2$ levels exceeding the 95$^{th}$ percentile (9.9 ppbv).

### 5.3.4 $NO_2$

Similarly, for the other gaseous species, the mean and median, as well as 5$^{th}$, 25$^{th}$, 75$^{th}$ and 95$^{th}$ percentiles were calculated for $NO_2$ concentrations measured at Elandsfontein for the entire sampling period and are presented in Table 5.6. The mean ambient concentration of $NO_2$ was calculated to be 12.5 ppbv for the two-year study period. In addition, the mean $NO_2$ concentration at Elandsfontein was also higher than the average $NO_2$ level of 8.5 ppbv reported for a site located in the industrialised and densely populated western Bushveld Complex in South Africa (Venter *et al.,* 2012). The mean of 12.5 ppbv is also higher than the annual mean measured in the South African industrial Highveld of 7.4 ppbv from March 2017 to February 2018 (Adesina *et al*., 2022). Furthermore, Collett *et al*. (2010) recorded a monthly high $NO_2$ concentration of ~4.2 ppbv from April 2005 to March 2006. It is evident from this that $NO_2$ emissions have increased at Elandsfontein at least. However, $NO_2$ levels at Elandsfontein were approximately two times lower than $NO_2$ concentrations measured at 323 sites of the 1485 sites where $NO_2$ was measured during the European Study of Cohorts for Air Pollution Effect (ESCAPE) (Cyrys *et al.,* 2012). In ESCAPE, the annual average $NO_2$ concentration at these 323 sites were in the order of or higher than 20 ppbv.

**Table 5.6** Mean and median, as well as the 5th, 25th, 75th and 95th percentile concentration values for $NO_2$ over the entire measurement period

| Description | Value (ppbv) |
|---|---|
| Mean | 12.5 |
| Median | 8.6 |
| 5th Percentile | 1.8 |
| 25th Percentile | 4.7 |
| 75th Percentile | 15.4 |
| 95th Percentile | 36.8 |

Also listed in Table 5.4 are the South African NAAQS (DEA, 2009) limit values and the European air quality standards for atmospheric $NO_2$, which are related to $NO_2$ measured in this study. According to these legislations, a 1-h standard (106 ppbv) and an annual standard (21 ppbv) are imposed for $NO_2$ ambient concentrations. The number of annual exceedances of these standard limits during the two-year sampling period is also presented. The mean 1-h average for the entire sampling period was 12.4 ppbv, with a maximum of 228.7 ppbv. The 1-hour standard limit was exceeded eight times throughout the study, which is substantially lower than 88 allowed number of exceedances. Adesina *et al*. (2022) recorded zero exceedances of the NAAQS and WHO standard for $NO_2$ from March 2017 to February 2018. Furthermore, a CLAPUFF dispersion model was used to estimate pollutant concentrations over the HPA based on emissions from 14 different sources in 2016 including the coal-fired power stations and Sasol refinery, where it was seen that both the 1-hour average and annual NAAQS limits were not exceeded in the model (Gray, 2019). This shows that although the HPA is considered an $NO_2$ hotspot, the $NO_2$ levels rarely exceed the NAAQS and WHO standard limits.

In Figure 5.11, box-and-whisker plots of monthly $NO_2$ levels determined in this study are presented. Higher $NO_2$ concentrations also generally occurred during the colder and/or dryer months, which are, similar to $SO_2$ levels, expected in the north-eastern South African interior (e.g. Colette *et al.,* 2010, Venter *et al.,* 2012, Adesina *et al*., 2022). Elevated $NO_2$ can also be attributed to pollution build-up, as well as an increase of low-level emissions mainly associated with domestic burning for space heating and open biomass burning (e.g. Graham, 1998; Makonese *et al*., 2017; Laban *et al.,* 2018). Therefore, these low-level emission sources likely make a substantial contribution to $NO_2$ concentrations determined at Elandsfontein. However, it is well-known that high-stack emissions associated with industrial activities, especially coal-fired power stations, are also major sources of $NO_2$ in this region (Rorich *et al*., 1998; Colette *et al.,* 2010; Gray, 2019; Swartz *et al.,* 2020; Laban *et al.,* 2018).

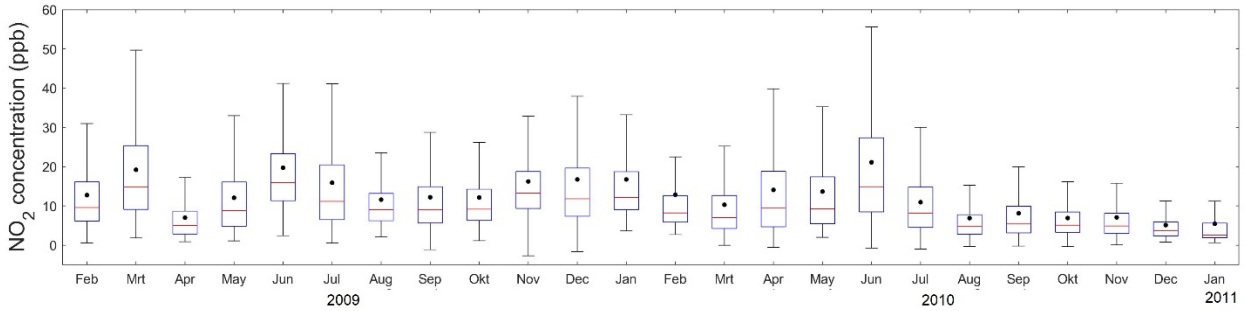


**Figure 5.11:** Box and whisker plots of the measured $NO_2$ concentrations for each month during the study period. The red line represents the median, the black dot the mean, the box the 25$^{th}$ and 75$^{th}$ percentiles and the whiskers are equal to 1.5 times the interquartile range.

It is also evident from the overall and seasonal diurnal patterns for $NO_2$ depicted in Figure 5.12 that $NO_2$ concentrations were higher during winter (red line) as observed in the monthly levels (Figure 5.11). A similar, yet less pronounced trend was seen by Adesina *et al*. (2022) and Collett *et al*. (2010). $NO_2$ levels increased just after 08:00 and reached a maximum peak just between 11:00 and 12:00 during all the seasons, which can also be ascribed to mixing down of high-stack emission during the break-up of inversion layers and increase in PBL layer (Garstang *et al.,* 1996; Korhonen *et al.,* 2014; Gierens *et al.,* 2018). A similar trend was observed by Collett *et al*. (2010). The latter is also supported by this peak being more prominent during winter due to more pronounced inversion layers and the lower PBL depth. However, a second, less pronounced peak is observed in the late afternoon/early evening, which steadily decreases up until midnight, after which slight increases in $NO_2$ are again observed. This same secondary peak was observed by Adesina *et al*. (2022). This is most likely related to low-level emissions of $NO_2$, which include household combustion, open biomass burning and traffic (Rorich *et al*., 1998; Graham, 1998; Makonese *et al*., 2017; Laban *et al.,* 2018). In addition, this could also be ascribed to aged high-stack emissions in which NO is converted to $NO_2$. Diurnal $NO_2$ trends determined by Venter *et al.* (2012) at a site in the highly industrialised and densely populated western Bushveld Complex, exhibited distinct bimodal peaks, which occurred in the morning (between 06:00 and 10:00) and late afternoon/early evening (between 17:00 and 10:00), which was attributed to low-level emissions (mainly household combustion). Lower $O_3$ and $OH^{\bullet}$ levels during night-time (e.g. Laban *et al.,* 2018) could also contribute to the higher $NO_2$ levels during night-time. The overall and season diurnal patterns for $O_3$ are presented in Figure 5.13, which clearly indicate the lowest $O_3$ concentrations during night-time for all four seasons. Tropospheric $NO_2$ and $O_3$ chemistry are interrelated with $NO_2$ being the only species from which tropospheric $O_3$ can be formed in the atmosphere (Seinfeld & Pandis, 2016). Laban *et al.* (2018) clearly indicated that the tropospheric $O_3$ production in this area is VOC-limited, which was attributed to high anthropogenic emissions of NOx (NO and $NO_2$). Therefore, according to these diurnal trends determined for $NO_2$ at Elandsfontein, it seems that a combination of high-stack and low-level emissions sources contribute to $NO_2$ concentrations measured at this site.

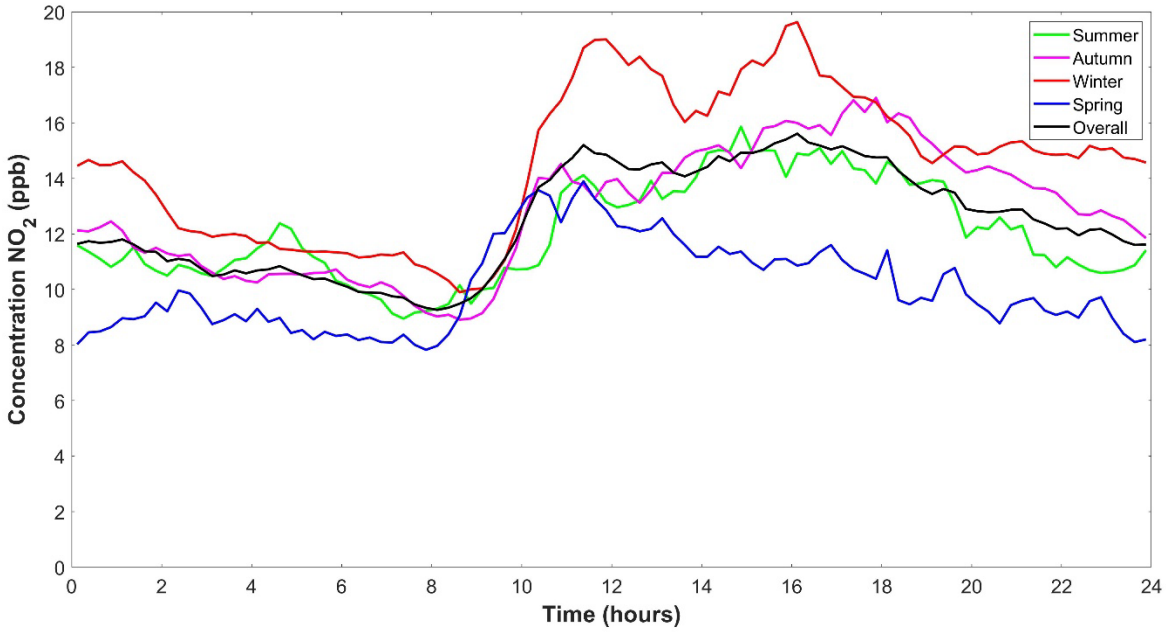


**Figure 5.12:** Diurnal patterns based on average 15 min data of $NO_2$ for the entire measurement period, as well as separate average patterns for each season (Summer = December, January and February; Autumn = March, April and May; Winter = June, July and August; Spring = September, October and November).

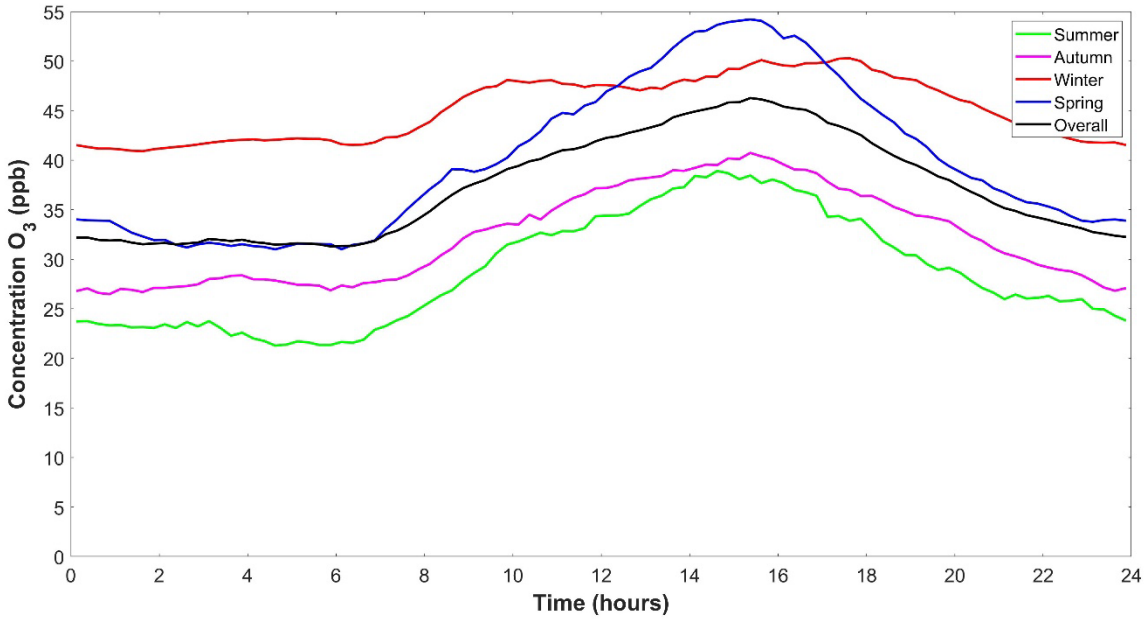


**Figure 5.13:** Diurnal patterns based on average 15 min data of $O_3$ for the entire measurement period, as well as separate average patterns for each season (Summer = December, January and February; Autumn = March, April and May; Winter = June, July and August; Spring = September, October and November).

The pollution and frequency roses for $NO_2$ concentrations higher than the annual average (12.5 ppbv) and 95$^{th}$ percentile (36.8 ppbv) are presented in Figure 5.14. $NO_2$ levels exceeding these threshold values were predominantly associated with winds from the west for northern sector, which correspond to the same

region contributing to higher $SO_2$ and NO levels measured at Elandsfontein. However, similar to $SO_2$ and NO, $NO_2$ concentrations exceeding the annual average were also associated with a larger fetch region, with the exception of $NO_2$ levels corresponding with southerly winds. There are, especially, a relatively higher frequency of increased $NO_2$ concentrations coinciding with winds from the east-south-east, which is also observed for $SO_2$ (to a lesser extent) and NO. Chiloane *et al.* (2018) attributed $NO_2$ concentrations from the east at Elandsfontein to nearby traffic emissions. Similarly, Rorich *et al*. (1998) found high NOx emissions related to traffic at a monitoring site in Bedworth Park. However, it should be noted that this was within an urban area. This also points to various potential sources (low-level and high-stack emissions) of $NO_2$ as revealed by the diurnal patterns. The frequency rose indicates that high concentrations of $NO_2$ are most frequently encountered from the western sector where numerous coal-fired power stations are situated within proximity of the Elandsfontein measurement station. The highest $NO_2$ concentrations were also observed for winds from this region. The pollution and frequency roses for NO, $SO_2$ and $NO_2$ reveal similar sources for these species. However, $SO_2$ levels at Elandsfontein are more frequently associated with winds from the north, which are most likely due to the influence of pyrometallurgical smelters (as observed for $H_2S$ with higher $H_2S$ concentrations related with northerly winds). Comprehensive source apportionment with the method developed in study is also presented in Chapter 6.

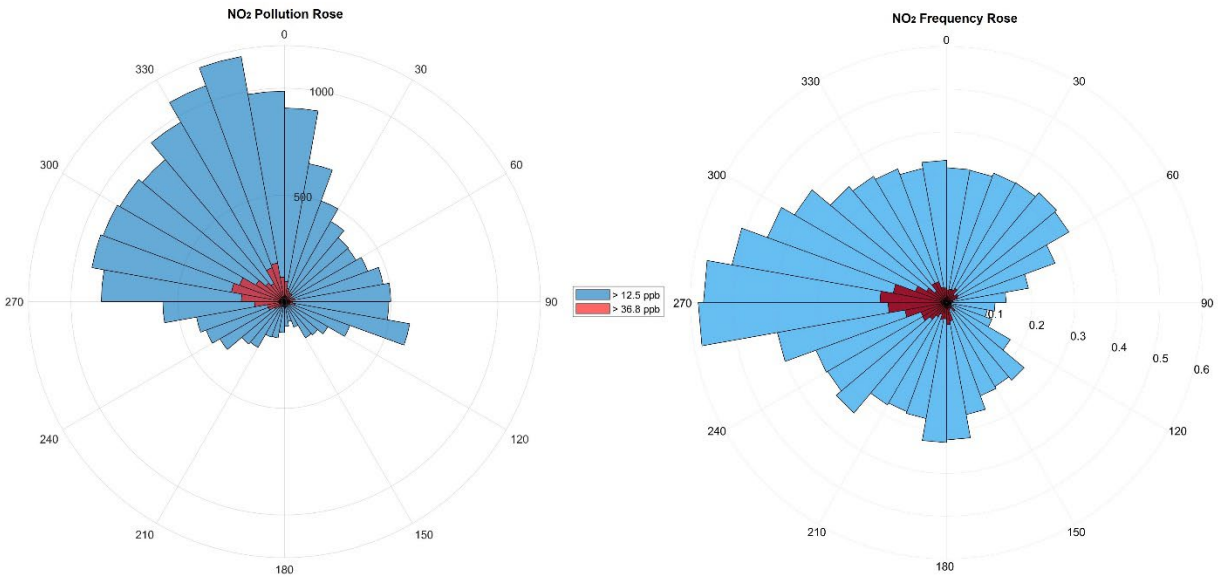


**Figure 5.14:** Pollution (left) and frequency roses (right) associated with NO concentrations (15-min averages) measured at Elandsfontein. Indicated in blue are wind directions corresponding with $SO_2$ concentrations exceeding 12.5 ppbv (annual mean concentration), while red represents wind directions associated with $SO_2$ levels exceeding the 95$^{th}$ percentile (36.8 ppbv).

## 5.4 Chapter 5: Conclusion

Average data coverage for the species under investigation was approximately 81%, which could be considered as good data coverage for the period. Gaps in the data could mostly be attributed to rolling power outages during the study period as South Africa was in an energy crisis (Pretorius *et al.,* 2015), and these gaps were spread out over time and probably will not cause bias in the seasonal analysis. Remaining data was subject to rigorous quality assurance to ensure a high-quality dataset (Laakso *et al.*, 2012; Beukes *et al.,* 2015).

There were very few exceedances of the NAAQS standards, $SO_2$ only exceeded its 10-minute standard of 191 ppbv twice and the 1-hour standard of 134 ppbv six times (total allowable exceedance of 526 and 88 annually respectively). $NO_2$ only exceeded it 1-hour standard of 106 ppbv eight times throughout the study period and the annual standard of 21 ppbv was not exceeded (total allowable exceedance of 88 and 0 times annually respectively). This is interesting, as the HPA is considered a hotspot for $NO_2$ and $SO_2$ (Wenig *et al.,* 2003; Toenges-Schuller *et al.*, 2006; Ghede *et al*., 2009; Lourens *et al*., 2012); however, the ambient air quality with regard to the aforementioned rarely exceeds the allowable NAAQS and WHO standards. Currently, the South African DFFE is considering the formulation of regional-specific $H_2S$ ambient air quality standard limits. If the envisaged legislation is applied to only focus on large industrial point sources, it will likely reduce the occurrence of so-called "high $H_2S$" days (a day on which an one-hour average $H_2S$ concentration exceeds 29 ppbv), but possibly not reduce the overall ambient levels. Thirteen such "high $H_2S$" days were recorded at Elandsfontein during the two-year measurement period considered in this study, which were attributed to different sources.

Generally, most species presented some seasonal variation, with average concentrations reaching maximums during the colder and drier months of the year. Seasonal and diurnal patterns of the $H_2S$ concentration at the Elandsfontein measurement site suggest that surface emissions are the predominant sources of $H_2S$ in the region. $SO_2$, NO and $NO_2$ concentrations all seemed to be influenced mostly by high stack emissions observed as a large single peak just after the breakup of inversion layer(s) and the increase in PBL height.

Considering the effect of wind direction on the gas concentrations, NO, $NO_2$ and $SO_2$ presented highest frequency of high concentrations (>95$^{th}$ percentile) for westerly winds. In this direction, the closest major sources are coal-fired power plants. The Jhb/Pta megacity and numerous pyrometallurgical smelters are also situated in this region, but are further away. Interestingly, $H_2S$ had a bi-directional pattern with concentrations > 95$^{th}$ percentile arriving at high frequency from the north and southwest. The southwest $H_2S$ peak is most likely due to a petrochemical plant; however, the origin of the north peak is not as obvious. Possible sources for the northern sector could be pyrometallurgical plants in the Middelburg/Witbank area or spontaneous combustion of coal.

# Chapter 6: Trace gas source contributions

**In this chapter,** the source contributions determined for $H_2S$, $SO_2$, NO and $NO_2$ with the novel method developed in study and presented in Chapter 3.1 are discussed. In section 6.1, example case studies are presented to illustrated how the chemical composition of plumes were related to sources, while the source contributions associated of each gaseous species are discussed in section 6.2. The contribution of sources to atmospheric $H_2S$ in this region, as well as the case studies introduced in this chapter, has been published in the research article *Concentration contextualisation, temporal patterns and sources of hydrogen sulphide at a site on the South African Highveld* published in *Atmospheric Environment* (Cogho *et al.,* 2023). This chapter concludes in section 6.3.

## 6.1 Source contribution case studies for the identified sources

In this section, example case studies will be presented to further illustrate how plumes from major sources were identified and related to the sources. Since an example for the petrochemical operations was already presented in section 3.6, an example for this source type is not repeated here. In addition, a table that describes the chemical characteristics/footprint of each source was presented in Table 3.1 to further explain how the sources were differentiated.

### 6.1.1 Urban

As previously stated, the term “urban” within the context of this study refers to plumes associated with a town/city/in- or semiformal settlement, which excluded the Jhb-Pta megacity. Figure 6.1 presents a Google Earth image of the small-town of Bethal, which is approximately 25 km from Elandsfontein. It is evident that this town has a number of regions that hold different sources from which trace gases can be emitted, e.g. residential coal burning for heating and cooking purposes in informal settlements, industrial activities and waste treatment facilities in the small industrial area, as well as vehicle emissions from all the areas in this town. Due to the relatively small size of each individual source and the close proximity thereof to one another, such sources were considered as a single source area, i.e. “urban”, in the source quantification.

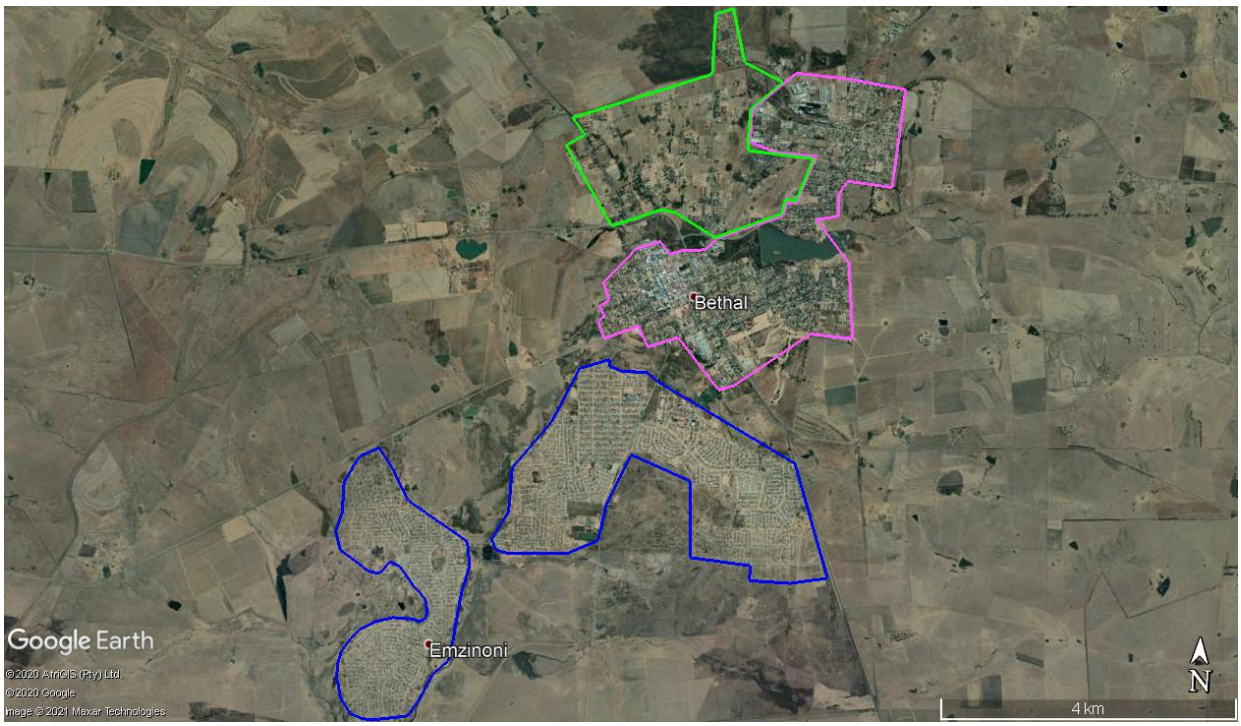


**Figure 6.1**: Google Earth image of the small town of Bethal. The purple polygon indicates the formal residential, small industry and business areas of Bethal, while the blue polygons the semi- and informal settlements. The surrounding area consist of small agricultural holdings (green polygon), as well as larger farmlands.

In Figure 6.2, increases in $H_2S$, $SO_2$ and $NO_2$ are observed, together with a small increase in eBC, but no increase in NO, between 14:00 and 17:00 on 10 January 2011. As previously indicated, a peak with coincidental increase of these species is indicative of household combustions on the Mpumalanga Highveld (Chiloane *et al.,* 2017). Although roughly 90% of households in South Africa are electrified (Noor, 2015), electricity is rarely used for cooking (Makonese *et al*., 2018). A study done in Bushbuckridge, South Africa, observed that although households received electricity with a free basic allowance of 6 kWh per month, 90% of the households still used firewood for cooking and heating activities (Madubansi *et al*., 2007). Coal is the most abundant fuel source for residential burning in the Mpumalanga Province due to its availability and low cost (Balmer, 2007; Langerman *et al.,* 2018, 2019). Ineffective household combustion processes applied, especially in in-/semiformal settlements do not oxidise all the sulphur in the fuel to $SO_2$, and therefore $H_2S$ can also be emitted. It was found that low ventilation coal stove emissions can contain more than 800 ppm $H_2S$ during pyrolysis and about 900 ppm $SO_2$ during the coking phase (Makonese *et al.,* 2015).

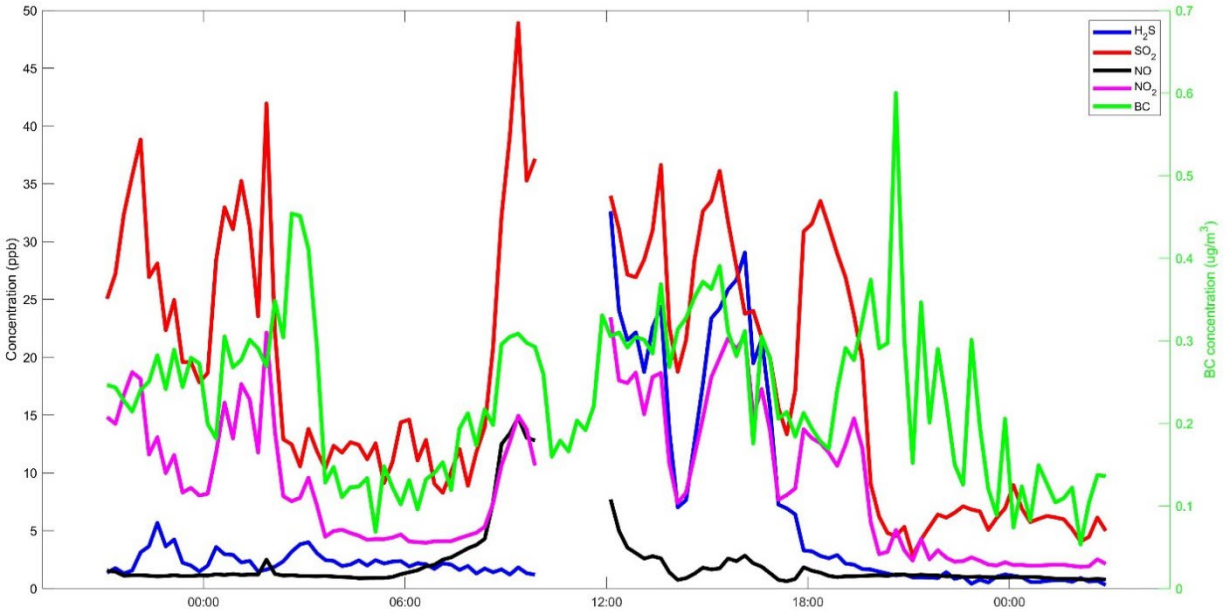


**Figure 6.2**: 24hr ± 3hr concentration *vs*. time graphs of co-incidental increases of $H_2S$, $SO_2$, $NO_2$ and eBC on the 10th of January 2011.

The timing of the co-incidental concentration peaks (Figure 6.2) does not exclude the possibility of high stack emissions (e.g. from coal-fired power stations, or a petrochemical operation) as the plume is observed during daytime when strong inversions are not present and the PBL is higher (compared to early mornings and night-time), which will allow downward mixing of high stack pollutants (Garstang *et al.,* 1996; Korhonen *et al.,* 2014; Gierens *et al.,* 2018). However, air mass history indicates strong emission sensitivity over the nearby town Bethal (Figure 6.3) directly south of Elandsfontein, as well as other small towns within the area. Although air mass history in Figure 6.3 indicates the possible influence of industry, i.e. a small fraction of air masses passing over industrial point sources, lower emission sensitivities were associated with these sources in this case study. Considering the aforementioned FLEXPART back trajectories, this plume was attributed to the "urban" source type.

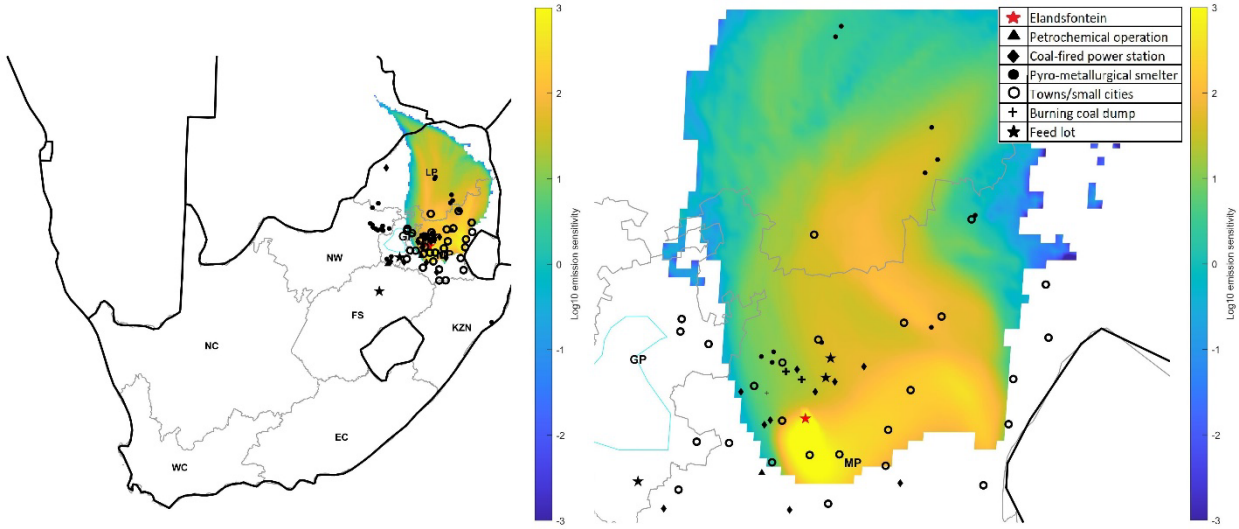


**Figure 6.3:** Summed up FLEXPART air mass emission sensitivities for the example co-incidental trace gas plume depicted in Figure 6.2

### 6.1.2 Jhb-Pta megacity

The Jhb-Pta megacity was categorised separately from the other urban sources in this study since it is a very large conurbation compared to other urban areas. In Figure 6.4, co-incidental increases in levels of $H_2S$, $SO_2$, $NO_2$ and eBC are evident between 00:00 and 03:00 on 26 August 2009, but no NO was observed. The Jhb-Pta megacity is further from the measurement site than the smaller towns/cities/settlements in this region, which allows more time for $O_3$ to react with NO to produce $NO_2$ during night-time transport.

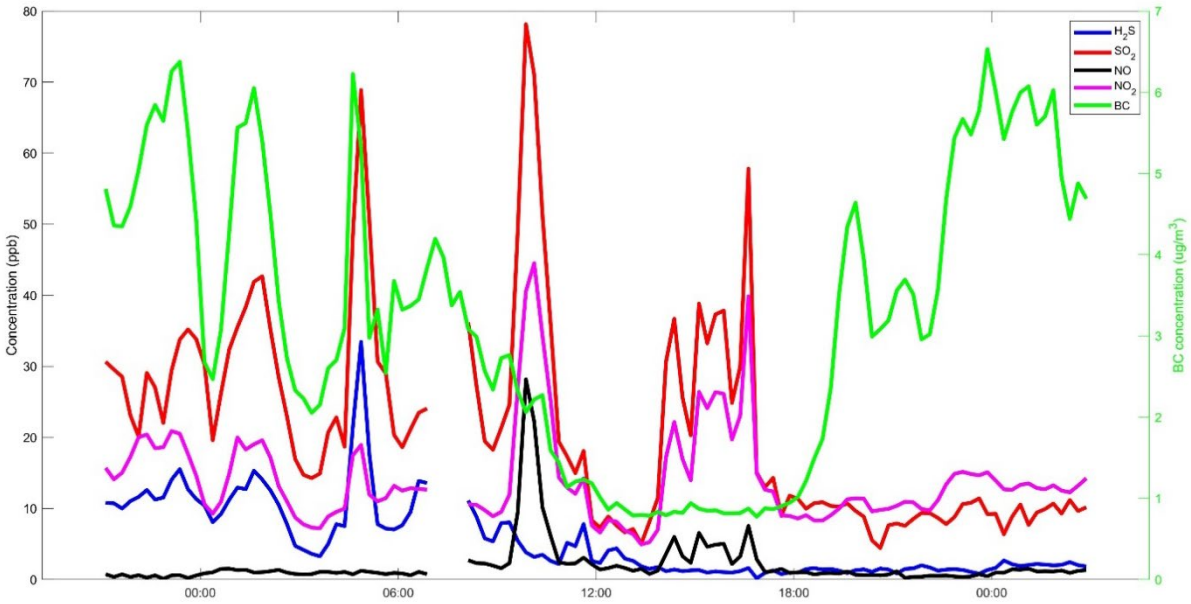


**Figure 6.4:** 24hr ± 3hr concentration *vs*. time graphs of co-incidental increases of $H_2S$, $SO_2$, $NO_2$ and eBC between 00:00 and 03:00 on the 26$^{th}$ of August 2009

The timing of the co-incidental concentration peaks suggests low-level emissions to be the origin as it is observed early in the morning, which makes it very unlikely that downward mixing of high stack pollutants would occur (Garstang *et al.,* 1996; Korhonen *et al.,* 2014; Gierens *et al.,* 2018). Air mass history in Figure 6.5 also indicated air masses passing over the Jhb-Pta megacity (blue polygon) and close to a coal-fired power plant, but the absence of NO rules out influence of fresh power plant emissions. Although further upwind air mass passed over pyrometallurgical smelters in the western bushveld igneous complex (BIC), their influence is considered small in relation to the number of air masses passing over the Jhb-Pta conurbation (Figure 6.5). Considering all the aforementioned, it is likely that the plume is dominated by the Jhb-Pta megacity emissions.

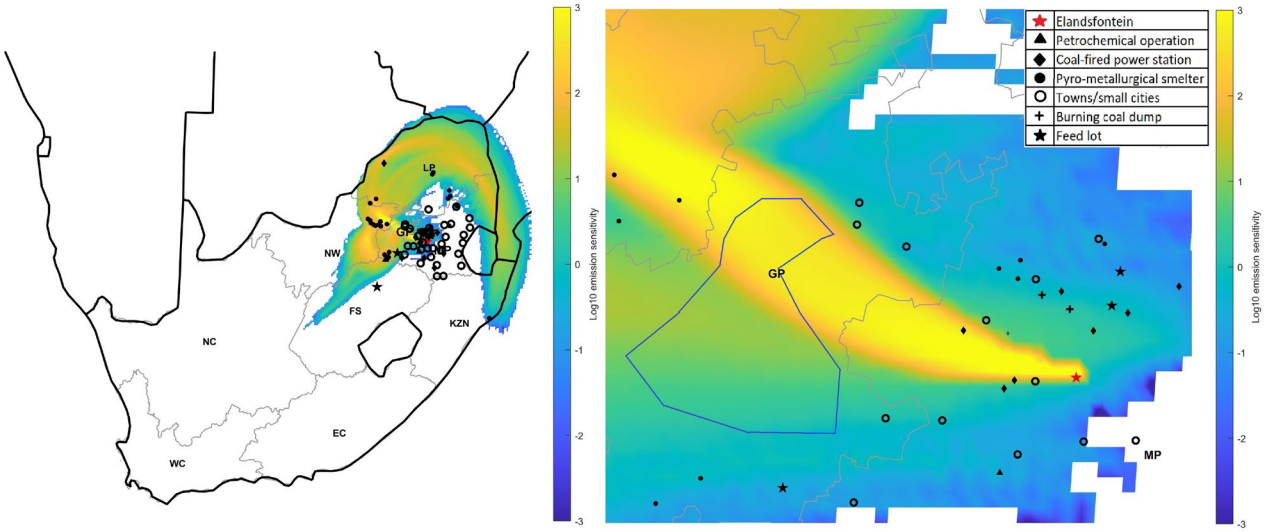


**Figure 6.5:** Summed up FLEXPART air mass emission sensitivit*ies* for the example co-incidental trace gas plume depicted in Figure 6.4

### 6.1.3 Pyrometallurgical smelter

Plumes from pyrometallurgical smelters on the Mpumalanga Highveld are usually characterised by coincidental increases of $SO_2$, $NO_2$ and eBC, together with $H_2S$ (Chiloane *et al.,* 2017). $H_2S$ in these plumes are expected, since pyrometallurgical smelting is a reductive process that is conducive to the formation of $H_2S$. However, a significant fraction of the $H_2S$ will be oxidised to $SO_2$ during off-gas combustion above the material bed in open and/or semi-closed furnaces (Beukes *et al.* 2017), or during flaring of cleaned off-gas by closed furnaces (Du Preez *et al.,* 2015; Beukes *et al.,* 2017). In Figure 6.6, the co-incidental increase of $H_2S$, $SO_2$, eBC and some $NO_2$ is observed between 04:00 and 10:00 on 24 April 2009, which is the first indication that this plume might have originated from a pyrometallurgical smelters.

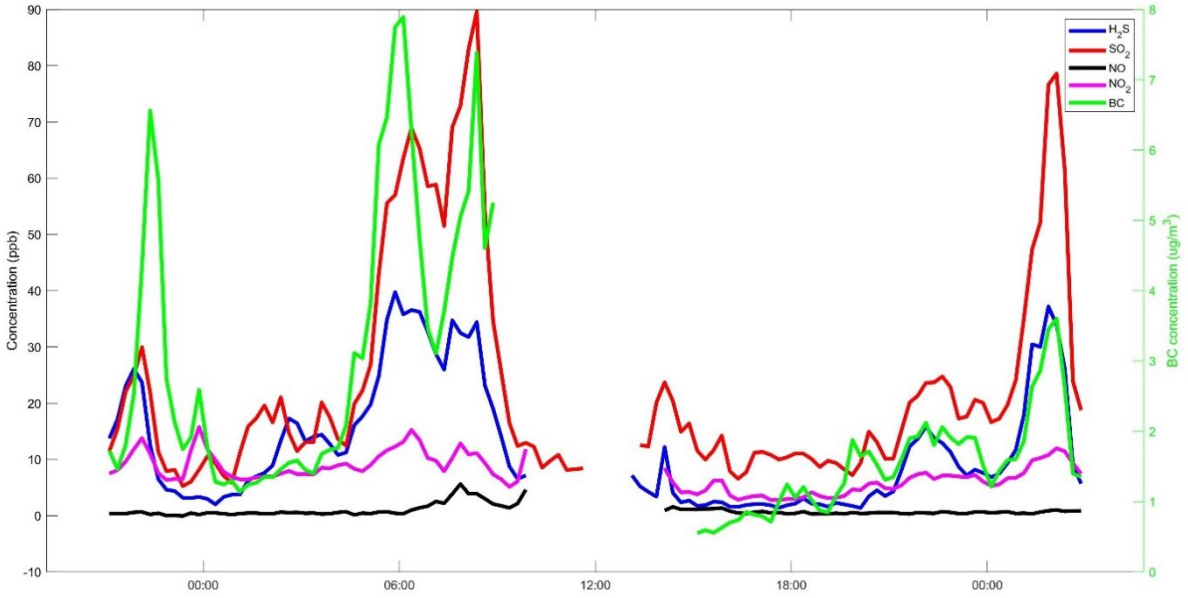


**Figure 6.6**: 24hr ± 3hr concentration *vs*. time graphs of co-incidental increases of $H_2S$, $SO_2$, NO, $NO_2$ and eBC on the 24th of April 2009

One would expect emissions from pyrometallurgical smelters to be released *via* high stacks. However, in South Africa, the stacks of pyrometallurgical smelters are typically not very tall. For example, the highest stack at the Lion Ferrochrome smelter of Glencore in Steelpoort is 58 m and on average the stacks at this smelter are just 45 m tall (Airshed Planning Professionals, 2004). According to the Rustenburg Local Municipality air quality management plan (Piketh *et al.,* 2005), only some platinum group metal (PGM) smelters have stacks that are higher than 100 m, while most other smelters typically have stacks lower than 50 m. PGM smelters emit significant quantities of $SO_2$ since they consume sulphide-rich ore (Xiao & Laplante, 2004). However, on the Mpumalanga Highveld there are no PGM smelters, just ferrochrome, ferromanganese and ferrovanadium smelters, as well as a steel mill. Therefore, these pyrometallurgical smelters will emit pollutants below low-level thermal inversion layer(s) (Gierens *et al.,* 2018) over the Highveld, where it can be trapped and concentrated during night-time and early mornings. Plumes from these smelters could therefore be observed at Elandsfontein during any time of the day. It is evident from Figure 6.7 that air masses arriving at 06:00 at Elandsfontein on this specific day passed over three pyrometallurgical smelters (filled black dots) that are located in the Witbank area, which are most likely the main source of $H_2S$ in this case study.

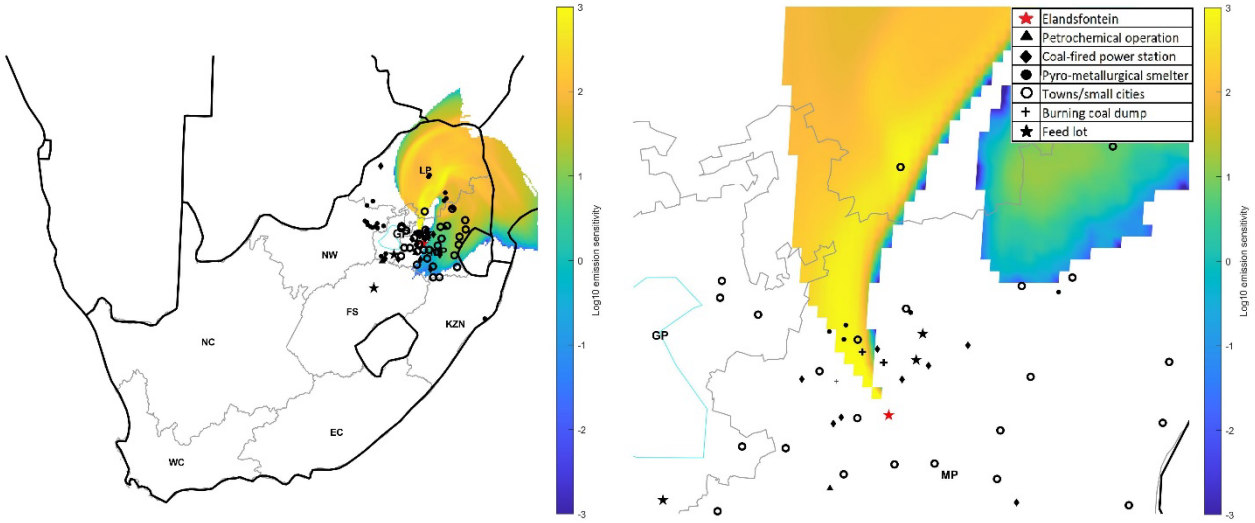


**Figure 6.7**: Summed up FLEXPART air mass emission sensitivit*ies* for the example co-incidental $H_2S$ plume depicted in Figure 6.6

### 6.1.4 Coal-fired power station

It was not expected to observe significant $H_2S$ emissions associated with coal-fired power station at Elandsfontein, since boilers at these facilities burn at exceptionally high temperatures (~1200 °C at full load, ESKOM, 2019) in an oxidising environment. However, $H_2S$ was observed in some plumes from coal-fired power station and therefore two case studies are presented. The first will be, what is considered a normal (more common) coal-fired power station plume without $H_2S$, while the second case study will investigate a less commonly observed coal-fired power station plume with $H_2S$ being present.

i. Coal-fired power station plume without $H_2S$

Typically, plumes associated with high stack coal-fired power generation emissions in the South African interior are observed at ground level after growth of the PBL depth and breakup of low-level thermal inversion layer(s) in the morning. This often results in a sharp increase in pollutant concentrations as downward mixing occurs. Such a plume is visible in Figure 6.8, where a sharp increase in $SO_2$, $NO_2$ and NO, but not $H_2S$, was observed between 11:00 and 17:00 on 11 May 2009, suggesting that these species are emitted from a coal-fired power station (Collet *et al.,* 2010; Lourens *et al.,* 2011). Furthermore, air mass history (with a starting time at 10:00) also reveal that air masses passed over two coal-fired power stations in Figure 6.9. Taking into account the co-incidental increases of NO, $NO_2$ and $SO_2$, the timing and amplitude of the co-incidental increases, and air mass origin, it is evident that the plume originated from the coal-fired power stations.

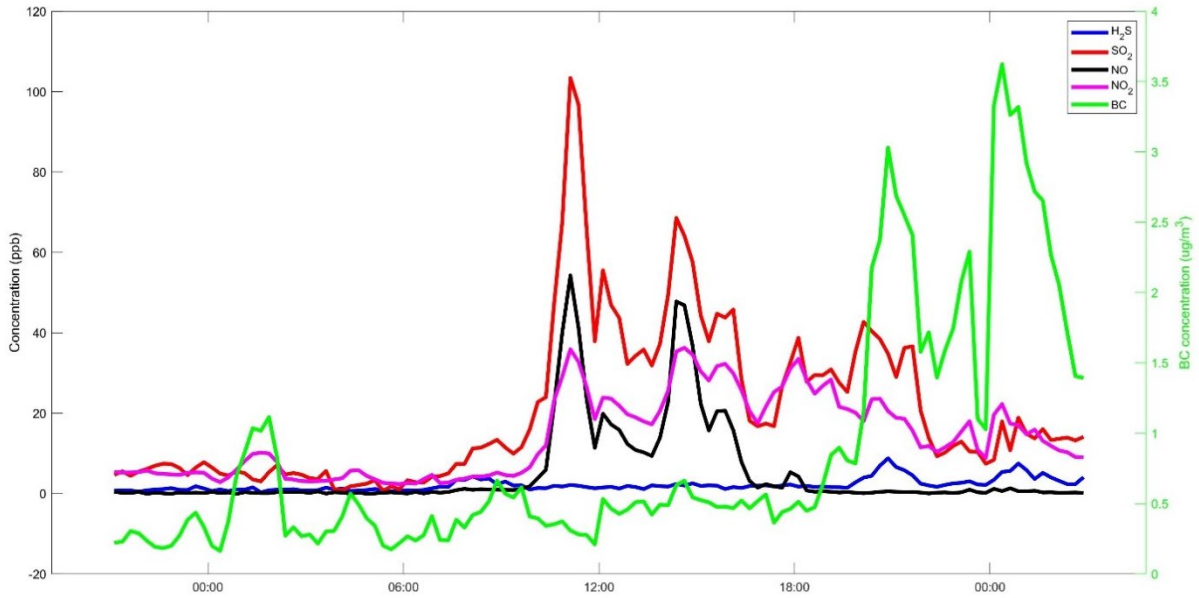


**Figure 6.8:** 24hr ± 3hr concentration *vs*. time graphs on the 11th of May 2009. Co-incidental increases of $SO_2$, NO and $NO_2$ between 11:00 and 17:00 are analysed.

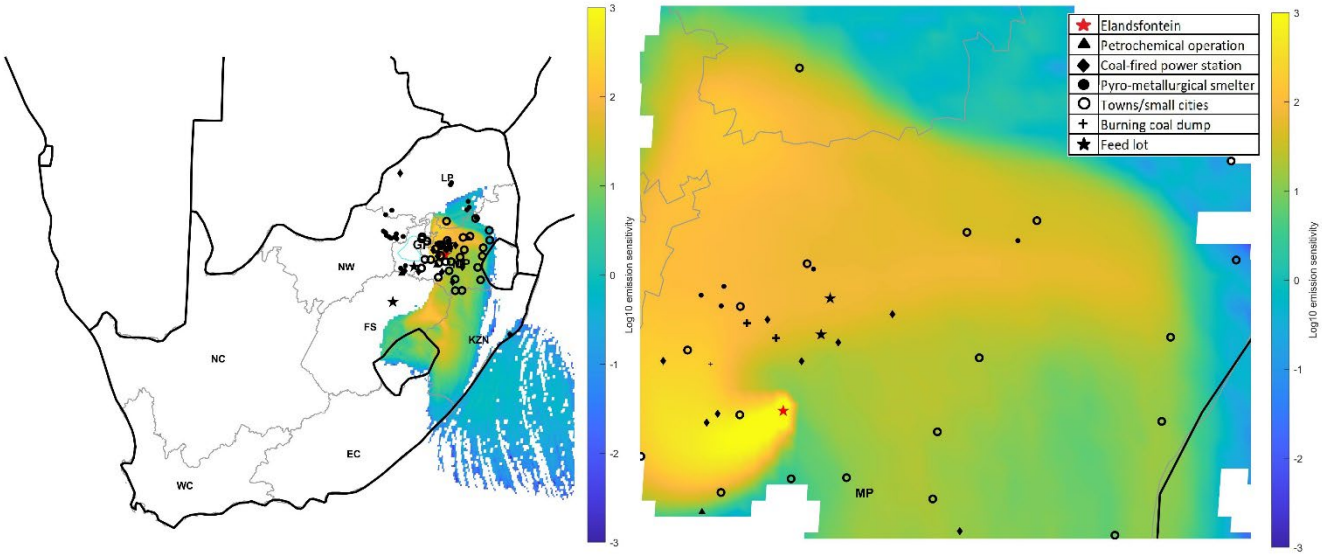


**Figure 6.9**: Summed up FLEXPART air mass emission sensitivit*ies* for the example co-incidental trace gas plume depicted in Figure 6.8

ii. Coal-fired power station plume with $H_2S$

As indicated in Figure 6.10, coincidental increases in $SO_2$, $NO_2$, eBC and $H_2S$ were observed between 17:00 and 19:00 on 26 May 2010. The absence of NO in the plume is indicative of an aged plume with NO being oxidised to $NO_2$. As explained earlier, the timing and amplitude of the co-incidental peak suggest that the plume is of high stack origin, i.e. either from a coal-fired power station or the petrochemical operation near Secunda. Due to the presence of $H_2S$ in the co-incidental peaks considered in this case study, it could very

easily be assumed that the plume originated from the petrochemical operation. However, the emission profile does not look similar than that of a petrochemical operation. $H_2S$ is evident as a peak, which has approximately the same profile as the observed $NO_2$ and $SO_2$, but it is not as concentrated. In addition, the co-incidental increase in eBC is not present in plumes associated with the petrochemical operation. It is also evident from air mass history for this case study (Figure 6.11) that air masses passed over or close to coal-fired power plants (Matla and Kriel power plants) to the west of the Elandsfontein station.

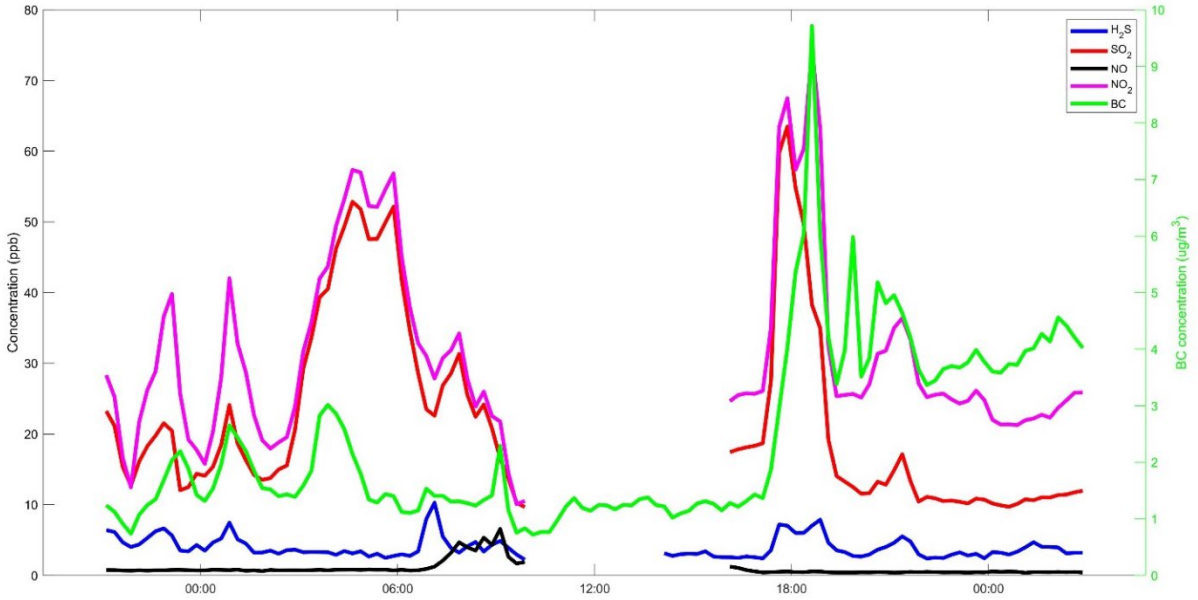


**Figure 6.10:** 24hr ± 3hr time series concentration graphs of co-incidental increases of $H_2S$, $SO_2$, NO and $NO_2$ on 26 May 2010

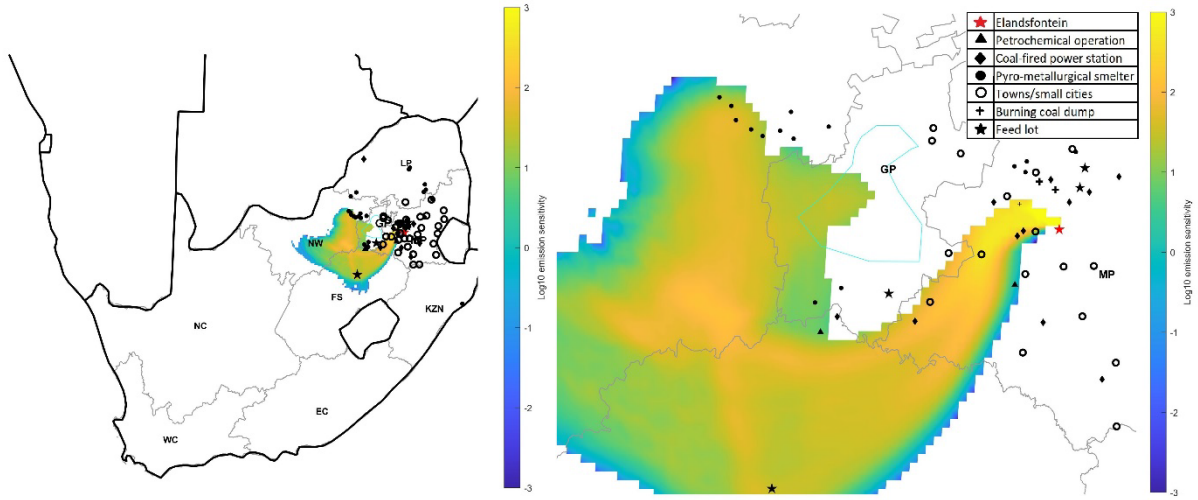


**Figure 6.11**: Summed up FLEXPART air mass emission sensitivit*ies* for the example co-incidental trace gas plume depicted in Figure 6.10

As indicated earlier, it is well known that pollution from coal-fired power stations in South Africa is characterised by coincidental increases in $SO_2$, $NO_2$ and NO (Collet *et al.,* 2010; Lourens *et al.,* 2011; Belaid *et al.,* 2014; Pretorius *et al.,* 2015). However, according to Shirai *et al.* (2012), it is possible for $H_2S$ to be formed during coal-fired power generation if low-$NO_x$ ($NO_x$ = NO + $NO_2$) combustion principles are applied. Several papers have been published that indicate that the sole electricity supplier in South Africa, ESKOM, has indeed been switching to low-$NO_x$ burners in order to move closer to compliance with more stringent $NO_x$ emission standards (e.g. Van der Merwe *et al.,* 2017; Engineering News, 2017). However, neither Matla nor Kriel power plants have been retrofitted with low-NOx burners yet (ESKOM, 2014). Another reason for the presence of $H_2S$ is that a non-ideal oxidative environment is experienced when a coal-fired boiler is started up, which could lead to some $H_2S$ also being emitted. Typically, a cold boiler is initially started by injecting fuel oil at a high pressure through nozzles (ESKOM, 2019), which does not represent boiler conditions at full load and temperature (ESKOM, 2019). South Africa has been in an energy crisis since 2007 due to an increase in electricity demand and poor maintenance of the coal-fired power stations (Pretorius *et al.,* 2015). These factors have resulted in more than normal breakdowns (and associated cold start-ups) of coal-fired power station boilers. Since the power stations have not been retrofitted with low-NOx burners yet, the latter explanation is the most likely cause of $H_2S$ emissions from the stations.

### 6.1.5 Cattle feed lot

There are three large cattle feedlots relatively close to the Elandsfontein measurement station with Figure 6.12 depicting a Google Earth image of the Kanhym feedlot (25° 53’40 S, 29° 33’31 E). These feedlots emit pollutants at surface level and are characterised by emissions of reduced sulphur compounds such as $H_2S$, as well as nitrogen oxides, depending on the type of animals and feed used at the feedlot (Koelsch *et al.,* 2004; Feilberg *et al.,* 2017). The $H_2S$ is formed by bacterial decomposition of sulphate containing organic compounds under anaerobic conditions (Arogo *et al.,* 2000). The cattle feedlots on the Mpumalanga Highveld are open, dry feedlots, meaning that animals are not kept in confined environments. However, at the Kanhym cattle feedlot, there is also a very large piggery. The pigs are housed in closed buildings and could also contribute to gaseous emissions. In Figure 6.13, a simultaneous increase of $H_2S$, $SO_2$ and $NO_2$ is observed between 23:00 on 30 November and 02:00 on 1 December 2009. It was not expected to observe an increase in $SO_2$ in a feedlot plume, but this could be due to fractional oxidation of emitted $H_2S$ during transport of the air mass. The north-eastern interior of South Africa is in general characterised by relatively high $O_3$ concentrations (e.g. Collett *et al*., 2010; Laban *et al.,* 2018; Adesina *et al*., 2022), which will contribute to high levels of the hydroxyl radical (OH•) (albeit not characterised and quantified yet in South Africa) (Seinfeld & Pandis, 2006). Additionally, co-emission of $SO_2$ from combustion sources at the feedlot (e.g. heavy vehicles, refuse combustion and household combustion) could also have contributed to it being measured as a co-incidental species.


**Figure 6.12**: Google Earth image of the Kanhym feedlot and piggery. The blue polygon indicates active feedlots, the green polygon shows inactive feedlots, the yellow polygons indicate the piggery, the purple polygon is a waste treatment dam, the pink polygons are silage production areas and the cyan polygon indicates a stagnant water body that has discoloured, likely due to manure runoff (a run-off path from the one end of the feedlot to the dam is clearly visible).

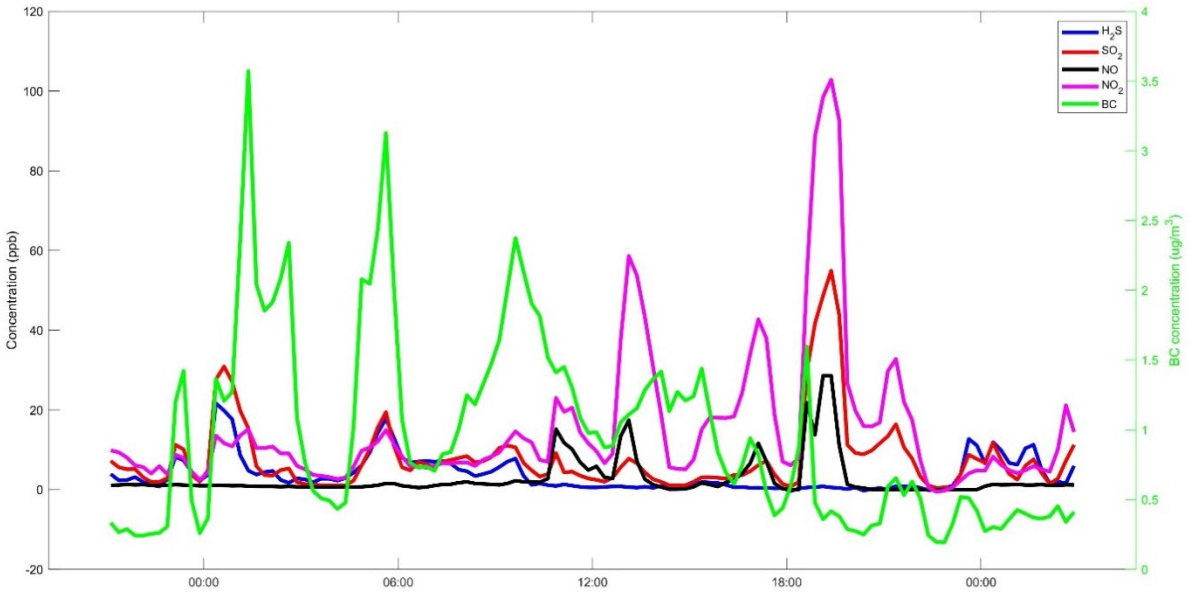


**Figure 6.13:** 24hr ± 3hr concentration *vs*. time graphs of co-incidental increases of $H_2S$, $SO_2$ and $NO_2$ on 30 November 2009.

Figure 6.14 clearly indicates air masses that had passed over the Kanhym and SIS feedlot. However, three power plants and one pyrometallurgical smelter lie within this FLEXPART footprint area. The timing of the co-

incidental concentration peaks does not eliminate high stack emissions as a potential source, but it makes it very unlikely since it was observed late at night when low-level thermal inversion layers are present (Garstang *et al.,* 1996; Korhonen *et al.,* 2014; Gierens *et al.,* 2018). Furthermore, the peak amplitudes were not indicative of a fresh coal-fired power station plume. Although the contribution from a coal-fired power station cannot be completely excluded, this plume was associated mainly with feedlot emissions.

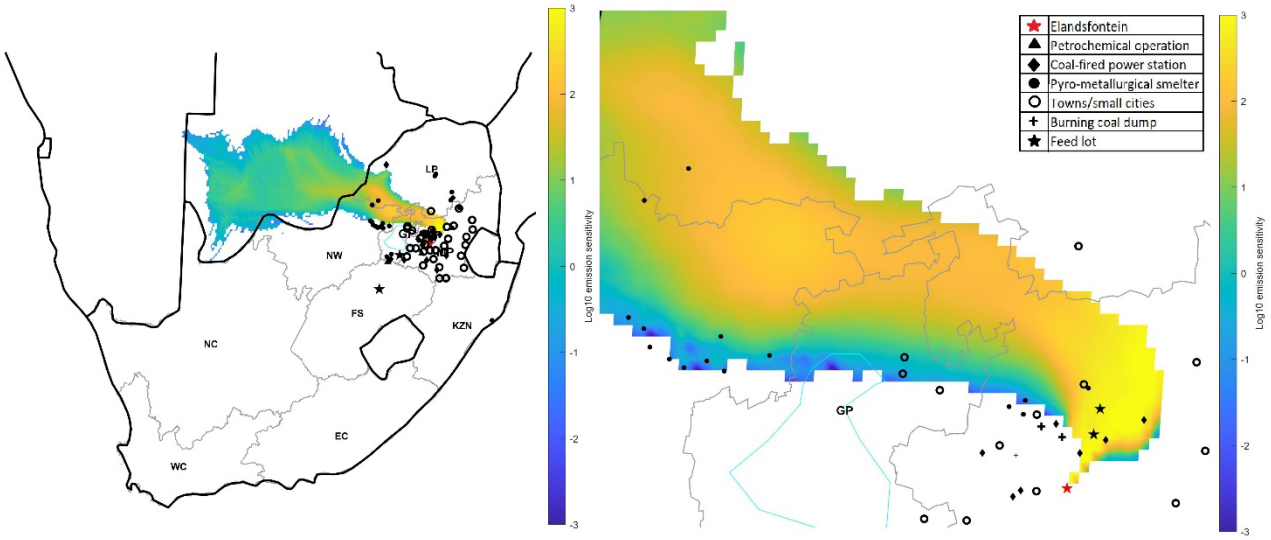


**Figure 6.14**: Summed up FLEXPART air mass emission sensitivit*ies* for the example co-incidental trace gas and eBC plume depicted in Figure 6.27

### 6.1.6 Burning coal dumps

Emissions from spontaneous combustion of coal (coal dumps/seams) on the Mpumalanga Highveld have recently been semi-quantified in a study where fire radiative power observations were used to determine these activities (Cogho *et al.,* 2022). Coal mining is a prevalent activity in this region and a consequence is the exposure of coal to oxygen, which can cause spontaneous combustion of coal. It has been suggested that the spontaneous combustion of coal may have significant environmental impacts (Pone *et al.,* 2007, Cogho, 2022), since the ineffective combustion of sulphur containing coal will emit $H_2S$ (Sussman & Mulhern, 1964). The formation of $H_2S$ from burning coal dumps could be from two possible reaction pathways (Reactions 6.1 – 6.3) (Sussman & Mulhern, 1964)

$$H_2SO_4 + FeS \rightarrow FeSO_4 + H_2S \qquad (6.1)$$

$$C + 2SO_2 \rightarrow CS_2 + 4H_2O \qquad (6.2)$$

$$CS_2 + 2H_2O \rightarrow 2H_2S + CO_2 \qquad (6.3)$$

In Figure 6.15, a simultaneous increase of $H_2S$, $SO_2$ and a slight increase in eBC is observed between 07:00 and 09:00 on 20 September 2010. These increases were unlikely to be from high stack emissions, due to the timing of the co-incidental peaks, as previously indicated (Garstang *et al.,* 1996; Korhonen *et al.,* 2014;

Gierens *et al.,* 2018). This co-incidental increase in $H_2S$, $SO_2$ and eBC is not necessarily indicative of the emissions of burning coal, as it is similar to the emissions of other low-level sources (e.g. urban and feedlot emissions). However, from inspection of the back-trajectory paths (Figure 6.16), it is evident that the air masses passed directly over an actively burning coal field that was identified with the method presented by Beukes *et al.* (2018) and Cogho *et al.* (2022) (explained in section 3.5 and Chapter 4).

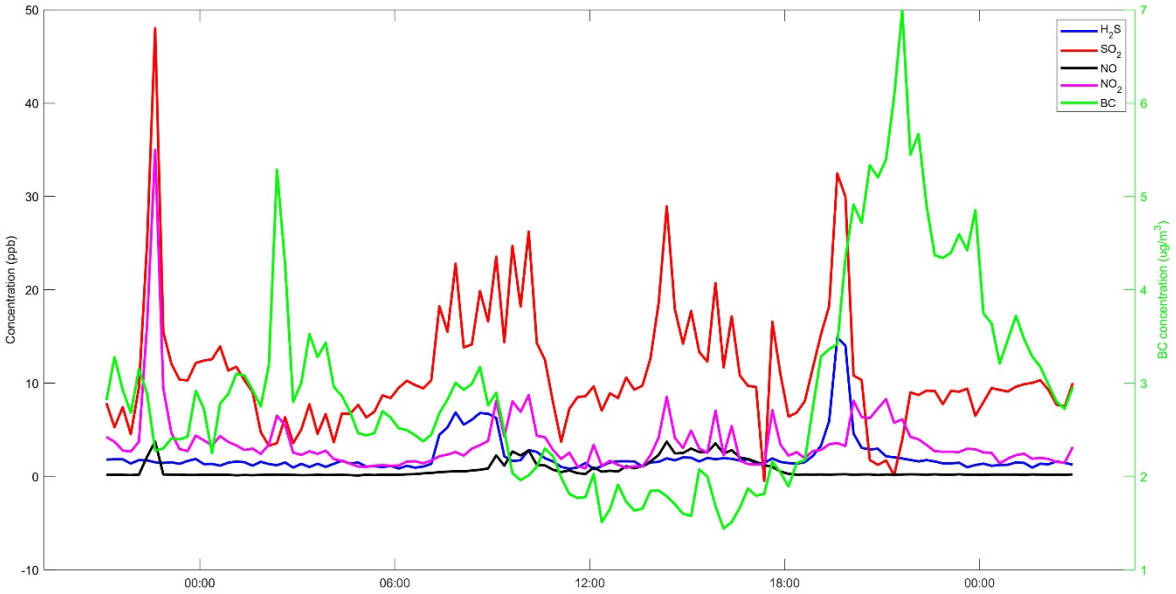


**Figure 6.15:** 24hr ± 3hr time series concentration graphs of co-incidental increases of $H_2S$, $SO_2$, $NO_2$ and eBC on 20 September 2010

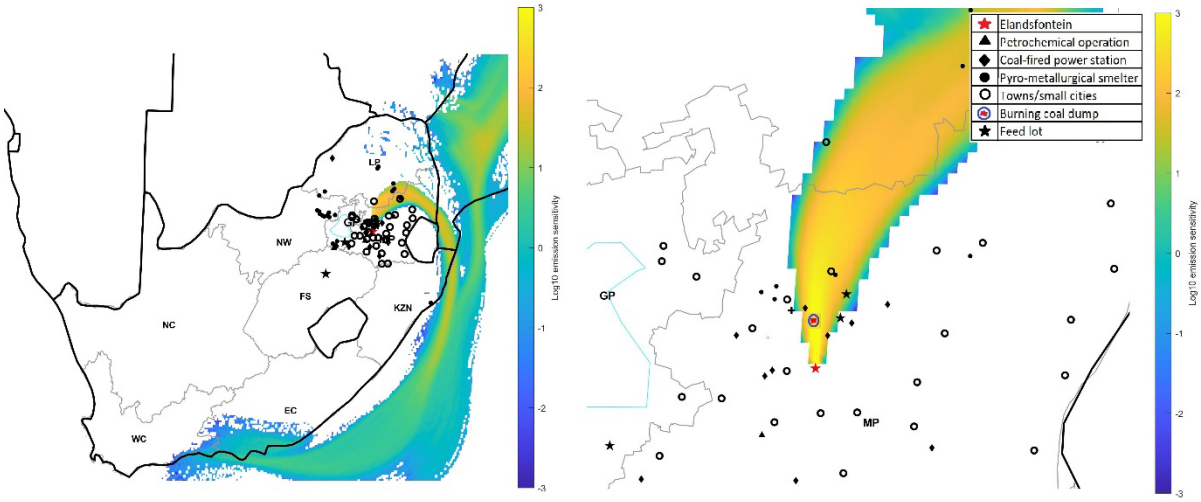


**Figure 6.16:** Summed up FLEXPART air mass emission sensitivities for the example co-incidental trace gas and eBC plume depicted in Figure 6.15

In the Google Earth image presented in Figure 6.17, a polygon indicating the area surrounded by the blue circle in Figure 6.16 is presented. Historically, the coal fields in the area were mined by using a room and pillar technique. This is an underground mining practice in which pillars of coal are left within a coal seam to provide support for the roof of the underground operation, while the coal surrounding the pillars are mined to form "rooms" (Bell *et al.,* 2001; Pone *et al.,* 2007). More recently, opencast mining operations to mine the left over "pillars" exposed the coal "pillars" to an influx of oxygen, which resulted in the spontaneous combustion of some of the coal (Bell *et al.,* 2001; Pone *et al.,* 2007). The combustion process can become self-sustaining in the presence of oxygen once the coal is burning hot enough and large quantities of coal is available, which makes containing these fires extremely difficult (Bell *et al.,* 2001).

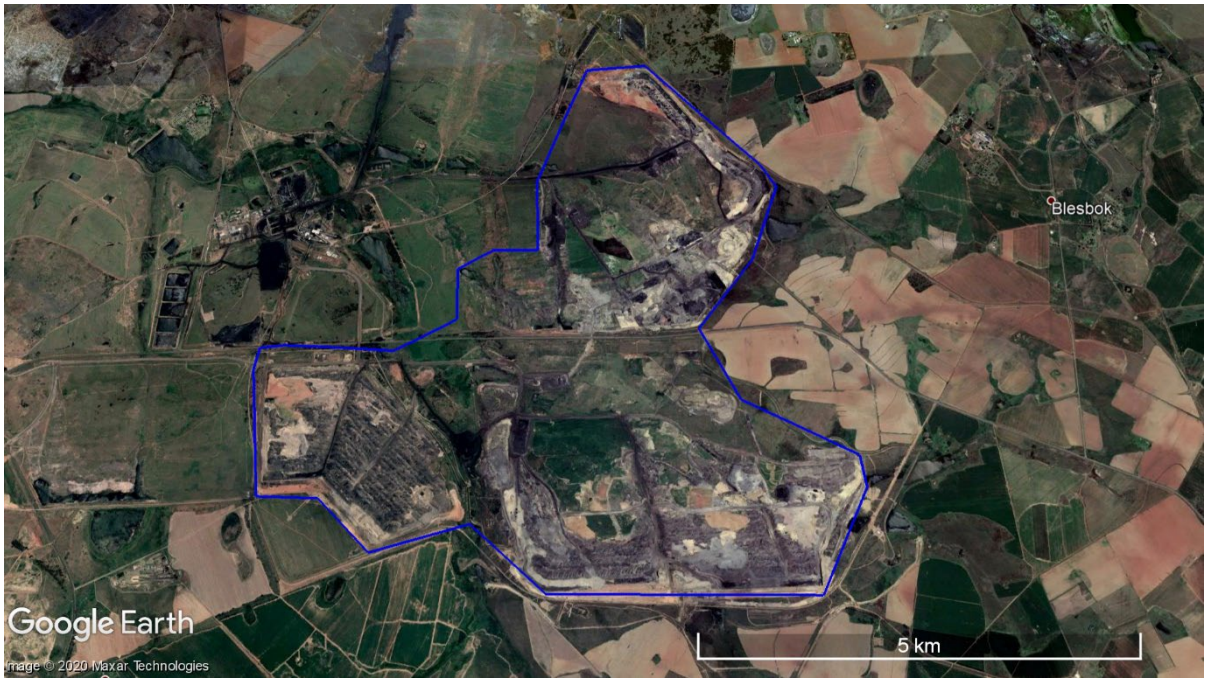


**Figure 6.17:** Google Earth image of the area identified as a burning coal field in Figure 6.16.

### 6.1.7 Traffic

Chiloane *et al.* (2017) related air mass plumes comprising eBC and $NO_2$ to traffic emissions east of Elandsfontein, i.e. a provincial road (R35) situated approximately 4.7km east of Elandsfontein, which is mostly utilised for the transportation of coal with diesel trucks. Furthermore, numerous tarred roads are located north and northwest of Elandsfontein, which include the national N4 and N12 highways. Throughout the study period, several plumes with coincidental increases in $NO_2$ and eBC were identified, with most of these air masses passing over the area east of Elandsfontein. In Figure 6.19, one such plume that exhibits a simultaneous increase in $NO_2$ and eBC between 16:00 and 18:00 is presented as a case study. Air mass history associated with this plume presented in Figure 6.20 clearly indicates that this plume arrived form this region to the east of Elandsfontein.

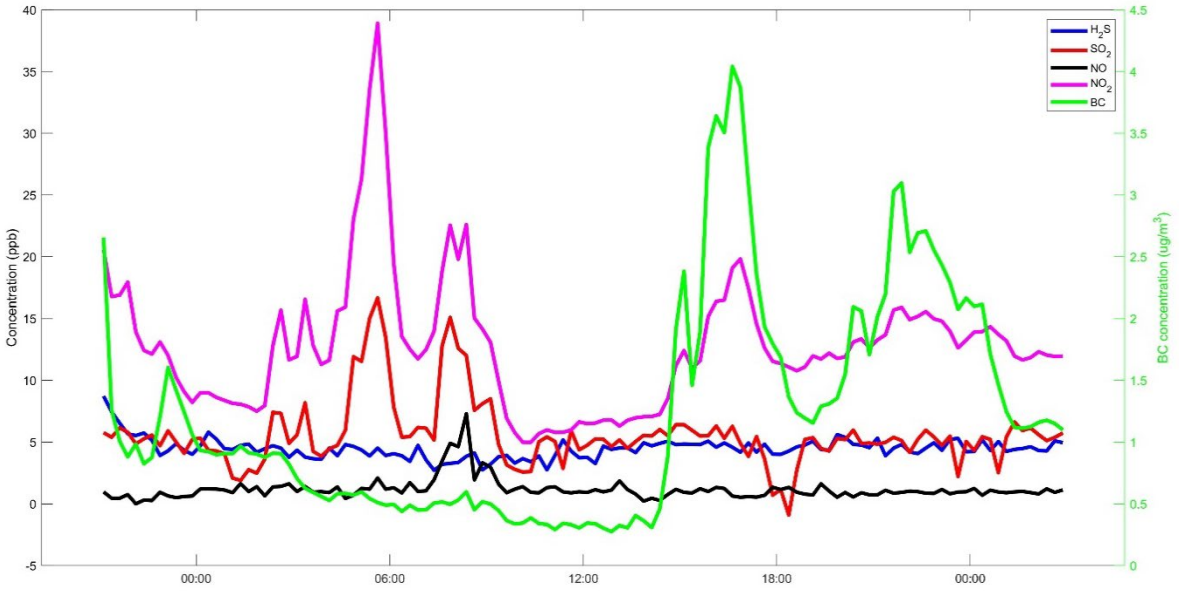


**Figure 6.19:** 24hr ± 3hr concentration *vs*. time graphs of co-incidental increases of $NO_2$ and eBC between 16:00 and 18:00 on 29 June 2009

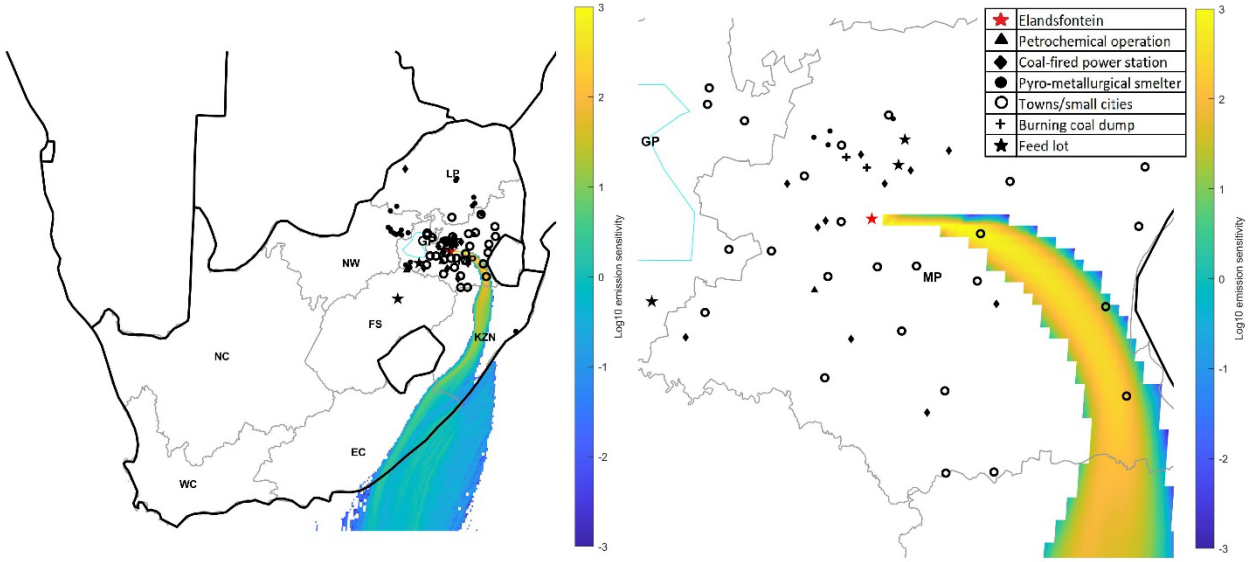


**Figure 6.20:** Summed up FLEXPART air mass emission sensitivit*ies* for the example co-incidental $NO_2$ and eBC plume depicted in Figure 6.19

## 6.2 Source contributions

The source apportionment of $H_2S$, $SO_2$, NO and $NO_2$ as measured at Elandsfontein in excess of the baseline is presented in the sections below. It should be noted that the study only focused on co-incidental increases in pollution species in excess of the baseline. The total time of these co-incidental increases only added up to

approximately 20% of the total time of the study period. Thus, 80% (in time) of the measured trace gas concentrations remains non-apportioned to a specific source.

### 6.2.1 $H_2S$ source contributions

Figure 6.21 presents a simple bar plot of the $H_2S$ source contributions to ambient $H_2S$ concentrations in excess of the baseline (which was 2.7 ppbv, when plume periods were excluded), conducted with the method introduced and discussed in section 3.6. Co-incidental concentration peaks were allocated to eight different sources, namely the petrochemical operation near Secunda (indicated as "Petrochemical"), coal-fired power stations (indicated as "Power station"), pyrometallurgical smelters (indicated as "Pyrometallurgical), urban (not including the Jhb-Pta megacity), Jhb-Pta megacity, feedlots, burning coal dumps (indicated as "Coal dumps") and mixed.

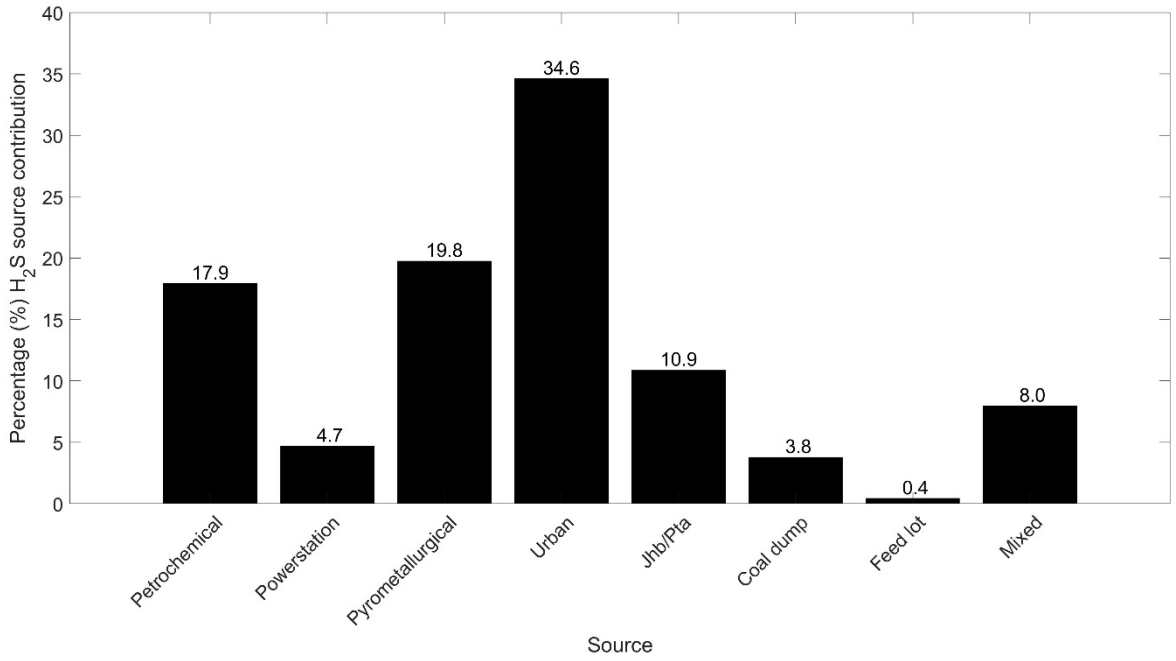


**Figure 6.21:** Percentage $H_2S$ source contributions in excess of the baseline concentrations for each of the identified sources as calculated with the method introduced in Section 3.6

It is evident from Figure 6.21 that the largest contributor to ambient $H_2S$ levels measured in excess of the baseline concentrations observed at Elandsfontein were urban emissions, i.e. 34.6% of the total H2S measured in excess of the baseline. As previously stated, these urban emissions include all $H_2S$ emissions associated with cities/towns/in- and semiformal settlements (excluding emissions from the Jhb-Pta megacity), e.g. household combustion, waste water treatment facilities, landfills, small industries, as well as traffic emissions, especially, from older diesel vehicles (Kourtidis *et al.,* 2004; Sengupta, 2014; Colomer *et al.,* 2012; Hac Ko *et al.,* 2015). In the diurnal $H_2S$ patterns (Figure 5.1), bimodal peaks were identified in the early mornings and evenings, which were attributed to low-level emissions that can be trapped near the surface (Garstang *et al.,* 1996; Korhonen *et al.,* 2014; Gierens *et al.,* 2018). Therefore, the afore-mentioned result, i.e. urban emissions having the largest contribution to $H_2S$ measured at Elandsfontein, agrees with the

deductions made from the seasonal and diurnal patterns. It should be noted, though, that the urban category may include some industrial emissions in rare cases, where night-time mixing brings high stack emissions down to the surface. It is also possible that a plume from a more distant point source that reached ground level the previous day would be observed during night-time at Elandsfontein. Therefore, the contribution here is an upper limit value and deficiencies associated with this defined source group are acknowledged. However, it is still a good indication of $H_2S$ (and other gaseous species discussed in this chapter) emissions associated with urban areas.

It is well known that the petrochemical operation near Secunda emits $H_2S$, since the coal pyrolysis gasification process applied (Bunt & Waanders, 2008) suppresses the formation of $SO_2$ (the corresponding oxidised gaseous species). Therefore, high contributions to ambient $H_2S$ measured at Elandsfontein are expected. However, according to the receptor source quantification results presented in this study, i.e. contribution of 17.9% to the $H_2S$ (Figure 6.21) measured in excess of the baseline concentrations at Elandsfontein, it is evident that it is not the main contributor of $H_2S$ measured in excess of the baseline at Elandsfontein. Chiloane *et al.* (2017) found that the pyrometallurgical smelters in the Middelburg/Witbank area contributed to $H_2S$ measured at Elandsfontein; however, the fractional contribution of this industry sector was not quantified in the aforementioned study. The results presented in this chapter (Figure 6.21) indicated that the pyrometallurgical smelters in the area contributed 19.8% to $H_2S$ measured in excess of the baseline concentrations. The Jhb-Pta megacity was also indicated to be a significant contributor to $H_2S$ measured in excess of the baseline concentrations at Elandsfontein, with a contribution of 10.9% (Figure 6.21). Combined, the urban- and Jhb-Pta sources accounted for 45.5% of the $H_2S$ in excess of the baseline.

Coal-fired power stations also contributed to the ambient $H_2S$ measured in excess of the baseline concentrations at Elandsfontein, with a smaller, but not insignificant contribution of 4.7% (Figure 6.21). It was not expected to measure $H_2S$ in plumes originating from coal-fired power stations, since the combustion process requires oxidising conditions that favour the formation of $SO_2$ and not $H_2S$. However, two possible explanations for $H_2S$ emission associated with coal-fired power stations were considered, i.e. use of low-NOx burners (Shirai *et al.,* 2012; Van der Merwe *et al.,* 2017; Engineering News, 2017) and a non-ideal oxidative environment experienced during boiler start-ups (ESKOM, 2019). These are explained in greater detail in section 6.1.4.ii.

Burning coal dumps had a small, but not insignificant, contribution to ambient $H_2S$ in excess of the baseline, contributing 3.8% to the total ambient $H_2S$ measured at Elandsfontein. In relation to the relatively small number, size and sporadic activities of these burning coal dumps, they make a surprisingly large contribution to the ambient $H_2S$ levels. Feedlots had the smallest individual contribution to the ambient $H_2S$ measured in excess of baseline concentrations at Elandsfontein, i.e. 0.4%. Three very large feedlots, each with ≥ 20 000 animals, could be identified as sources. These animals do not directly emit $H_2S$, but there are generally two sources at feedlots where $H_2S$ is produced, i.e.: i) in waste runoff retention structures or treatment lagoons,

and ii) accumulation of manure in pens and manure storage areas (Preece *et al.,* 2018). In both of these locations, anaerobic wet conditions allow for the decomposition of manure to produce $H_2S$ (Rubright *et al.,* 2017; Preece *et al.,* 2018). Additionally, anaerobic decomposition of silage feed could also serve as a small $H_2S$ source, but, as far as the authors could determine, no studies have been conducted to assess this potential source. It is generally accepted that feedlots do not emit $H_2S$ in very large quantities (Koelsch *et al.,* 2004). Lastly, the co-incidental concentration peaks that were attributed to "Mixed" sources contributed approximately 8% of the $H_2S$ measured in excess of the baseline concentrations at Elandsfontein.

In addition to the abovementioned source contributions, statistics of the ratios of baseline corrected $H_2S$ concentrations divided by baseline corrected concentrations of the other species relevant to each source type are presented in Table 6.1. As previously stated, very little $H_2S$ data is available for South Africa in the peer-reviewed public domain. Therefore, such ratios can be used in future modelling studies as approximated emission factors to estimate $H_2S$, if only concentration(s) of other species are known. However, care should be taken when these ratios are used, since atmospheric conversion processes of the various species cited in Table 6.1 are influenced by plume age, methodological conditions (e.g. high stack emission mostly observed during certain times of the day on the South African Highveld) and ambient conditions (e.g. difference between daytime and night-oxidation processes).

**Table 6.1:** Mean and median, as well as the 5th, 25th, 75th and 95th percentile concentration values the calculated $H_2S$ ratios

| Source | Ratio | | | | | | | | | | | |
|---|---|---|---|---|---|---|---|---|---|---|---|---|
| | $H_2S/SO_2$ | | | | | | $H_2S/NO_2$ | | | | | |
| | Mean | Median | 5th | 25th | 75th | 95th | Mean | Median | 5th | 25th | 75th | 95th |
| **Power** | 0.5 | 0.2 | 0.0 | 0.1 | 0.6 | 2.0 | 0.6 | 0.3 | 0.0 | 0.1 | 0.6 | 2.5 |
| **Petro** | 1.2 | 0.9 | 0.1 | 0.6 | 1.5 | 2.9 | 0.9 | 0.8 | 0.1 | 0.5 | 1.1 | 2.0 |
| **Pyro** | 0.8 | 0.7 | 0.2 | 0.4 | 1.0 | 1.5 | 1.5 | 1.2 | 0.2 | 0.6 | 2.2 | 3.5 |
| **Urban** | 1.6 | 0.6 | 0.2 | 0.4 | 0.9 | 3.5 | 1.5 | 0.9 | 0.2 | 0.5 | 1.8 | 4.1 |
| **Jhb/Pta** | 0.6 | 0.5 | 0.1 | 0.3 | 0.7 | 1.3 | 1.9 | 1.1 | 0.2 | 0.6 | 2.0 | 3.4 |
| **Coal** | 1.0 | 0.7 | 0.2 | 0.4 | 1.0 | 2.8 | 1.8 | 1.1 | 0.1 | 0.6 | 2.9 | 4.9 |
| **Feed** | 1.0 | 1.0 | 0.1 | 0.7 | 1.2 | 2.2 | 1.0 | 0.9 | 0.1 | 0.3 | 1.5 | 2.7 |
| | $H_2S/NO$ | | | | | | $H_2S/eBC$ | | | | | |
| | Mean | Median | 5th | 25th | 75th | 95th | Mean | Median | 5th | 25th | 75th | 95th |
| **Power** | 10.8 | 4.7 | 0.6 | 3.0 | 8.3 | 37.5 | 5.2 | 0.5 | 0.0 | 0.1 | 2.4 | 27.5 |
| **Petro** | 7.8 | 2.5 | 0.2 | 0.9 | 5.7 | 40.2 | 34.6 | 18.2 | 2.9 | 8.3 | 42.8 | 98.2 |
| **Pyro** | 35.5 | 10.2 | 0.5 | 3.6 | 35.9 | 154.9 | 7.2 | 4.9 | 1.0 | 3.0 | 7.9 | 25.7 |
| **Urban** | 24.1 | 8.6 | 0.4 | 2.5 | 26.7 | 94.5 | 14.8 | 7.0 | 1.3 | 3.2 | 13.5 | 55.9 |
| **Jhb/Pta** | 31.2 | 14.8 | 0.8 | 4.5 | 33.6 | 138.3 | 9.0 | 5.5 | 1.7 | 3.5 | 10.0 | 24.7 |
| **Coal** | 27.5 | 8.8 | 0.8 | 2.9 | 28.9 | 103.9 | 10.9 | 6.8 | 1.5 | 4.2 | 12.1 | 27.1 |
| **Feed** | 5.5 | 2.4 | 0.0 | 1.2 | 5.3 | 25.0 | 14.9 | 7.4 | 3.1 | 4.9 | 11.3 | 66.1 |

Correlation coefficients of $H_2S$ with other species measured in this study were also calculated for each source type and are presented in Table 6.2. Each source should have a unique chemical footprint, which could be

derived from these correlations and enable differentiation between sources. These correlation coefficients corresponded with the criteria applied when allocating plumes to specific sources. In plumes associated with the petrochemical sector, $H_2S$ had moderate correlations with $NO_2$, $SO_2$ and NO (0.6, 0.4 and 0.3, respectively). Weak correlations are observed between $H_2S$ and, $SO_2$, $NO_2$ and eBC in plumes associated with coal-fired power stations with no correlation with NO. A moderate correlation is observed between $H_2S$ and $SO_2$ in air masses passing over pyrometallurgical smelters, while it also weakly correlated with eBC. Similar correlation coefficients were calculated for urban sources and the Jhb-Pta megacity with strong and moderate correlations determined between $H_2S$ and $SO_2$, respectively for these two sources. Differences between correlation coefficients of the latter sources could be attributed to the Jhb-Pta megacity being a large, combined source with mostly the same chemical composition whereas urban sources are more varied in composition depending on activities/processes within these urban sources. Weak correlations between $H_2S$, and $SO_2$, $NO_2$ and eBC were determined for coal dump plumes with no correlation with NO. $H_2S$ emissions associated with the spontaneous combustion of coal can occur at lower temperature during pyrolysis, while larger quantities of $SO_2$ and $NO_2$ are emitted at higher temperatures. $H_2S$ did not correlate with any species in air masses associated with feedlots, which can be attributed these emissions being related to natural decomposition and not combustion processes (Koelsch *et al.,* 2004; Feilberg *et al.,* 2017).

**Table 6.2:** Correlation coefficients of $H_2S$ with the other measured gaseous species and eBC for each of the different sources

| Source | Correlation coefficient | | | | Source | Correlation coefficient | | | |
|---|---|---|---|---|---|---|---|---|---|
| | $SO_2$ | $NO_2$ | NO | eBc | | $SO_2$ | $NO_2$ | NO | eBc |
| Petrochemical | 0.4 | 0.6 | 0.3 | 0 | Jhb_Pta | 0.7 | 0.2 | 0 | 0.4 |
| Coal-fired Power stations | 0.1 | 0.2 | 0 | 0.1 | Coal dump | 0.3 | 0.1 | 0 | 0.2 |
| Pyrometallurgical Smelters | 0.5 | 0.1 | -0.1 | 0.3 | Feedlot | 0 | -0.2 | -0.1 | -0.2 |
| Urban | 0.5 | 0.3 | 0 | 0.2 | | | | | |

### 6.2.2 $SO_2$ source contributions

A bar plot of $SO_2$ source contributions to ambient $SO_2$ concentrations exceeding the baseline level (7.4 ppbv) as determined with the method develop in this study (section 3.6) is presented in Figure 6.22. Here, co-incidental concentration peaks were allocated to seven different sources, i.e. the petrochemical operation near Secunda (indicated as “Petrochemical”), coal-fired power stations (indicated as “Power station”), pyrometallurgical smelters (indicated as “Pyrometallurgical), urban (not including the Jhb-Pta megacity), the Jhb-Pta megacity, burning coal dumps (indicated as “Coal dumps”) and a combination of sources as (indicated as “Mixed”).

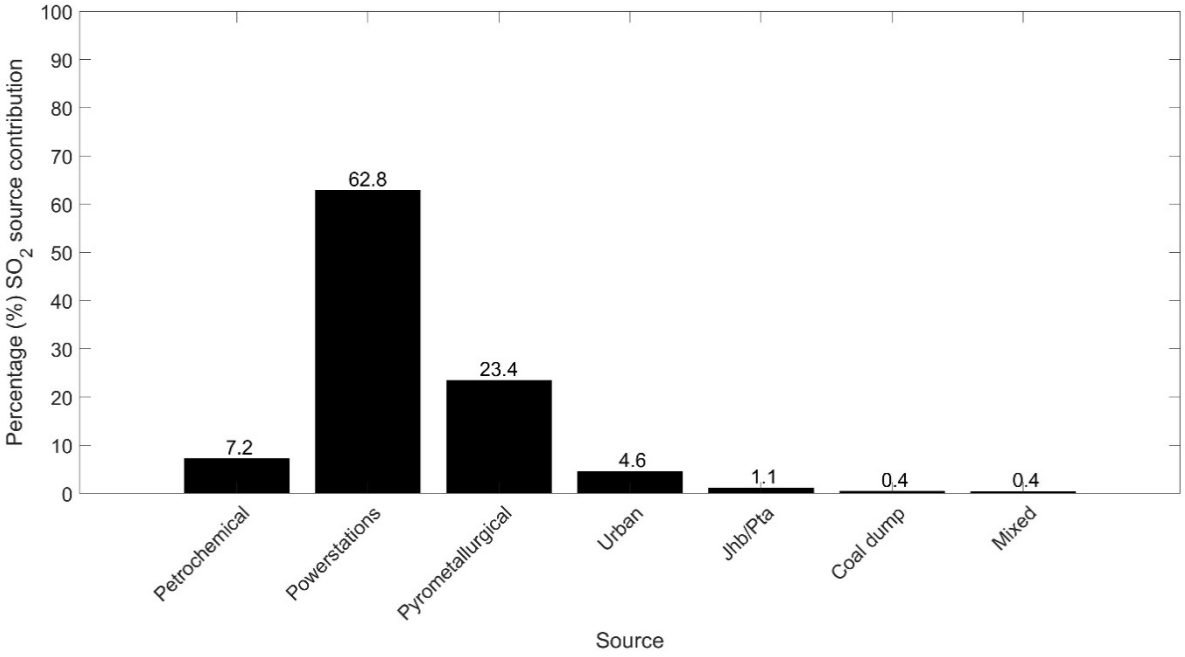


**Figure 6.22:** Percentage $SO_2$ source contributions in excess of the baseline concentrations for each of the identified sources as calculated with the method introduced in section 3.5

The three largest contributors to $SO_2$ levels in excess of baseline $SO_2$ concentrations at the monitoring site were high-stack emissions, i.e. coal-fired power stations, pyrometallurgical smelters and the petrochemical industry, which correspond with the deductions made from the temporal patterns presented for $SO_2$ levels in Chapter 5. Therefore, higher $SO_2$ concentrations are mostly measured during daytime when the depth of the PBL increases and vertical mixing occurs (Garstang *et al.,* 1996; Korhonen *et al.,* 2014; Gierens *et al.,* 2018). Coal-fired power stations made a substantially larger contribution (64%) to ambient $SO_2$ levels compared to the other sources, including pyrometallurgical smelters (23.4%) and the petrochemical industry (7.2%), which can be expected at Elandsfontein located within proximity of nine coal-fired power stations (Colette *et al.,* 2012, Chiloane *et al.,* 2017). Previous studies estimated that between 90 and 100% of sulphur entering coal-fired boilers are expected to appear as sulphur oxides ($SO_x$) in the flue gas (Cuffe *et al.,* 1964). The predominant sources of anthropogenic $SO_2$ in South Africa are coal-fired power plants with a contribution of 70% to ambient $SO_2$ estimated by the South African government (Department of Environmental Affairs, 2012), which is in the same order as the source contribution (64%) determined for $SO_2$ in this study (Figure 6.22).

The pyrometallurgical sector made the second largest contribution to atmospheric $SO_2$ concentrations exceeding the baseline at Elandsfontein. As previously mentioned, several metallurgical smelters are located in this region impacting air masses measured at Elandsfontein, while it was also indicated that these smelters are an important source of $H_2S$. The platinum group metal (PGM) smelters, especially, are associated with high $SO_2$ emissions due to the sulphite-rich ore utilised in the production of these metals (Xiao & Laplante, 2004). The third largest contributor to $SO_2$ concentrations in excess of baseline levels were the petrochemical

operations near Secunda. However, the contribution was relatively low compared the contributions from coal-fired power plants and pyrometallurgical smelters, which can be ascribed to the coal pyrolysis gasification process that inhibits the formation of $SO_2$, as previously mentioned.

The contribution from low-level emissions sources, i.e. urban, Jhb-Pta megacity and coal dumps to ambient $SO_2$ concentrations measured in excess of the baseline at Elandsfontein were 4.6%, 1.1% and 0.4 %, respectively, which is significantly lower than the contributions of these sources to $H_2S$ levels. These small contributions from low-level sources to ambient $SO_2$ levels can be expected due to the nature of these sources (e.g. only certain types of fuels utilised for household combustion contributing to ambient $SO_2$), which was also revealed by the temporal patterns of $SO_2$. Mixed sources contributed 0.4% to $SO_2$ levels in excess of baseline concentrations. Similar to $H_2S$, statistics of the ratios of baseline corrected $SO_2$ concentrations divided by baseline corrected concentrations of the other species relevant to each source type are presented in Table 6.3 for future modelling purposes.

**Table 6.3:** Mean and median, as well as the 5th, 25th, 75th and 95th percentile concentration values the calculated $SO_2$ ratios

| Source | Ratio | | | | | | | | | | | |
|---|---|---|---|---|---|---|---|---|---|---|---|---|
| | $SO_2/NO_2$ | | | | | | $SO_2/NO$ | | | | | |
| | Mean | Median | 5th | 25th | 75th | 95th | Mean | Median | 5th | 25th | 75th | 95th |
| Power | 1.6 | 1.3 | 0.4 | 0.8 | 2.2 | 3.7 | 5.5 | 2.4 | 0.6 | 1.3 | 4.0 | 12.8 |
| Petro | 1.0 | 0.8 | 0.3 | 0.5 | 1.3 | 2.6 | 7.6 | 2.7 | 0.6 | 1.2 | 5.0 | 29.0 |
| Pyro | 3.1 | 2.2 | 0.5 | 1.3 | 4.1 | 8.1 | 67.6 | 27.9 | 3.2 | 11.2 | 64.0 | 265.2 |
| Urban | 1.9 | 1.0 | 0.4 | 0.6 | 2.0 | 7.9 | 41.8 | 20.4 | 1.4 | 8.9 | 46.0 | 211.4 |
| Jhb/Pta | 3.9 | 2.4 | 0.4 | 1.2 | 4.4 | 13.2 | 103.2 | 57.0 | 5.1 | 16.8 | 223.6 | 275.8 |
| Coal | 3.8 | 2.9 | 0.3 | 0.9 | 5.9 | 11.1 | 80.4 | 19.6 | 2.1 | 6.7 | 69.4 | 576.1 |
| | $SO_2/H_2S$ | | | | | | $SO_2/eBC$ | | | | | |
| | Mean | Median | 5th | 25th | 75th | 95th | Mean | Median | 5th | 25th | 75th | 95th |
| Power | 23.9 | 17.0 | 2.4 | 8.9 | 31.3 | 63.4 | 69.3 | 40.9 | 6.6 | 19.7 | 81.3 | 233.7 |
| Petro | 5.8 | 1.3 | 0.5 | 0.8 | 3.6 | 21.1 | 61.0 | 27.1 | 6.3 | 12.5 | 60.1 | 202.3 |
| Pyro | 2.7 | 1.9 | 0.7 | 1.4 | 2.8 | 7.3 | 14.2 | 9.1 | 2.5 | 5.7 | 16.2 | 43.4 |
| Urban | 17.9 | 6.7 | 1.4 | 2.6 | 18.9 | 68.7 | 61.5 | 21.4 | 3.7 | 9.3 | 54.1 | 314.1 |
| Jhb/Pta | 7.2 | 4.8 | 1.6 | 2.9 | 12.5 | 16.9 | 30.2 | 30.5 | 1.2 | 8.0 | 44.2 | 92.3 |
| Coal | 3.3 | 1.7 | 0.5 | 1.2 | 3.7 | 15.7 | 29.1 | 23.6 | 3.6 | 10.9 | 31.3 | 121.2 |

In Table 6.4, the correlation coefficients calculated for $SO_2$ in relation to other species measured in this study for each source type are presented. These correlation coefficients also agreed with the criteria applied when allocating plumes to specific sources of $SO_2$. Strong correlations are observed between $SO_2$, and $NO_2$ and NO in plumes related to the petrochemical source (0.7 and 0.8, respectively) and coal-fired power stations (0.7) with no correlations with eBC. $SO_2$ had strong correlations with $H_2S$ in air masses passing over pyrometallurgical smelters, urban areas, the Jhb-Pta megacity and coal dumps (between 0.7 and 0.9), while

$SO_2$ associated with pyrometallurgical smelters, urban sources and the Jhb-Pta conurbation also correlated moderately with $NO_2$ and eBC.

**Table 6.4:** Correlation coefficients of $SO_2$ with the other measured gaseous species and eBC for each of the different sources

| Source | Gaseous/Aerosol species | | | | Source | Gaseous/Aerosol species | | | |
|---|---|---|---|---|---|---|---|---|---|
| | $H_2S$ | $NO_2$ | NO | eBc | | $H_2S$ | $NO_2$ | NO | eBc |
| Petrochemical | 0.3 | 0.7 | 0.8 | 0 | Urban | 0.7 | 0.5 | 0.2 | 0.5 |
| Coal-fired Power stations | 0.1 | 0.7 | 0.7 | 0 | Jhb_Pta | 0.9 | 0.6 | 0.2 | 0.7 |
| Smelters | 0.8 | 0.5 | 0.1 | 0.4 | Coal dump | 0.7 | 0.2 | 0 | 0.1 |

### 6.2.3 NO source contributions

It is estimated that the energy sector is responsible for 55% of the NOx emissions in South Africa (Department of Environmental Affairs, 2012). NO emitted from sources is relatively rapidly converted to $NO_2$, which is therefore usually associated with fresher plumes. In Figure 6.23, the contributions of three different sources to NO levels in excess of baseline NO concentrations (1.3 ppbv) at Elandsfontein are presented, i.e. the petrochemical operation near Secunda (indicated as “Petrochemical”), coal-fired power stations (indicated as “Power stations”) and pyrometallurgical smelters (indicated as “Pyrometallurgical). Other sources considered in this study made a combined contribution <0.1% to NO levels measured, which were therefore not presented and discussed.

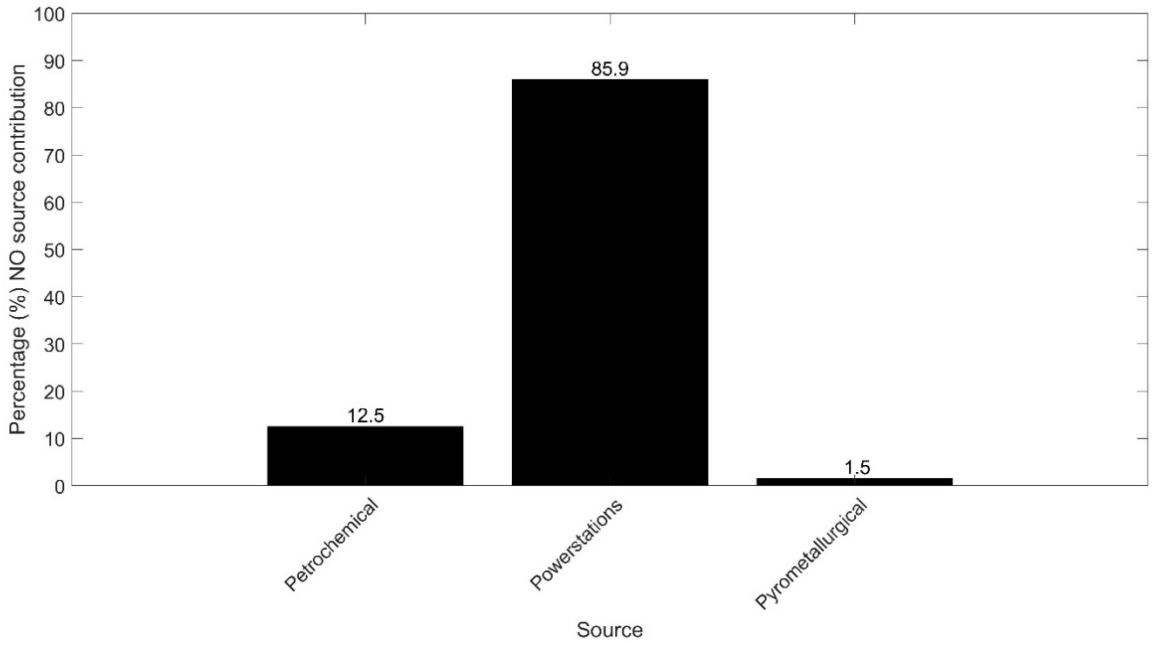


**Figure 6.23:** Percentage NO source contributions in excess of the baseline concentrations for each of the identified sources as calculated with the method introduced in section 3.5

It is evident from Figure 6.23 that the contribution of coal-fired power stations to NO levels higher than the baseline concentration measured were ~86% at this monitoring site. The second largest contributor to NO was the petrochemical plant, i.e. 12.5%, while the pyrometallurgical industry had a contribution of 1.5%. As indicated in the previous chapter, temporal patterns of NO revealed high-stack emissions to be the predominant sources of NO measured at Elandsfontein. Therefore, source contributions determined with the source apportionment method introduced in this study, correspond with these observations, since high-stack emissions are associated with these three sources identified. The highest contribution from coal-fired power stations can be expected due to these power stations being in proximity of Elandsfontein as previously mentioned. A large petrochemical plant located south-west of Elandsfontein also contributes to fresher NO-containing plumes. A very small, but not insignificant, contribution to NO levels was calculated for pyrometallurgical smelters. Considering the distance of these smelters to Elandsfontein, especially those within the BIC, most of the NO within the plumes would already be converted/oxidised to $NO_2$ by the time of arrival. Some fresher plumes arrived from the Witbank area with substantial NO concentrations. As previously mentioned, statistics of the ratios of baseline corrected NO concentrations divided by baseline corrected concentrations of the other species relevant to each source type can be used in modelling studies and are presented in Table 6.5.

**Table 6.5:** Mean and median, as well as the 5th, 25th, 75th and 95th percentile concentration values the calculated NO ratios

| Source | Ratio | | | | | | | | | | | |
|---|---|---|---|---|---|---|---|---|---|---|---|---|
| | $NO/SO_2$ | | | | | | $NO/NO_2$ | | | | | |
| | Mean | Median | 5th | 25th | 75th | 95th | Mean | Median | 5th | 25th | 75th | 95th |
| Power | 2.3 | 1.7 | 0.4 | 1.1 | 3.0 | 5.7 | 1.6 | 1.3 | 0.3 | 0.8 | 2.2 | 3.6 |
| Petro | 2.4 | 2.1 | 0.6 | 1.1 | 3.4 | 5.5 | 1.1 | 0.9 | 0.3 | 0.5 | 1.3 | 2.9 |
| Pyro | 3.2 | 3.0 | 0.5 | 1.3 | 3.9 | 8.3 | 1.7 | 1.4 | 0.3 | 0.8 | 2.2 | 4.5 |
| | $NO/H_2S$ | | | | | | NO/eBC | | | | | |
| | Mean | Median | 5th | 25th | 75th | 95th | Mean | Median | 5th | 25th | 75th | 95th |
| Power | 29.3 | 21.3 | 2.8 | 10.5 | 41.0 | 77.8 | 110.7 | 51.0 | 9.1 | 30.4 | 109.2 | 355.9 |
| Petro | 9.5 | 1.3 | 0.4 | 0.7 | 5.2 | 55.6 | 68.7 | 38.8 | 6.6 | 20.0 | 74.4 | 226.0 |
| Pyro | 14.6 | 2.2 | 0.3 | 1.3 | 7.4 | 61.7 | 64.1 | 20.5 | 1.1 | 5.4 | 51.1 | 323.4 |

In Table 6.6, the correlation coefficients calculated for NO with other species measured in this study for the three source types identified as the sources of NO are presented. Strong corelations are evident between NO, and $SO_2$ and $NO_2$ (0.8 and 0.7, respectively) for air masses passing over the petrochemical plant. A strong correlation (0.7) was also calculated between NO and $NO_2$ in plumes associated coal-fired power station, while a moderate correlation is observed between NO and $SO_2$ (0.5) in these plumes. Moderate correlations were determined between NO, and $SO_2$ and $NO_2$ in plumes arriving from pyrometallurgical smelters at Elandsfontein. Weak correlations were determined between NO and $H_2S$ for each of the sources, with no correlation with eBC.

**Table 6.6:** Correlation coefficients of NO with the other measured gaseous species and eBC for each of the different sources

| Source | Gaseous/Aerosol species | | | |
|---|---|---|---|---|
| | $H_2S$ | $NO_2$ | $SO_2$ | eBc |
| Petrochemical | 0.2 | 0.7 | 0.8 | -0.1 |
| Coal-fired Power stations | 0.1 | 0.7 | 0.5 | 0 |
| Smelters | 0.2 | 0.5 | 0.4 | 0 |

### 6.2.4 $NO_2$ source contributions

Figure 6.24 presents a bar plot of the $NO_2$ source contributions to ambient $NO_2$ concentrations in excess of the baseline (9.1 ppbv). Eight different sources corresponded with increased $NO_2$ levels at Elandsfontein, namely the petrochemical operation near Secunda (indicated as "Petrochemical"), coal-fired power stations (indicated as "Power stations"), pyrometallurgical smelters (indicated as "Pyrometallurgical"), urban sources excluding the Jhb/Pta megacity and traffic emissions (indicated as "Urban"), Jhb/Pta megacity emissions (indicated as "Jhb/Pta"), traffic emissions as identified by Chiloane *et al.* (2018) (indicated as "Traffic"), spontaneous combustion of coal dumps/seams (indicated as "Coal dump") and lastly a combination of sources (indicated as "Mixed").

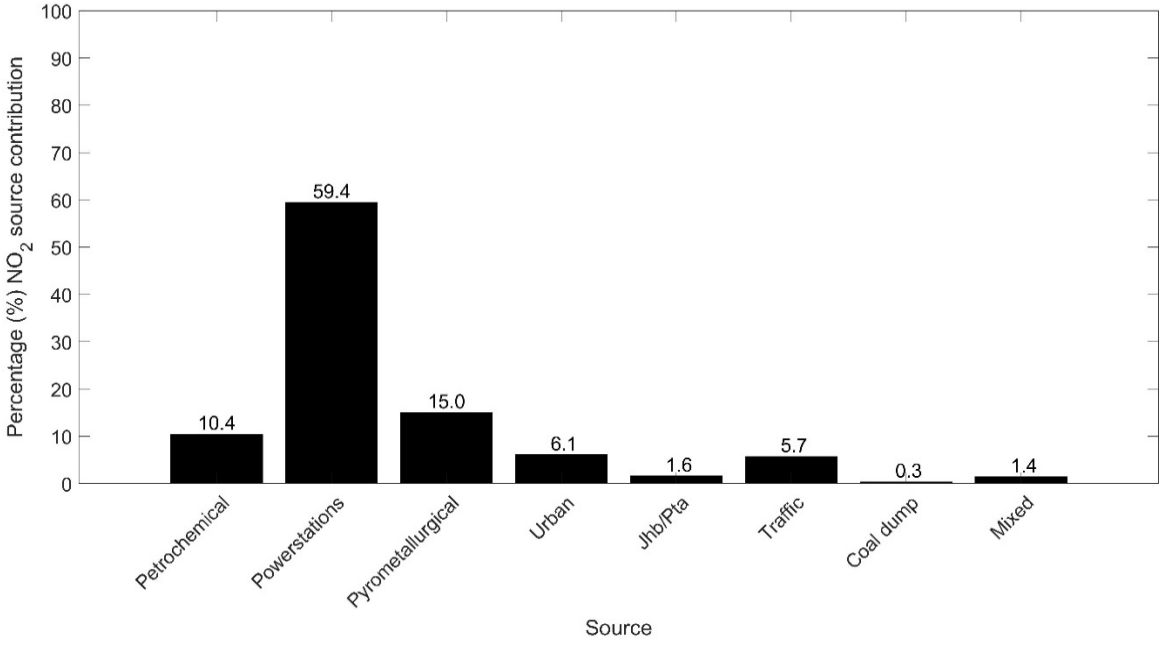


**Figure 6.24:** Percentage $NO_2$ source contributions in excess of the baseline concentrations for each of the identified sources as calculated with the method introduced in section 3.5

The largest contributor to ambient $NO_2$ concentrations measured in excess of the baseline concentrations was observed at Elandsfontein emissions from coal-fired power stations, i.e. 59.4%, which also made the largest contribution to the NO as indicated above. It is well known that the coal-fired power generation sector is a major source of atmospheric $NO_2$ in this north-eastern region of South Africa (Colette *et al.,* 2010; Swartz *et al.,* 2020; Laban *et al.,* 2018). $NO_2$ is not emitted directly into the atmosphere in large quantities from coal-fired power stations with NO being primarily emitted. Gerstle *et al.* (1965), for example, indicated that less than 1% of $NO_x$ in flue gas emissions from coal-fires power stations were $NO_2$. However, after NO is emitted, it is rapidly oxidised in the atmosphere to form $NO_2$ (Elshout & Beilke, 1985). As previously indicated,

Elandsfontein is located within proximity of nine coal-fired power stations influencing air masses measured at this site. The second largest source of $NO_2$ above the baseline was found to be the pyrometallurgical smelters (15%), while the petrochemical sector was the third largest contributor (10.4%). These percentage contributions from these three predominant sources of $NO_2$ correspond to the source contribution determined for $SO_2$. Therefore, high-stack emissions were also a major source of $NO_2$ as revealed through the temporal patterns of $NO_2$ (Chapter 5). Considering that emissions attributed to petrochemical operation were from one plant, in relation to numerous coal-fired power stations and pyrometallurgical plants, this percentage contribution to $NO_2$ (and to $SO_2$) measured at Elandsfontein is significant. The difference between the source contribution from petrochemical operation and pyrometallurgical smelters to NO and $NO_2$ levels measured, i.e. being the second and third largest contributors to NO, respectively, while it is the third and second largest contributors to $NO_2$, respectively, can be attributed to the distance of these sources from Elandsfontein as discussed for NO above. Furthermore, a larger percentage source contribution from pyrometallurgical smelters to ambient $SO_2$ concentrations compared to the percentage contribution of this source to $NO_2$ can also be ascribed to the sulphite-rich ore from which these metals are extracted with these smelters also being an important source of $H_2S$ (Xiao & Laplante, 2004).

Urban and traffic emissions contributed 6.1% and 5.7%, respectively to $NO_2$ levels exceeding baseline concentrations thereof at Elandsfontein, while the Jhb-Pta megacity contributed 1.6%. The percentage contributions from urban sources and the Jhb-Pta megacity were similar than the contributions of these sources to $SO_2$, with a combined contribution of 7.7% to $NO_2$ in excess of the baseline. Furthermore, since urban emissions also included traffic emissions as stated above, these three sources could be combined, which contribute 13.4% to $NO_2$ above the baseline. Therefore, considering this combined percentage contribution and the temporal $NO_2$ patterns presented in Chapter 5, these low-levels sources also make an important contribution to $NO_2$ levels measured at Elandsfontein. A very small contribution to $NO_2$ concentrations measured at Elandsfontein was determined for burning coal-dumps (0.3%), which is similar to the contribution of this source type to ambient $SO_2$ levels. Mixed source contributed to 1.4% of $NO_2$ in excess of baseline levels. Ratios of baseline corrected $SO_2$ concentrations divided by baseline corrected concentrations of the other species relevant to each source type is presented in Table 6.7.

**Table 6.7:** Mean and median, as well as the 5th, 25th, 75th and 95th percentile concentration values the calculated $NO_2$ ratios

| Source | Ratio | | | | | | | | | | | |
|---|---|---|---|---|---|---|---|---|---|---|---|---|
| | $NO_2/SO_2$ | | | | | | $NO_2/NO$ | | | | | |
| | Mean | Median | 5th | 25th | 75th | 95th | Mean | Median | 5th | 25th | 75th | 95th |
| Power | 0.8 | 0.6 | 0.1 | 0.3 | 1.1 | 2.0 | 0.8 | 0.5 | 0.1 | 0.3 | 0.8 | 1.9 |
| Petro | 0.4 | 0.3 | 0.0 | 0.1 | 0.4 | 0.9 | 0.5 | 0.3 | 0.0 | 0.2 | 0.7 | 1.4 |
| Pyro | 0.1 | 0.1 | 0.0 | 0.0 | 0.2 | 0.5 | 0.1 | 0.1 | 0.0 | 0.0 | 0.1 | 0.3 |
| Urban | 0.2 | 0.1 | 0.0 | 0.1 | 0.2 | 0.5 | 0.4 | 0.1 | 0.0 | 0.1 | 0.3 | 1.7 |
| Jhb/Pta | 0.1 | 0.1 | 0.0 | 0.0 | 0.2 | 0.4 | 0.2 | 0.1 | 0.0 | 0.0 | 0.2 | 0.8 |
| Traffic | 0.1 | 0.1 | 0.0 | 0.0 | 0.2 | 0.3 | 0.4 | 0.2 | 0.0 | 0.1 | 0.4 | 1.1 |
| Coal | 0.2 | 0.1 | 0.0 | 0.1 | 0.3 | 0.5 | 0.3 | 0.1 | 0.0 | 0.0 | 0.3 | 1.4 |
| | $NO_2/H_2S$ | | | | | | $NO_2/eBC$ | | | | | |
| | Mean | Median | 5th | 25th | 75th | 95th | Mean | Median | 5th | 25th | 75th | 95th |
| Power | 13.5 | 6.7 | 0.4 | 2.6 | 15.0 | 51.2 | 43.6 | 18.1 | 0.7 | 6.9 | 44.9 | 165.9 |
| Petro | 0.8 | 0.4 | 0.0 | 0.2 | 0.8 | 4.4 | 14.5 | 5.7 | 0.1 | 1.3 | 15.1 | 66.7 |
| Pyro | 0.5 | 0.1 | 0.0 | 0.0 | 0.3 | 1.2 | 1.8 | 0.4 | 0.0 | 0.1 | 1.2 | 3.6 |
| Urban | 3.3 | 0.4 | 0.0 | 0.2 | 1.1 | 6.7 | 5.5 | 1.2 | 0.2 | 0.5 | 3.0 | 25.6 |
| Jhb/Pta | 1.6 | 0.4 | 0.0 | 0.1 | 0.8 | 7.7 | 3.7 | 0.5 | 0.1 | 0.2 | 1.3 | 39.4 |
| Traffic | 0.9 | 0.5 | 0.1 | 0.2 | 1.1 | 2.4 | 0.8 | 0.5 | 0.1 | 0.2 | 0.8 | 3.7 |
| Coal | 0.7 | 0.2 | 0.0 | 0.1 | 0.7 | 3.1 | 3.0 | 2.5 | 0.1 | 0.6 | 3.8 | 12.1 |

$NO_2$ was also correlated with other species measured in this study. Correlation coefficients for each source type are presented in Table 6.8, which also corresponded with coincidental peaks of species used to classify source types. As expected, $NO_2$ had a strong correlation with NO (0.7) in plumes related to the petrochemical industry, while it a correlated moderately with $SO_2$ and $H_2S$ (0.6 and 0.4, respectively) in these plumes. Strong relationships are determined between $NO_2$, and $SO_2$ and NO (0.7) in air masses passing over coal-fired power station with no correlation with $H_2S$ and eBC in these plume events, which also supports coal-fired power station not being an important source of $H_2S$. For pyrometallurgical smelters, weak correlations are evident between $NO_2$ and other species with no correlation with $H_2S$. In plumes associated with traffic, urban sources and the Jhb-Pta megacity, weak or no correlation was determined between $NO_2$, and other species considered in this study. Although the contribution from burning coal-dump to $NO_2$ concentrations was very low, moderate correlations were calculated between $NO_2$, and $SO_2$ and $H_2S$ (0.4 and 0.6, respectively) in plumes related to this source type.

**Table 6.8:** Correlation coefficients of $NO_2$ with the other measured gaseous species and eBC for each of the different sources

| Source | Gaseous/Aerosol species | | | | Source | Gaseous/Aerosol species | | | |
|---|---|---|---|---|---|---|---|---|---|
| | $H_2S$ | $SO_2$ | NO | eBc | | $H_2S$ | $SO_2$ | NO | eBc |
| Petrochemical | 0.4 | 0.6 | 0.7 | -0.1 | Urban | 0 | 0.2 | 0 | 0 |
| Coal-fired Power stations | 0 | 0.7 | 0.7 | -0.1 | Jhb_Pta | 0 | 0.2 | 0.1 | -0.1 |
| Smelters | 0 | 0.2 | 0.1 | 0.1 | Coal dump | 0.4 | 0.6 | 0.2 | 0.1 |
| Traffic | 0 | 0.2 | 0 | 0.1 | | | | | |

## 6.3 Chapter 6: Conclusion

As the study focused only on co-incidental increases of trace gases and eBC in excess of the measured baseline to determine source contributions, a significant portion (80% in time) of the measured concentration data remains non-apportioned. Therefore, these contributions are only for the measured co-incidental concentration increases and not the measured baseline or noise, which this method is not suited for as it requires a clear and identifiable concentration peak.

Although this is a well-studied region in South Africa, ambient $H_2S$ concentrations and sources were investigated in detail for the first time in southern Africa in this study. Measurements reveals that $H_2S$ forms a considerable fraction (>20%) of the total gas phase sulphur burden over the industrial hub of South Africa. Seasonal and diurnal patterns of the $H_2S$ concentration at the Elandsfontein measurement site suggest that surface emissions are the predominant source of $H_2S$ in the region.

A review of industrial and other anthropogenic activities in the Mpumalanga Highveld suggests a number of potential sources of $H_2S$ in the region. Investigation into $H_2S$ plumes in excess of the baseline concentrations indicates substantial contributions from most of these sources. Emissions from urban areas (excluding the Jhb-Pta megacity) were identified as the largest contributor, which accounted for 34.6% of the $H_2S$ in excess

of the baseline concentrations. This was not expected; however, a similar deduction could be made from the bi-modal concentration peaks observed in the diurnal graph for $H_2S$ in section 5.3.1. In addition, the Jhb-Pta megacity contributed another 10.9%, which was a bit lower than the contribution from the petrochemical operation near Secunda (17.9%). It should be noted that the petrochemical operation is a single source and plumes from this source would only be measured if meteorological conditions are favourable. Pyrometallurgical smelters, coal-fired power stations, burning coal dumps and large feedlots contributed approximately 19.8, 4.7, 3.8 and 0.4%, respectively. However, it should be noted that especially urban and megacity categories may contain contributions from surrounding industrial sources. As noted in sections 6.1.4.ii and 6.2.1, it was not expected for coal-fired power stations to contribute to the $H_2S$ measured in excess of the baseline. However, due to the energy crises in South Africa and frequent stop and start of power stations, $H_2S$ can be produced.

Currently, the South African DFFE is considering the formulation of regional-specific $H_2S$ ambient air quality standard limits. The results from this study should be used to inform this process. The combined contributions from urban regions (excluding Jhb-Pta megacity) and the Jhb-Pta megacity were 45.5% to $H_2S$ concentrations in excess of the baseline in the Mpumalanga Highveld. This indicated that the focus should foremost be on poverty alleviation, which will reduce household combustion of low grade coal in semi- and informal settlements, as well as matters controlled by local and municipal government, e.g. uncontrolled refuse combustion, mismanaged sewage water facilities (e.g. Tempelhoff, 2009) and poorly maintained diesel vehicles that are allowed to be used – all of which are likely sources to contribute to the observed emissions associated with urban emissions of $H_2S$.

The temporal assessment of $SO_2$ indicated that the main contributor of ambient $SO_2$ measured at Elandsfontein was of high stack origin. This deduction agrees with what is seen in Figure 6.22, the source contribution graph for $SO_2$. Here it was clear that coal-fired power stations had the biggest contribution of $SO_2$ measured above the baseline at Elandsfontein with 62.8%. The next largest contributor of $SO_2$ was the pyrometallurgical sector with 23.4%, followed by the petrochemical sector with 7.2%. Urban, Jhb/Pta, coal-dumps and mixed sources each contributed 4.6%, 1.1%, 0.4% and 0.4% respectively to the total quantity of $SO_2$ measured at Elandsfontein above the baseline.

For NO, only three sources could be identified, e.g. coal-fired power stations, the petrochemical plant and pyrometallurgical smelters. These sources could all be considered high-stack emission sources, and this agrees with the temporal assessment for NO in section 5.3, which indicated that high-stack emissions dominated the measured ambient NO.

In section 5.3, it was indicated that high-stack emissions also dominated ambient $NO_2$. This makes sense, as $NO_2$ is not emitted directly but as a by-product of NO emissions as NO gets oxidised to $NO_2$. Therefore, if the primary emissions of NO were of high-stack origin, $NO_2$ would follow suit. From the calculated source

contributions of $NO_2$ measured above the baseline (Figure 6.24), it was evident that high-stack sources dominated the emissions, and the coal-fired power station source was the main contributor with 59.4%. The pyrometallurgical and petrochemical sectors contributed 15% and 10.4%, respectively, followed by urban (6.1%) and traffic emissions (5.7). The Jhb/Pta conurbation, coal dumps and mixed sources contributed 1.6%, 0.3% and 1.4% to the total $NO_2$ measured at Elandsfontein above the baseline, respectively.

In addition to the abovementioned source contributions, statistics of the ratios of baseline- corrected concentrations divided by baseline-corrected concentrations of the other species relevant to each source type were presented. Such ratios can be used in future modelling studies as approximated emission ratios to estimate trace gas concentrations, if only concentration(s) of other species are known. However, care should be taken when these ratios are used, since atmospheric conversion processes of the various species are influenced by plume age, methodological conditions (e.g., high stack emissions mostly observed during certain times of the day on the South African Highveld) and ambient conditions (e.g. difference between daytime and night-oxidation processes). A great limitation of the method is that it is dependent on the user ultimately to decern what the most appropriate source of the plume is and could often result in erroneous attribution to source categories. This is seen in the discrepancies between the ratio statistics presented in Tables 6.1, 6.3, 6.5 and 6.7. Similar ratios should be observed for species pairs when comparing the same sources; however, this was not observed. This, therefore,, points to erroneous inclusion of plumes in source categories.

# Chapter 7: Conclusions, project evaluation and recommendations

**In this chapter,** the main conclusions from the study are summarised in section 7.1, followed by a project evaluation (section 7.2) in terms of the successes and shortcomings of this study in relation to the general aim and objectives presented in Chapter 1. Lastly, recommendations for future research stemming from the main findings in this thesis are presented in section 7.3.

## 7.1 Conclusions

In this study, the first receptor-oriented source quantification for hydrogen sulphide ($H_2S$) on the Mpumalanga Highveld is presented, which also included burning coal dumps as a source as established with a novel and unique application of satellite observations. In addition, this method was also applied to determine sources of other trace gas species measured at this site located in the Mpumalanga Highveld (Elandsfontein), i.e. nitric oxide (NO), nitrogen dioxide ($NO_2$) and sulphur dioxide ($SO_2$), of which $NO_2$ and $SO_2$ are criteria pollutants, according to South African legislation. Existing receptor source apportionment techniques are not suited for trace gas source apportionment, while source-oriented models were not considered, since a comprehensive peer-reviewed South African-specific emission inventory was not available in the public domain at the time when this study commenced. The main deductions from the study are subsequently considered in relation to each of the results chapters presented in this thesis.

### 7.1.1 Chapter 4: Spontaneous combustion activities associated with coal mining on the Mpumalanga Highveld

Spontaneous combustion of coal in the Mpumalanga Highveld has a large environmental impact, especially on-air quality. Through the use of fire radiative power (FRP) data, it was found that five sites in the Mpumalanga Highveld were prone for spontaneous combustions over a 19-year period. These sites were all opencast mines situated on top of old board-and-pillar mines.

Of these five sites, two sites (labelled as sites A and B) were particularly active, recording burning throughout the period. A relatively well-developed seasonal variation was observed within the spontaneous combustion activities, with combustion events more common during winter months as a result of the suppression of these events during rain events in the summer season.

Considering the frequent activity of these spontaneous combustion events and pollutants released from these events, a detailed characterisation of these emissions is urgently needed. The FRP-based method used here demonstrates that remote sensing observations can be utilised to determine when there is active burning at a site. Furthermore, it offers a way to incorporate emissions associated with these spontaneous combustion of coal events in air quality models (see Sofiev *et al.,* 2009), once the emission factors have been quantified. However, factors limiting the quantification with this approach include the resolution of the Moderate Resolution Imaging Spectroradiometer (MODIS) measurement instrumentation and frequency of satellite pass-overs over a specific area under investigation.

### 7.1.2 Chapter 5: Air quality in the rural Mpumalanga Highveld

Data coverage for the species under investigation, i.e. $SO_2$, NO, $NO_2$ and $H_2S$ were 82%, 85%, 83% and 75%, respectively, which can be considered good data coverage. Data gaps were mostly attributed to rolling power outages/load shedding, as South Africa was plagued by an energy crisis (Pretorius *et al.,* 2015). However, these gaps were evenly distributed throughout the sampling period and were not clustered to provide bias. Other small gaps in the data were attributed to quality assurance/-control procedures during which data points considered questionable and uncertain were removed to ensure a high-quality dataset (Laakso *et al.,* 2012; Beukes *et al.,* 2015).

There were very few exceedances of the national ambient air quality standards (NAAQS) of the criteria pollutants assessed in the study. $SO_2$ only exceeded the 10-minute standard limit of 191 ppbv twice (526 exceedance allowed annually) and the 1-hour standard limit of 134 ppbv six times (88 exceedance allowed annually). $NO_2$ exceeded the 1-hour standard of 106 ppbv eight times throughout the study period (88 exceedance allowed annually), while the annual standard of 21 ppbv was not exceeded. Although $H_2S$ does not have an NAAQS limit, a single hourly average concentration exceeding 29 ppbv is considered a high $H_2S$ day. The measured $H_2S$ exceeded this guideline 47 times on 13 different days (Table 5.2). This is interesting as the Mpumalanga Highveld, or more specifically the Highveld Priority Area, is considered to be a pollution hotspot with regard to $SO_2$ and $NO_2$. However, the criteria pollutants experienced very little exceedances of the NAAQS and WHO ambient air quality standards.

A distinct seasonal variation was observed in most of the investigated gases with trace gas concentrations reaching highs in the colder winter months when more pronounced meteorological conditions trap pollutants and there is an increase in biomass burning activities. Furthermore, from diurnal variations of the species, it was seen that ambient $H_2S$ concentrations were mostly ascribed to low-level emissions (as depicted by bimodal peaks). However, there was also an important contribution from high-stack emissions to $H_2S$ levels measured at Elandsfontein. $SO_2$, NO and $NO_2$ concentrations were mostly influenced by high-stack emissions, which is not uncommon for this area, as particularly revealed through a large single peak in the diurnal pattern, which is attributed to the downward mixing of high-stack emission after the break-up of low-level inversion layers and an increase in the planetary boundary layer (PBL) height.

### 7.1.3 Chapter 6: Trace gas source contributions

Various case studies were presented to illustrate how plumes from sources comprising different compositions of major trace gas species and equivalent black carbon (eBC) were identified and categorised. Case studies presented plumes associated with urban sources (excluding Jhb-Pta megacity), the Jhb-Pta megacity, pyrometallurgical smelters, coal-fired power stations, cattle feed lots, burning coal dumps and traffic emissions.

The source contribution derived with the novel method developed in this study corresponded with the temporal patterns. It was shown that low-level emission sources were the main contributor to ambient $H_2S$ measured at Elandsfontein, with high- stack emissions also being an important (but not dominant) source. Here, the *urban* source made the largest contribution (34.6%) in excess of the baseline, while the Jhb-Pta megacity source contributed 10.9% to $H_2S$ concentrations measured at Elandsfontein. Therefore, if the contributions from these defined sources are combined, it is evident that urban sources contribute significantly to $H_2S$ in the Mpumalanga Highveld. The pyrometallurgical and petrochemical sectors contributed 19.8% and 17.9%, respectively, which was somewhat surprising since these sources, especially the petrochemical plant, are generally considered $H_2S$ emitters. It is to be noted that the point source for the *petrochemical* category is a single point source and emission plumes would only be measured during favourable meteorological conditions. Since the combustion process in coal-fired power stations is not favourable for the formation of $H_2S$, it was not expected to see a significant contribution from this source. However, it was identified that the coal-fired power sector contributed 4.7% $H_2S$ in excess of the baseline. $H_2S$ produced here was most probably from non-ideal oxidative environments during boiler start-ups, and not the utilisation of low-NOx burners, as very few power stations were retrofitted with these burners during the study period. Burning coal dumps and feed lots had the lowest contributions to $H_2S$ levels measured at Elandsfontein, i.e. 3.8% and 0.4%, respectively, in excess of the baseline concentration.

Source apportionment of $SO_2$ also revealed high-stack emissions to be most significant source of $SO_2$ exceeding baseline levels as indicated by the temporal trends. Here it was indicated that coal-fired power stations made the largest contribution to $SO_2$ measured above the baseline at Elandsfontein, i.e. 62.8%. The second largest contribution (23.4%.) was the pyrometallurgical sector, while the petrochemical-, urban-, Jhb-Pta megacity- and coal dump sources contributed 7.2%, 4.6%, 1.1% and 0.4%, respectively, in excess of baseline levels.

For NO, three sources could be identified, i.e. coal-fired power stations, the petrochemical plant and pyrometallurgical smelters, with all three of these sources associated with high-stack emissions. Coal-fired power stations had the largest contribution of 85.9%, followed by the petrochemical sector and the pyrometallurgical sector with contributions of 12.5% and 1.5% measured above the baseline, respectively. As NO oxidises in the atmosphere into $NO_2$, NO was only observed in fresh plumes. Therefore, NO will also only be picked up by the method in very favourable meteorological conditions when freshly emitted plumes arrive at the measurement site.

The main sources of $NO_2$, determined with the novel method developed in this study, were also high-stack emissions, while a smaller, but not insignificant, contribution was related to low-level emissions. This also corresponded with the observed temporal patterns of $NO_2$. In addition, higher contributions to $NO_2$ levels were from similar sources than for $SO_2$ and NO. This is expected, since $NO_2$ forms from NO,

while it is also well-known that, especially coal-fired power stations emit $SO_2$ and $NO_x$. Therefore, it was no surprise that coal-fired power stations made the largest contribution, i.e. 59.4% to $NO_2$ in excess of the baseline. Other high-stack sources, which include the pyrometallurgical sector and petrochemical sector. contributed 15% and 10.4%, respectively. to $NO_2$ above the measured baseline. Low-level emissions had the lowest contributions. with urban, traffic, the Jhb-Pta megacity and burning coal dumps contributing 6.1%, 5.7%, 1.6% and 0.3%, respectively.

Ratio statistics and correlation coefficients were calculated and presented with the idea that these could be used in other source apportionment or modelling studies to estimate the concentration values of co-emitted species if they have not been measured. However, due to discrepancies between the ratios of different sources for the same species pairs, it was highlighted that these values might not be suitable and more work and refinement need to be completed on the method.

## 7.2 Project evaluation

In order to assess whether the general aim of the study presented in Chapter 1 has been met, the study is evaluated in terms of each of the four specific objectives listed in Chapter 1.

***I.) Contextualise $H_2S$, NO, $NO_2$ and $SO_2$ concentrations measured at Elandsfontein by comparison to appropriate ambient air quality legislation and measurements conducted elsewhere, as well as assess temporal patterns of these species***

In Chapter 5, the concentrations of $H_2S$, NO, $NO_2$ and $SO_2$ determined in this study were compared and contextualised to local and global air quality standards, as well as measurements of these species conducted in other parts of the world. It was successfully indicated that the two criteria pollutants, i.e. $SO_2$ and $NO_2$, were in compliance with ambient air quality standards limits, which were only exceed on a few occasions (well below the number of allowed exceedances). $H_2S$ does not have a standard limit, but could be contextualised in relation to the guideline of a single hourly average concentration exceeding 29 ppbv. This guideline was exceeded on 13 days. Comparison of these gaseous species with measurements thereof elsewhere indicated for the most part that $H_2S$, $SO_2$ and $N_2O$ were generally higher than other measurement sites within high industrial sectors.

***II.) Identify sources that could contribute to the inorganic trace gas concentrations at the site. This also included applying a novel method utilising satellite measurements to determine when coal dumps/seams were actively burning in the area surrounding Elandsfontein as a result of spontaneous combustion, which was one of the sources considered***

Using the method developed by Beukes *et al.* (2018), in which a novel application of MODIS FRP retrievals was used, actively burning coal dumps/seams in the Mpumalanga Highveld could also be successfully identified in this study. Most of the spontaneous combustion activities were related to open cast mines

located above old board-and-pillar mines, which are prone to spontaneous combustion when contact is made with oxygen during re-mining. Possible limitations associated with this methodology are the resolution of MODIS instrumentation that might not detect smaller thermal anomalies and therefore do not reveal smaller burning coal dumps/seams, while the frequency of pass-over times can also limit the application of this methodology. However, factors limiting the quantification with this approach include the resolution of the Moderate Resolution Imaging Spectroradiometer (MODIS) measurement instrumentation and frequency of satellite pass overs over a specific area under investigation.

The main sources identified to impact the ambient concentrations of $H_2S$, $SO_2$, $NO_2$ and NO at the measurement site (Elandsfontein) in the Mpumalanga Highveld included urban sources (excluding Jhb-Pta megacity), the Jhb-Pta megacity, pyrometallurgical smelters, coal-fired power stations, cattle feed lots, burning coal dumps and traffic emissions. Temporal (seasonal and diurnal) indicated that a combination of high-stack and low-level emissions had an influence on the ambient concentrations of these gaseous species, with predominant sources also revealed.

***III.) Conduct source apportionment and quantification of $H_2S$, $SO_2$, $NO_2$ and NO, as well as quantification and contextualisation of the measured baseline of these species, with the novel method developed in this study***

The method introduced by Chiloane *et al.* (2017) in which eBC measured at Elandsfontein was related to sources by exploring the chemical composition of plumes impacting the site, were further developed and successfully applied in this study. An algorithm/flow diagram for the novel source quantification method developed in this study for atmospheric gaseous species was compiled and presented, which could also be used in other studies. Prior to this study, source apportionment could only be conducted by establishing the chemical composition of atmospheric particulate matter, which is subjected to advances statistical methods.

This novel method was applied to determine the predominant sources of atmospheric $H_2S$, $SO_2$, $NO_2$ and NO at Elandsfontein. Furthermore, baseline concentrations of these gaseous species could also be established. For $H_2S$, 92% of plumes measured in excess of the baseline could be attributed to a specific source, while 100%, 98.6% and 99.6% of NO, $NO_2$ and $SO_2$, respectively, in excess of the baseline, could be related to a specific source. It was indicated that the low-level emissions associated with urban sources were the major sources of $H_2S$, while high-stack emissions related to coal-fired power stations, pyrometallurgical smelters and petrochemical operations made the largest contribution to ambient $SO_2$, $NO_2$ and NO in excess of baseline levels.

However, although the source apportionment method developed in this study could be applied to determine the main sources of atmospheric gaseous species, there are some limitations associated with this method. The contributions determined from each of the sources identified should be interpreted in terms of the number or percentages of plumes that impacted Elandsfontein from these sources and are not absolute

quantifications of the exact concentrations of these species emitted by these sources. Therefore, for instance, it is well known that the petrochemical plant impacting Elandsfontein emits high concentrations of $H_2S$, which could exceed $H_2S$ levels associated with urban sources determined in this study to make the largest contribution to the number of plumes comprising $H_2S$. Furthermore, this source apportionment method introduced in this study is tedious and laborious, which could be further developed and improved. Also, the method relies on the discretion of the user to allocate a measured plume to a specific source based on the plume timing, amplitude, species present, back trajectories and emission sensitivities. Therefore, if this requires a great understanding of the underlying chemistry and meteorology by the user in order to implement, the method and plumes can quite easily be erroneously attributed to a specific source. Furthermore, the ratio statistics, as presented in Chapter 6, still need some refinement in order to be used in other modelling studies. There are discrepancies between the ratios of species pairs of similar sources, and these values should be similar.

## 7.3 Recommendations

Although the objectives were achieved and a deeper understanding with regard to the contributions of sources of trace gas species in the Mpumalanga Highveld was gained, these new insights also brought about new scientific questions pertaining to the topic. In essence, this is what scientific research should do, i.e. answer existing questions, which lead to new questions. According to the candidate, at least the following five aspects should be addressed in future investigations:

- In the current study, only coincidental peaks in excess of the respective baseline concentrations were considered. The total time of all such peaks added up to approximately 20% of the overall time of the dataset for each trace gas species. Therefore, there is still a significant amount of gas unaccounted for (not attributed to a source), which is likely emitted by large point sources but had significant time to mix and dilute with other pollution sources or emitted by small/defuse sources. It is vital to quantify these background trace gas concentrations since it is important to understand the background trace gas levels before regulatory measures are considered and implemented.

- This study deemed it possible to do receptor-oriented source quantification of trace gas species at a site in the Mpumalanga Highveld. Therefore, to further strengthen the method, it is suggested to apply/employ this method to numerous sites with different source characteristics. This will provide valuable information on pollution sources.

- Only NO and $NO_2$ were investigated, as the combined $NO_x$ ambient concentrations were analysed, it would be prudent to further investigate and apply the source apportionment method to the measured $NO_x$.

- The method is not automated and requires rigorous input and advanced knowledge from the user. Further development of technologies such as machine learning, neural networks and other automation techniques should strive to automate the method to enable a broader user community.
- The FLEXPART emission sensitivity data is also not easily accessible and requires significant user and technical input, which is a crucial hindrance to overcome if the method is to be used by a wider audience.
- The South African government should continue to target high-stack emitters, especially coal-fired power operations, as well as low-level emissions, in particular household combustion and waste removal practices to reduce emissions of these gaseous species as determined in this study. The latter will require more comprehensive and intensive efforts since it entails in improvement of socio-economic circumstances.

# Bibliography

Aas, W., Mortier, A., Bowersox, V., Cherian, R., Faluvegi, G., Fagerli, H., Hand, J., Klimont, Z., Galy-Lacaux, C., Lehman, C.M.B., Mhyre, C.L., Mhyre, G., Olivie, D., Sato, K., Quaas, J., Rao, P.S.P., Schulz, M., Sh+Hindell, D., Skeie, R.B., Stein, A., Takemura, T., Tsyro, S., Vet, R. & Xu, X. 2019. Global and regional trends of atmospheric sulfur. *Scientific Reports*, 9:953. https://doi.org/10.1038/s41598-018-37304-0

Abdi, H. & Williams, L.J. 2010. Principal component analysis. *Interdisciplinary Reviews Computational Statistics,* 2(4):733-459, doi: https://doi.org/10.1002/wics.101.

Abdul-Wahab, S.A., Bakheit, C.S. & AL-ALAWI, S.M. 2005. Principal component and multiple regression analysis in modelling of ground-level ozone and factors affecting its concentrations. *Environmental Modelling & Software*, 20(10):1263-1271, doi: 10.1016/j.envsoft.2004.09.001.

Adesina, J.A., Piketh, S.J., Burger, R.P. & Mkhatshwa, G. 2022. Assessment of criteria pollutants contributions from coal-fired plants and domestic solid fuel combustion at the South African industrial highveld. *Cleaner Engineering and Technology,* 6:100358, doi: https://doi.org/10.1016/j.clet.2021.100358.

Adeyemi, A., Molnar, P. & Boman, J. 2021. Source apportionment of fine atmospheric particles using positive matrix factorization in Pretoria, South Africa*. Environmental Monitoring and Assessment*, 193:716, doi: https://doi.org/10.1007/s10661-021-09483-3.

Ahjum, F. 2020. SADC e-Mobility Outlook: Accelerating Low Carbon Transport Futures.

Airshed Planning Professionals. 2017. Atmospheric Impact Report: Sasol Secunda Synfuels Operations. Report no.: 16SAS03, Rev 1.

Air Resources Laboratory. 2014. National Oceanic and Atmospheric Administration (NOAA). http://www.arl.noaa.gov/ Date of access: 20 Jul. 2019.

Alfeus, A., Molnar, P., Boman, J., Hopke, P. & Wichmann, J. 2023. PM2.5 in Cape Town, South Africa: Chemical characterization and source apportionment using dispersion-normalised positive matrix factorization. *Atmospheric Pollution Research*, 15, doi: https://doi.org/10.1016/j.apr.2023.102025.

Arogo, J., Zhang, R.H., Riskowski, G.L., and Day, D.L. 2000. Hydrogen sulfide production from stored liquid swine manure: a laboratory study. *Transactions of the ASAE*. 43(5): 1241-1245.

Atkinson, R. 2000. Atmospheric chemistry of VOCs and NOx. *Atmospheric Environment,* 34(12-14):2063-2101.

Baars, H., Kanitz, T., Engelmann, R., Althausen, D., Heese, B., Komppula, M., Preißler, J., Tesche, M., Ansmann, A., Wandinger, U., Jae-Hyun L., Joon Young A., Stachlewska, I.S., Amiridis, V., Marinou, E., Seifert, P., Hofer, J., Skupin, A., Schneider, F. & BohlmanN, S. 2016. An overview of the first decade of

PollyNET: an emerging network of automated Raman-polarization lidars for continuous aerosol profiling. *Atmospheric Chemistry & Physics*, 16:5111-5137, doi: 10.5194/acp-16-5111-2016.

Backman, J., Virkkula, A., Vakkari, V., Beukes, J.P., Van Zyl, P.G., Josipovic, M., Piketh, S., Tiitta, P., Chiloane, K., Petäjä, T., Kulmala, M., Laakso, L. 2014. Differences in aerosol absorption Angstrom exponents between correction algorithms for a particle soot absorption photometer measured on the South African Highveld. *Atmospheric Measurement Techniques*, 7:4285-4298, doi: https://doi.org/10.5194/amt-7-4285-2014.

BalmER, M. 2007. Household coal use in an urban township in South Africa. *Journal of Energy in Southern Africa*, 18:27-32, doi: http://dx.doi.org/10.17159/2413-3051/2007/v18i3a3382.

Belaid, M., Falcon, R., Vainikka, P. 2014. Pulverized coal versus circulating fluidized-bed boilers Perspectives and challenges for South Africa. *South African Journal of Chemical Engineering*, 19:72-81.

Belis, C.A., Larson, B.R., Amato, F., El Haddad, I., Favez, O., Harrison, R.M., Hopke, P.K., Nava, S., Paatero, P., Quass, U., Vecchi, R., Viana, M. & Prevot, A. 2014. European Guide on Air Pollution Source Apportionment with Receptor Models; Joint Research Centre, Institute for Environment and Sustainability: Luxembourg: Publications Office of the European Union, doi: 10.2788/9307.

Beukes, J.P., Venter, A.D., Josipovic, M., Van Zyl, P.G., Vakkari, V., Jaars, K., Dunn, M. & Laakso, L. 2015. Automated continuous air monitoring. (*In* FORBES, P., *ed*. Monitoring of Air Pollutants – Sampling, Sample, Preparation and Analytical Techniques, Elsevier. In press.).

Beukes, J.P., Du Preez, S.P., Van Zyl, P.G., Paktunc, D., Fabritus, T., Päätalo, M. & Cramer, M. 2017. Review of Cr(VI) environmental practices in the chromite mining and smelting industry: Relevance to development of the Ring of Fire, Canada. *Journal of Cleaner Production*, 165:874-889, doi: http://dx.doi.org/10.1016/j.jclepro.2017.07.176.

Beukes, J.P., Van Zyl, P.G., Sifiev, M., Soares, J., Liebenberg-Enslin, H., Shackleton, N. & Sunström, A.-M. 2018. The use of satellite observations of fire radiative power to estimate the availabilities (activity patterns) of pyrometallurgical smelters. *The Journal of the Southern African Institute of Mining and Metallurgy*, 118:619-624, doi: http://dx.doi.org/10.17159/2411-9717/2018/v118n6a9.

Bhave, P.V., Fergenson, D.P., Prather, K.A. & Cass, G.R. 2001. Source apportionment of fine particulate matter by clustering single-particle data: Tests of receptor model accuracy. *Environmental Science and Technology*, 35:2060-2072. doi:10.1021/es0017413.

Blanchard, C.L., Tanenbaum, S. & Hidy, G.M. 2012. Source contributions to atmospheric gases and particulate matter in the Southeastern United States. *Environmental Science and Technology*, 46:5479-5488, doi: https://doi.org/10.1021/es203568t.

Bond, W.J., Keeley, J.E. 2005. Fire as a global “herbivore”: The ecology and evolution of flammable ecosystems. *Trends in Ecology and Evolution,* 20(7), 387 – 394, doi: https://doi.org/10.1016/j.tree.2005.04.025.

Bruwer, A.P. & Kornelius, G. 2017. Modeling the effects of biogenic NOx emissions on the South African Highveld and Waterberg regions. *Water, Air & Soil Pollution*, 228:326, doi: https://doi.org/10.1007/s11270-017-3526-y.

Brunekreef, B. & Holgate, S.T. 2002. Air pollution and health. *The Lancet*, 360(9341):1233-1242.

Bunt, J.R. & WAANDERS, F.B. 2008. Identification of the reaction zones occurring in a commercial-scale Sasol-Lurgi FBDB gasifier. *Fuel*, 87:1814-1823, doi: 10.1016/j.fuel.2007.11.012.

Camacho, A. 2009. Sulphur Bacteria. (*In* LIKENS, G.E., Plankton of Inland Waters, 1st ed.), pp. 261-279.

Cardoso, A.A., LIU, H. & DASGUPTA, P.K. 1997. Fluorometric fiber optic drop sensor for atmospheric hydrogen sulphide. *Talanta*, 44:1099-1106, doi: https://doi.org/10.1016/S0039-9140(96)02202-3.

Chiloane, K.E., Beukes, J.P., Van Zyl, P.G., Maritz, P., Vakkari, V., Josipovic, M., Venter, A.D., Jaars, K., Tiitta, P., Kulmala, M., Wiedensohler, A., Liousse, C., Mkhatshwa, G.V., Ramandh, A. & Laakso, L. 2017, Spatial, temporal and source contribution assessments of black carbon over the northern interior of South Africa. *Atmospheric Chemistry & Physics,* 17:6177-6196, doi: 10.5194/acp-17-6177-2017.

Chou, S., Ogden, J.M., Phol, H.R., Scinicariello, F., Ingerman, L., Barber, L. & Citra, M. 2016. Toxicological profile for hydrogen sulphide and carbonyl sulphide. Agency for Toxic Substances and Disease Registry: Atlanta, GA.

Cogho, E., Beukes, J.P., van Zyl, P.G. & Vakkari, V. 2022. The use of fire radiative power observations to determine spontaneous combustion event activities associated with coal mining on the Mpumalanga Highveld. *Clean Air Journal,* 32, doi: http://dx.doi.org/10.17159/caj/2022/32/2.12145.

Cogho, E., Beukes, J.P., van Zyl, P.G., Vakkari, V., Laakso, L., Josipovic, M. & Kulmala, M. 2023. Concentration contextualisation, temporal patterns and sources of hydrogen sulphide at a site on the South African Highveld. *Atmospheric Environment,* 315, doi: https://doi.org/10.1016/j.atmosenv.2023.120140.

Connel, D.W. 2005. Basic concepts of environmental chemistry. doi: https://doi.org/10.1201/b12378.

Conradie, E.H., Van Zyl, P.G., Pienaar, J.J., Beukes, J.P., Galy-Lacaux, C., Venter, A.D. & Mkhatshwa, G.V. 2016. The chemical composition and fluxes of atmospheric wet deposition at four sites in South Africa. *Atmospheric Environment*, 146:113-131, doi: http://dx.doi.org/10.1016/j.atmosenv.2016.07.033.

Collett, K.S., Piketh, S.J. & Ross, K.E. 2010. An assessment of the atmospheric nitrogen budget on the South African Highveld. *South African Journal of Science*, 106(5/6), Art. #220, doi: 10.4102/sajs.v106i5/6.220.

Colomer, F.L., Morató, H.E. & Iglesias, E.M. 2012. Estimation of hydrogen sulfide emission rates at several wastewater treatment plants through experimental concentration measurements and dispersion modelling. *Journal of the Air & Waste Management Association*, 62(7):758-766, DOI: 10.1080/10962247.2012.674008.

Contini, D., Cesari, D., Conte, M. & Donateo, A. 2016. Application of PMF and CMB receptor models for the evaluation of the contribution of a large coal-fired power plant to $PM_{10}$ concentrations. *Science of the Total Environment*, 560-561:131-140, doi: http://dx.doi.org/10.1016/j.scitotenv.2016.04.031.

Cooper, J.A. & Watson, JR. J.G. 1980. Receptor oriented methods of air particulate source apportionment. *Journal of the Air Pollution Control Association,* 30(10):1116-1125, doi: 10.1080/00022470.1980.10465157.

Cyrys, J., Eeftens, M., Heinrich, J., Ampe, C., Armengaud, A., Beelen, R., Bellander, T., Beregszaszi, T., Birk, M., Cesaroni, G. & Cirach, M. 2012. Variation of NO2 and NOx concentrations between and within 36 European study areas: results from the ESCAPE study. *Atmospheric Environment*, 62:374-390, doi: https://doi.org/10.1016/j.atmosenv.2012.07.080.

Dabrowski, J.M., Ashton, P.J., Murray, K., Leaner, J.J. & Mason, R.P. 2008. Anthropogenic mercury emissions in South Africa: Coal combustion in power plants. *Atmospheric Environment*, 42(27):6620-6626.

Daly, A., Zannetti, P. 2007. An introduction of air pollution: definitions, classifications, and history. (*In* Zannetti, P., Al-Ajmi, D. & Al-Rashied, S., *eds*. Ambient air Pollution, The Arab School for Science and Tegnology (ASST) and The EnviroComp Institue. 1-14 p.)

DAVIS, B.H. & HOWER, J.C. 2017. Coal technology for power, liquid fuels, and chemicals. In: Kent, J., Bommaraju, T., Barnicki, S. (eds). Handbook of industrial chemistry and biotechnology. Springer, Cham. https://doi.org/10.1007/978-3-319-52287-6_3

Delmas, R., Baudet, J., Servant, J. & Baziard, Y. 1980. Emissions and concentrations of hydrogen sulfide in the air of the tropical forest of the Ivory Coast and of temperate regions in France. *Journal of Geophysical Research*, 85:148-227, doi: 10.1029/JC085iC08p04468.

De Lange, A., Naidoo, M., Garland, R.M. & Dyson, L.L. 2021. The sensitivity of simulated surface-level pollution concentrations to WRF-ARW-model PBL parameterisation schemes over the Highveld of South Africa. *Atmospheric Research*, 254, doi: https://doi.org/10.1016/j.atmosres.2021.105517.

Department Of Cooperative Governance And Traditional Affairs. 2020. City of Tshwane Metropolitan GAU.

Department Of Cooperative Governance And Traditional Affairs. 2020. City of Johannesburg Metropolitan GAU.

Department Of Environmental Affairs. 2007, Government Gazette, 23 November, No. 30518.

Department Of Environmental Affairs. 2009, Government Gazette, 24 December, No. 32816.

Department Of Environmental Affairs. 2009, State of Air Report 2005. A report on the state of air in South Africa.

Department Of Environmental Affairs. 2010, The Highveld Priority Area Air Quality Baseline Assessment Report 2010.

Department Of Environmental Affairs. 2012.

Department Of Forestry, Fisheries And The Environment (DFFE). 1998. Terms of reference for the establishment of a national environmental consultative and advisory forum in terms of Section 3A of the National Environmental Management Act, 1998 (Act 107 of 1998) to advise the minister of forestry, fisheries and the environment on matters arising from applications for the suspension and postponement of compliance with the minimum emission standards and the applications for the issuance of provisional atmospheric emission licences.

Department Of Mineral Resources And Energy (DMRE). 2022. The South African Energy Sector Report 2022. ISBN: 978-1-920435-24-0.

Dhital, S., Rupakheti, D. 2019. Bibliometric analysis of global research on air pollution and human health. *Environmental Science and Pollution Research*, 26, 13103 – 13114, doi: https://doi.org/10.1007/s11356-019-04482-x.

Di, Q., Wang, Y., Zanobetti, A., Wang, Y., Koutrakis, P., Choirat, C., Dominici, F. & Schwartz, J.D. 2017. Air pollution and mortality in the medicare population. *The New England Journal of Medicine*, 376:2513-2522, doi: 10.1056/NEJMoa1702747.

Doraiswamy, P., Davis, W.T., Miller, T.L., Fu, J.S. 1995. Source apportionment of fine particles in Tennessee using a source-oriented model. *Journal of the Air & Waste Management Association,* 57:407-419, doi: 10.3155/1047-3289.57.4.407.

Draxler, R.R. & Hess, G.D. 2004. Description of the HYSPLIT 4 Modelling System. NOAA Technical Memorandum ERL ARL-224.

Du Preez, S.P., Beukes, J.P. & Van Zyl, P.G. 2015. Cr(VI) Generation During Flaring of CO-Rich Off-Gas from Closed Ferrochromium Submerged Arc Furnaces. *Metallurgical and Materials Transactions*, 46B, 1002-1010, doi: 10.1007/s11663-014-0244-3.

Ehn, M., Thornton, J., Kleist, E. *et al.* 2014. A large source of low-volatility secondary organic aerosol. *Nature,* 506:476-479. https://doi.org/10.1038/nature13032

Eldering, A. & Cass, G.R. 1996. Source-orientated model for air pollution effects on visibility. *Journal of Geophysical Research*, 101(D14). doi: 10.1029/95JD02928.

Engelbrecht, J.P., Swanepoel, L., Chow, J.C., Watson, J.G. & Egami, R.T. 2002, The comparison of source contributions from residential coal and low-smoke fuels, using CMB modelling in South Africa. *Environmental Science & Policy*. 5:157-167, doi: http://dx.doi. org/10.1016/S1462-9011(02)00029-1.

Engineering News. 2017. Camden power station to receive last of 164 burners. http://www.engineeringnews.co.za/article/camden-power-station-to-receive-last-of-164-burners-2017-01-27. Date of access [18 Feb 2019].

Environmental Protection Agency. Report to Congress on Hydrogen Sulfide Air Emissions Associated with the Extraction of Oil and Natural Gas." EPA-453/R-93-045, October 1993. p.III-4.

Environmental Protection Agency. 2009. Standard Operating Procedures. Thermo Environmental Instruments Model 43C $SO_2$ analyser. Version no. 2.0.

Environmental Protection Agency. Managing Air Quality – Emissions Inventories. https://www.epa.gov/air-quality-management-process/managing-air-quality-emissions-inventories. Last updated 16 January 2018. Date of access: [23 Jul 2018].

ESKOM. 2014. Response to request for additional information with regards to the Kriel power station postponement application for compliance to the minimum emissions standards. Reference number: ENV14-L211.

ESKOM. 2019. Power generation overview. www.eskom.co.za/AboutElectricity/FactsFigures/Documents/CO0002HowElecProducedCoalFiredRev11.pdf. Date of access: [22 Feb 2019].

Feig, G., Garland, R.M., Naidoo, S., Maluleke, A. & Van Der Merwe, M. 2019. Assessment of changes in concentrations of selected criteria pollutants in the Vaal and Highveld priority areas. *Clean Air Journal*, 29(2), doi: https://doi.org/10.17159/caj/2019/29/2.7464.

Feilberg, A., Hansen, M.J., Liu, D. & Nyord, T. 2017. Contribution of livestock H2S to total sulfur emissions in a region with intensive animal production. *Nature Communications*, doi: 10.1038/s41467-017-01016-2.

Fenger, J. 2009. Urban air pollution. (*In* HEWITT, C.N. & JACKSON, A.V., *eds*. Atmospheric science for environmental scientists. Chichester, W. Sussex: Wiley-Blackwell. 242-267 p.)

Freiman, M.T. & Piketh, S.J. 2002 Air transport into and out of the industrial Highveld Region of South Africa. *Journal of Applied Meteorology*, 42(7):994-1002, doi: 10.1175/1520-0450(2003)042<0994:ATIAOO>2.0.CO;2.

Garstang, M., Tyson, P.D., Swap, R., Edwards, M., Kållberg, P. & Lindesay, J.A. 1996. Horizontal and vertical transport of air over southern Africa. *Journal of Geophysical Research*, 101:721-736. http://dx.doi. org/10.1029/95JD00844.

Giannakaki, E., Pfülle, A., Korhonen, K., Mielonen, T., Laalso, L., Vakkari, V., Baars, H., Engelman, R., Beukes, J.P., Van Zyl, P.G., Josipovic, M., Tiitta, P., Chiloane, K., Piketh, S.J., Lihavainen, H., Lehtinen, K.E.J. & Komppula, M. 2015. One year of Ramen lidar observations of free-tropospheric aerosol layers over South Africa. *Atmospheric Chemistry and Physics*, 15:5429-5442, doi: 10.5194/acp-15-5429-2015.

Giglio, L., Descloitres, J., Justice, C.O. & Kaufman, Y.J. 2003, An enhanced contextual fire detection algorithm for MODIS. *Remote Sensing of Environment*, 87:2-3, doi: 10.1016/S0034-4257(03)00184-6.

Giglio, L., Schroeder, W. & Justice, C.O. 2016. The collection 6 MODIS active fire detection algorithm and fire products. *Remote Sensing of Environment*, 178, doi: 10.1016/j.rse.2016.02.054

Ghude, S.D., Van Der A, R.J., Beig, G., Fadnavis, S. & Polade, S.D. 2009. Satellite derived trends in $NO_2$ over the major global hotspots during the past decade and their inter-comparison. *Environmental Pollution*, 157:1873-1878, doi: https://doi.org/10.1016/j.envpol.2009.01.013.

Gierens, R.T., Henriksson, S., Josipovic, M., Vakkari, V., Van Zyl, P.G., Beukes, J.P., Wood, C.R. & O'connor, E.J. 2018. Observing continental boundary-layer structure and evolution over the South African savannah using a ceilometer. *Theoretical Applied Climatology*, doi: 10.1007/s00704-018-2484-7.

Gray, H.A. 2019. Air quality impacts and health effects due to large stationary source emissions in and around South Africa's Mpumalanga Highveld Priority Area (HPA).

Graham, J. 1998. Emissions and efficiencies of domestic appliances burning various fuels in South Africa. University of Cape Town.

Godish, T. 2004. Air quality, Fourth Edition. Lewis Publishers: Boca Raton, Florida.

Goar, B.G. 1986. Sulfur Recovery Technology". *Energy Progress*, 6:71-75.

Hales, J.M., Wilkes, J.O. & York, J.L. 1974. Some recent measurements of $H_2S$ oxidation rates and their implications to atmospheric chemistry. *Tellus*, 26(1-2):277-283, doi: 10.3402/tellusa.v26i1-2.9795.

Hac Ko, J., Xu, Q. & Jang, Y.-C. 2015. Emissions and control of hydrogen sulfide at landfills: a review. *Critical Reviews in Environmental Science and Technology*, 45(19):2043-2083, doi: 10.1080/10643389.2015.1010427.

Harvey, P.J. & GRAB, S.W. 2021. Southern African temperature responses to major volcanic eruptions since 1883: Simulated by CMIP5 models. *International Journal of Climatology*, 41:5386-5405, doi: https://doi.org/10.1002/joc.7135.

Hakkarainen, J., Ialongo, I., Oda, T., Szelag, M.E., O'dell, C.W., Eldering, A. & Crisp, D. 2023. Building a bridge: characterizing major anthropogenic point sources in the South African Highveld region using OCO-3 carbon dioxide snapshot area maps and Sentinal-5P/TROPOMI nitrogen dioxide columns. *Environmental Research Letters*, 18, doi: 10.1088/1748-9326/acb837.

Held, G., Snyman, G.M. & Scheifinger, H. 1993. Seasonal variation and trends of atmospheric particulates on the South African Highveld, *The Clean Air Journal*, 8(8):4-11.

Held, G., Gore, B.J., Surridge, A.D., Tosen, G.R., Turner, C.R. & Walmsley, R.D. 1996. Air pollution and its impacts on the South African Highveld, Environmental Scientific Association, Cleveland, 144pp.

Henry, R.C. 1987. Current factor analysis receptor models are ill-posed. *Atmospheric Environment*, 21:1815-1820, doi: https://doi.org/10.1016/0004-6981(87)90122-3.

Henry, R.C. 1991. Multivariate receptor models. *Receptor modelling for air quality management, Hopke PK (ed*). Elsevier: Amsterdam, 117-147.

Hinz, R. 2011. Hydrogen sulphide in Rotorua, New Zealand: personal exposure assessment and health effects. Palmerston North: Massey University. (Dissertation – MSc) 166p.

Holmes, N.S. 2007. A review of particle formation events and growth in the atmosphere in the various environments and discussion of mechanistic implications. *Atmospheric Environment*, 41(10):2183-2201, doi: https://doi.org/10.1016/j.atmosenv.2006.10.058.

Hopke, P.K. 2008. The use of Source apportionment for air quality management and health assessments. *Journal of Toxicology and Environmental Health*, Part A, 71(9-10):555-563, doi: 10.1080/15287390801997500.

Hopke, P.K. & Cohen D.D. 2011. Application of receptor modelling methods. *Atmospheric Pollution Research*, 2:122-125, doi: 10.5094/APR.2011.016.

Hopke, P.K. 2016. Review of receptor modelling methods for source apportionment. *Jounal of the Air & Waste Management Association*, 66(3):237-259, doi: 10.1080/10962247.2016.1140693.

Hyvärinen, A.-P., VAKKARI, V., LAAKSO, L., HOODA, R.K., SHARMA, V.P., PANWAR, T.S., BEUKES, J.P., VAN ZYL, P.G., JOSIPOVIC, M., GARLAND, R.M., ANDREAE, M.O., PÖSCHL, U. & PETZOLD, A. 2013. Correction

for a measurement artefact of the Multi-Angle Absorption Photometer (MAAP) at high black carbon mass concentration levels. *Atmospheric Measurement Techniques*, 6:81-90.

IPCC. 2021. Climate Change 2021: The Physical Science Basis. Contribution of Working Group I to the Sixth Assessment Report of the Intergovernmental Panel on Climate Change. Cambridge University Press, Cambridge, United Kingdom and New York, NY, USA, In press, doi:10.1017/9781009157896.

Intergovernmental Panel On Climate Change. 2013. Climate Change 2013: The physical science basis. *Contribution of Working Group I to the Fifth Assessment Report of the Intergovernmental Panel on Climate Change.* Cambridge University Press, Cambridge, United Kingdom and New York, NY, USA, 1535 pp. http://www.ipcc.ch/report/ar5/wg1/ Date of access: 25 Feb. 2019.

IPCC, 2007: Climate Change 2007: Impacts, Adaptation and Vulnerability. Contribution of Working Group II to the Fourth Assessment Report of the Intergovernmental Panel on Climate Change. Cambridge University Press, Cambridge, UK, 976pp.

Jaars, K., Van Zyl, P.G., Beukes, J.P., Hellén, H., Vakkari, V., Josipovic, M., Venter, A.D., Räsänen, M., Knoetze, L., Cilliers, D.P., Siebert, S.J., Kulmala, M., Rinne, J., Guenther, A., Laakso, L. & Hakola, H. 2016. Measurements of biogenic volatile organic compounds at a grazed savannah grassland agricultural landscape in South Africa. *Atmospheric Chemistry and Physics*, 16:15665-15688, doi: 10.5194/acp-16-15665-2016.

Jaars, K., Vestenius, M., Van Zyl, P.G., Beukes, J.P., Hellén, H., Vakkari, V., Venter, M., Josipovic, M. & Hakola, H. 2018. Receptor modelling and risk assessment of volatile organic compounds measured at a regional background site in South Africa. *Atmospheric Environment*, 172:133-148, doi: 10.1016/j.atmosenv.2017.10.047.

Jayaratne, E.R. & Verma, T.S. 2001. The impact of biomass burning on the environmental aerosol concentration in Gaborone, Botswana. *Atmospheric Environment*, 35:1821-1828, doi: 10.1016/S1352-2310(00)00561-6.

Jones, R.T. 2005. An overview of Southern African PGM smelting. *Nickel and Cobalt:*147-178.

JURY, M.R. & TOSEN, G.R. 1989. Characteristics of the winter boundary layer over the African Plateau: 26 S. *Boundary-Layer Meteorology*, 49(1-2):53-76, doi: https://doi.org/10.1007/BF00116405.

Kampa, M. & Castanas, E. 2008. Human health effects of air pollution. *Environmental Pollution*, 151:362-367.

Kleeman, M.J. & Cass G.R. 2001. A 3D eulerian source-oriented model for an externally mixed aerosol. *Environmental Science and Technology*, 25:4834-4848, doi:10.1021/es010886m.

Koelsch, R.K., Woodbury, B.L., Stenberg, D.E., Miller, D.N. & Schulte, D.D. 2004. Hydrogen sulfide concentration in vicinity of beef cattle feedlots. *Nebraska Beef Cattle Reports*, 198, https://digitalcommons.unl.edu/animalscinbcr/198.

Korhonen, K., Giannakaki, E., Mielonen, T., Pfuller, A., Laakso, L., Vakkari, V., Baars, H., Engelman, R., Beukes, J.P., Van Zyl, P.G., Ramandh, A., Ntsangwane, L., Josipovic, M., Tiitta, P., Fourie, G., Ngwana, I., Chiloane, K. & Komppula, M. 2014. Atmospheric boundary layer top height in South Africa: measurements with lidar and radiosonde compared to three atmospheric models. *Atmospheric Chemistry and Physics,* 14:4264-4278, doi: 10.5194/acp-14-4263-2014.

Kourtidis, K., Kelesis, A. & Petrakakis, M. 2007. Hydrogen sulphide ($H_2S$) in urban ambient air. *Atmospheric Environment*, 42, 7476-7482, doi: https://doi.org/10.1016/j.atmosenv.2008.05.066.

Kuik, F., Lauer, A., Beukes, J. P., Van Zyl, P.G., Josipovic, M., Vakkari, V., Laakso, L. & Feig, G.T. 2015: The anthropogenic contribution to atmospheric black carbon concentrations in southern Africa: a WRF-Chem modeling study, *Atmospheric Chemistry and Physics*, 15:8809-8830, doi:10.5194/acp-15-8809-2015.

Laakso, L., Laakso, H., Aalto, P.P., Keronen, P., Petäjä, T., Nieminien, T., Pohja, T., Siivola, E., Kulmala, M., Kgabi, N., Molefe, M., Mabaso, D., Phalatse, D., Pienaar, K. & Kerminen, V.-M. 2008. Basic characteristics of atmospheric particles, trace gases and meteorology in relatively clean Southern Africa Savannah environment. *Atmospheric Chemistry and Physics*, 8:4823-4839, doi: https://doi.org/10.5194/acp-8-4823-2008.

Laakso, L., Vakkari, V., Virkkula, A., Laakso, H., Backman, J., Kulmala, M., Beukes, J.P., Van Zyl, P.G., Titta, P., Josipovic, M., Pienaar, J.J., Chiloane, K., Gilardoni, S., Vignati, E., Wiedensohler, A., Tuch, T., Birmili, W., Piketh, S., et al. 2012. South African EUCAARI measurements: seasonal variation of trace gases and aerosol optical properties. *Atmospheric Chemistry and Physics*, 12:1847-1864, doi: https://doi.org/10.5194/acp-12-1847-2012.

Laakso, L., Merikanto, J., Vakkari, V., Laakso, H., Kulmala, M., Molefe, M., Kgabi, N., Mabaso, D., Carslaw, K. S., Spracklen, D. V., Lee, L. A., Reddington, C. L. & Kerminen, V.-M. 2013. Boundary layer nucleation as a source of new CCN in savannah environment. *Atmospheric Chemistry and Physics*, 13:1957-1972, doi:10.5194/acp13-1957-2013.

Laban, T.L., Van Zyl, P.G., Beukes, J.P., Vakkari, V., Jaars, K., Borduas-Dedekind, N., Josipovic, M., Thompson, A.M., Kulmala, M. & Laakso, L. 2018. Seasonal influences on surface ozone variability in continental South Africa and implications for air quality. *Atmospheric Chemistry and Physics,* 18:15491-15514, doi: https://doi.org/10.5194/acp-18-15491-2018.

Langerman, K.E., Pauw, C.J., Smith, H.J. & Piketh, S.J. 2018. Moving households to cleaner energy through air quality offsets. In 2018 International Conference on the Domestic Use of Energy (DUE), 1-8, doi: 10.23919/DUE.2018.8384405.

Mulumba, K.J., Langerman, K.E. & Marnewick, A.L. 2019. Determining the optimal energy use mix in a low-income household. In 2019 International Conference on the Domestic Use of Energy (DUE):25-33, ISBN: 978-0-6399647-3-7

Last, J.A., Sun, W.M. & Witschi, H. 1994. Ozone, NO, and NO2: oxidant air pollutants and more. *Environmental Health Perspectives*, 102 (10):179-184, doi: https://doi.org/10.1289/ehp.94102s10179.

Legal Resources Centre. 2014. Submission on SASOL and Natref's applications for postponement of compliance with the minimum emission standards (MES) under section 21 of the National Environmental Air Quality Act (AQA). https://cer.org.za/wp-content/uploads/2014/06/2014-06-16-LRC-SASOL-NATREF-postponement.pdf. Date of access: [31 May 2019].

Lourens, A.S.M., Beukes, J.P., Van Zyl, P.G., Fourie, G.D., Burger, J.W., Pienaar, J.J., Read, C.E. & Jordaan, J.H. 2011. Spatial and temporal assessment of the gaseous pollutants in the Highveld of South Africa. *South African Journal of Science*, 107(1/2), Art.#297, 8 pages, doi: 10.4102/sajs.v107i1/2.269.

Lourens, A.S.M., Butler, T.M., Beukes, J.P., Van Zyl, P.G., Beirle, S., Wagner, T.K., Heue, K., Pienaar, J.J., Fourie, G.D. & Lawrence, M.G. 2012. Re-evaluating the $NO_2$ hotspot over the South African Highveld. *South African Journal of Science*, 108(11/12), Art. #1146, 6 pages, doi: http://dx.doi.org/10.4102/sajs.v108i11/12.1146.

Lourens, A.S.M., Butler, T.M., Beukes, J.P., Van Zyl, P.G., Fourie, G.D. & Lawrence, M.G. 2016, Investigating atmospheric photochemistry in the Johannesburg-Pretoria megacity using a box model, *South African Journal of Science*, 112(1/2), Art. #2015-0169, 11 pages, doi: http://dx.doi.org/10.17159/sajs.2016/2015-0169.

Madubansi, M., Shackleton C.M. 2007. Changes in fuelwood use and selection following electrification in the Bushbuckridge lowveld, *South African Journal of Environmental Management*, 83:416-426, doi: https://doi.org/10.1016/j.jenvman.2006.03.014.

Maenhaut, W., Salma, I., Cafmeyer, J., Annegarn, H.J., Andreae, M.O. 1996. Regional atmospheric aerosol composition and sources in the eastern Transvaal, South Africa, and impact of biomass burning. *Journal of Geophysical Research*, 101:631-650.

Makonese, T., Masekameni, D.M., Annegarn, H.J. Forbes, P.B., 2017. Emission factors of domestic coal-burning braziers. *South African Journal of Science*, 113(3-4):1-11, doi: http://dx.doi.org/10.17159/sajs.2017/20160187.

Makonese, T., Ifegbesan, A.P. & Rampedi, I. 2018. Household cooking fuel use patterns and determinants across southern Africa: Evidence from the demographic and health survey data. *Energy and Environment*, 29:19-48, doi: https://doi-org.nwulib.idm.oclc.org/10.1177/0958305X17739475.

Malinowski, E.R. 2002. *Factor analysis in chemistry*; John Wiley and Sons, Inc.: New York, NY.

Manisalidis, I., Stavropoulou, E., Stravropoulos, A. & Bezirtzoglou, E. 2020. Environmental and health impacts of air pollution: A review. *Frontiers in Public Health,* 8, doi: 10.3389/fpubh.2020.00014.

Maseko, B., Feig, G. & Burger, R. 2021. Estimating lightning NOx production over South Africa. *South African Journal of Science*, 117:9-10, doi: http://dx.doi.org/10.17159/sajs.2021/8035.

Mathuthu, M., Dudu, V. & Manjoro, M. 2019. Source apportionment of air particulates in South Africa: a review. *Atmospheric and Climate Sciences*, 9:100-113. doi: 10.4236/acs.2019.91007.

Monks, P.S., Archibald, A.T., Colette, A., Cooper, O., Coyle, M., Derwent, R., Fowler, D., Granier, C., Law, K.S., Mills, G.E., Stevenson, D.S., Tarasova, O., Thouret, V., Von Schneidemesser, E., Sommariva, R., Widl, O. & Williams, M.L. 2015. Tropospheric ozone and its precursors from the urban to the global scale from air quality to short-lived climate forcer. *Atmospheric Chemistry and Physics,* 15:8889-8973, doi: https://doi.org/10.5194/acp-15-8889-2015.

Moritz, M.A., Parisien, M.A., Batllori, M.A., Van Doorm, J., Ganz, D.J. & Hayhoe, K. 2012. Climate change and disruptions to global fire activity. *Ecosphere,* 3(6):1-22, doi: https://doi.org/10.1890/es11-00345.1.

Mphepya, J.N., Pienaar, J.J., Galy-Lacaux, C., Held, G. & Turner, C. R. 2004. Precipitation chemistry in semi-arid areas of Southern Africa: a case study of a rural and an industrial site. *Journal of Atmospheric Chemistry*, 47:1-24, doi:10.1023/B:JOCH.0000012240.09119.c4.

Mphepya, J.N., Galy-Lacaux, C., Galy-Lacaux, J.P., Held, G. & Pienaar, J.J. 2006. Precipitation chemistry and wet deposition in the Kruger National Park, South Africa, *Journal of Atmospheric Chemistry*, 53, 169–183, doi:10.1007/s10874-005-9005-7.

Mucina, L. & Rutherford, M.C. 2007. The vegetation of South Africa, Lesotho and Swaziland. SANBI, Pretoria, ISBN: 978-1-919976-21-1.

National Traffic Information System (NaTIS). 2023. Available at: https://www.natis.gov.za/index.php/statistics/live-vehicle-population/live-vehicle-population-2022.

Nkosi, N.C., Piketh, S.J. & Burger, R.P. 2018. Fine PM emission factors from residential burning of solid fuels using traditional cast-iron coal stoves. *Clear Air Journal*, 28, doi: http://dx.doi.org/10.17159/2410-972X/2018/v28n1a10.

Notice of intention to declare the Highveld Priority Area in terms of Section 18(1) of the National Environmental Management. Air Quality Act, 2004. Act no. 39 of 2004. Proclamation no. 396, 2007.

Novelli, P. 2003. Carbon monoxide in the atmosphere. (*In* POTTER, T.D. & COLMAN, B.R., *eds*. *Handbook of weather, climate and water*. Hoboken, N.J.: John Wiley and Sons, Inc. 78-88 p.)

Noor, J. 2015. Options for the supply of electricity to rural homes in South Africa. *Journal of Energy South Africa,* 26:58-65. ISI.

Peterson, J., Fisher, G.W. & Timpany, G. 1998. Survey of background hydrogen sulphide in Rotorua – 1996/67. AK98013, NIWA.

Petzold, A., Ogren, J.A., Fiebig, M., Laj, P., Li, S.-M., Holzer-Popp, T., Kinne, S., Pappalardo, G., Sugimoto, N., Wehrli, C., Wiedensohler, A. & Zhang, X.-Y. 2013. Recommendations for reporting "black carbon" measurements. *Atmospheric Chemistry and Physics*, 13:8365-8379, doi: 10.5194/acp-13-8365-2013.

Piketh, S.J., Van Nierop, M., Rautnbach, C., Walton, N., Ross, K., Holmes, S. & Richards, T. 2005. Rustenburg Local Municipality Air Quality Management Plan, Palace consulting engineers ltd. Republic of South Africa.

Pires, J.C.M., Sousa, S.I.V., Pereira, M.C., Alvim-Ferraz, M.C.M. & Martins, F.G. 2007. Management of air quality monitoring using principal component and cluster analysis-Part I: $SO_2$ and PM10. *Atmospheric Environment*, 42:1249-1260, doi: 10.1016/j.atmosenv.2007.10.044.

Pires, J.C.M., Sousa, S.I.V., Pereira, M.C., Alvim-Ferraz, M.C.M. & Martins, F.G. 2008. Management of air quality monitoring using principal component and cluster analysis-Part II: CO, $NO_2$ and $O_3$. *Atmospheric Environment*, 42:1249-1260, doi: 10.1016/j.atmosenv.2007.10.041.

Poschl, D. 2005. Atmospheric aerosols: Composition, transformation, climate and health effects. *Angewandte Chemie International Edition*, 44(46):7520-7540, doi: https://doi.org/10.1002/anie.200501122.

Pretorius, R.W., Aur, T.I., Held, G., Brassel, K.M., Danford, I.R. & Waldie, D.D. 1986. The climatology of the boundary layer over the eastern Transvaal highveld and its impact on sulphur dioxide concentrations at ground level. A Report for The Foundation for Research Development, CSIR Report ATMOS/86/16, Pretoria, 1-212.

Pretorius, O.J. 2007. The atmospheric impact of SASOL Synfuels operations on adjacent residential development. *Clean Air Journal*, 16(1):18-24, https://hdl.handle.net/10520/EJC27333.

Pretorius, I., Piketh, S.J., Burger, R. & Neomagus, H. 2015. A perspective on South African coal fired power station emissions. *Journal of Energy in Southern Africa*, 26:27-40.

Rayner-Canham, G. & Overton, T. 2009. The group 16 elements the chalcogens, in: *Descriptive Inorganic Chemistry*, W.H. Freeman and Compony, New York, NY, pp. 387-388.

Reff, A., Eberly, S.I. & Bhave, P.V. 2007. Receptor modelling of ambient particulate matter data using positive matrix factorization: review of existing methods. *Journal of the Air & Waste Management Association,* 57(2):146-154, doi: 10.1080/10473289.2007.10465319.

Reisell, A., Macdonald, C., Roberts, P. & AREY, J. 2003. Characterization of biogenic volatile organic compound and meteorology at Azusa during the SCOS97- NARSTO. *Atmospheric Environment*, 37(Suppl 2):181-196, doi: 10.1016/S1352-2310(03)00390-X.

Riddle, E.E., Voss, P.B., Stohl, A., Holcomb, D., Maczka, D., Washburn, K. & Talbot, R.W. 2006, Trajectory model validation using newly developed altitude-controlled balloons during the International Consortium for Atmospheric research and Transport and transformations 2004 campaign. *Journal of Geophysical Research*, 111, D23S57, doi: 10.1029/2006JD007456.

Road Traffic Management Corporation (RTMC). 2009. Road Traffic Report – June 2009. Available at: https://www.rtmc.co.za/index.php/publications/reports/traffic-reports/quarterly-year-reports.

RORICH, R.P. & GALPIN, I. 1998. Air quality in the Mpumalanga Highveld region, South Africa. South *African Journal of Science*, 94(3):109-114, doi: https://hdl.handle.net/10520/AJA00382353_133.

Ross, K.E., Piketh, S.J., Bruintjes, T., Burger, R.P., Swap, R.J. & Annegarn, H.J. 2003. Spatial and seasonal variations in CCN distribution and the aerosol-CCN relationship over southern Africa. *Journal of Geophysical Research*, 108:17-18.

Rubright, S.L.M., Pearce, L.L. & Peterson, J. 2017. Environmental toxicology of hydrogen sulfide. *Nitric Oxide,* 71:1-13, doi: 10.1016/j.niox.2017.09.011.

Sakirkin, S.L.P., Casey, K.D. & Auvermann, B.W. 2012. Hydrogen sulfide emissions from open/dry-lot-cattle-feeding operations. A*ir Quality Education in Animal Agriculture*, http://www.extension.org/pages/15538/air-quality-in-animal-agriculture.

Sangeetha, S.K., Sivakumar, V. & Gebreslasie, M. 2018. Long-range transport of SO2 over South Africa: A case study of the Calbuco volcanic eruption in April 2015. *Atmospheric Environment*, 185, 78-90, doi: https://doi.org/10.1016/j.atmosenv.2018.04.056.

Sangeetha, S.K. & Sivakumar, V. 2019. Long-term temporal and spatial analysis of SO2 over Gauteng and Mpumalanga monitoring sites of South Africa. *Journal of Atmospheric and Solar-Terrestrial Physics*, 191:105044, doi: https://doi.org/10.1016/j.jastp.2019.05.008.

Scheepers, C.C.W. 2011. Physiological and biochemical constraints on photosynthesis of leguminous plants induced by elevated ozone in open-top chambers (Thesis, North-West University).

SchoemaN, A. 2016. Risk mapping of eMalahleni municipal area with focus on coal mining impacts. Potchefstroom: NWU. (Dissertation – MSc) 134p.

Scott, B. 1992. Written communication from Bruce Scott, Bruce Scott, Inc., San Rafael, CA, to David Hendricks, Pacific Environmental Services, Inc., Research Triangle Park, NC, February28.

Scorgie, Y. 2012. Urban air quality management and planning in South Africa. University of Johannesburg.

Sehloho, T., Beukes, J.P., Van Zyl, P.G., Vakkari, V., Josipovic, M., Gilardoni, S., Vignati, E., Gianelle, V., Kulmala, M. & Laakso, L. 2019. Aerosol composition on the South African Highveld, in preparation for *Atmospheric Environment*.

Seinfeld, J.H. & Pandis, S.N. 2006, Atmospheric chemistry and physics: from air pollution to climate change. 2nd ed. P 219. John Wiley & Sons, Inc.

Sengupta, A. 2014. Preliminary hydrogen sulfide emission factors and emission models for wastewater treatment plant headworks. *University of New Orleans Theses and Dissertations*. 1829. https://scholarworks.uno.edu/td/1829.

Shirai, H., Ikeda, M. & Aramaki, H. 2012. Characteristics of hydrogen sulphide formation in pulverized coal combustion. *Fuel*, 114:114-119, doi: http://dx.doi.org/10.1016/j.fuel.2012.03.028.

Shikawambana, L., Mhangara, P. & Mbatha, N. 2020. Trend analysis and first time observations of sulphur dioxide and nitrogen dioxide in South Africa using TROPOMI/Sentinal-5 P data. *International Journal of Applied Earth Observations and Geoinformation*, 91, doi: https://doi.org/10.1016/j.jag.2020.102130.

Skrtic, L. 2006. Hydrogen sulfide, oil and gas, and people's health. Berkeley: University of California. (Dissertation – MSc) 77p.

Slatt, B.J., Natusch, D.F.S., Prospero, J.M. & Savoie, D.L. 1967. Hydrogen sulphide in the atmosphere of the northern equatorial Atlantic Ocean and its relation to the global sulfur cycle. *Atmospheric Environment*, 12:981-991, doi: https://doi.org/10.1016/0004-6981(78)90342-6.

SMITH, K.A., Mctaggart, I.P. & TSURUTA, H. 1997. Emissions of N2O and NO associated with nitrogen fertilization in intensive agriculture, and the potential for mitigation. *Soil Use and Management*, 13:296-304, doi: https://doi.org/10.1111/j.1475-2743.1997.tb00601.x.

Sousa, S.I.V., Martins, F.G., Alvim-Ferraz, M.C.M. & Pereira, M.C. 2007. Multiple linear regression and artificial neural networks based on principal components to predict ozone concentrations. *Environmental Modelling & Software*, 22:97-103, doi: 10.1016/j.envsoft.2005.12.002.

Stern, D.I. 2006. Reversal of the trend of global anthropogenic sulphur emissions. *Global Environmental Change*, 16:207-220.

Stohl, A. 1998, Computation, accuracy and application of trajectories: a review and bibliography. *Atmospheric Environment*, 32:947-966, doi: 10.1016/S1352-2310(97)00457-3.

Su, L., Yuan, Z., Fung, J.C.H. & Lau, A.K.H. 2014. A comparison of HYSPLIT backward trajectories generated from two GDAS datasets. *Science of the Total Environment*:506-507, 527-537, doi: http://dx.doi.org/10.1016/j.scitotenv.2014.11.072.

Suwa, T., Hogg, J.C., Quinlan, K.B., Ohgami, A., Vincent, R. & Van Eeden, S.F. 2002. Particulate air pollution induces progression of atherosclerosis. *Journal of the American College of Cardiology*, 39(6):35-942 doi: https://doi.org/10.1016/S0735-1097(02)01715-1.

Sussman, V.H. & Mulhern, J.J. 1964. Air pollution from coal refuse disposal areas. *Journal of the Air Pollution Control Association*, 14(7):279-284, doi: 10.1080/00022470.1964.10468282.

Swap, R.J., Annegarn, H.J., Suttles, J.T., King, M.D., Platnick, S., Privette, J.L. & Scholes, R.J. 2003. Africa burning: A thematic analysis of the Southern African Regional Science Initiative (SAFARI 2000). *Journal of Geophysical Research: Atmospheres***,** 108(D13), doi: 10.1029/2003JD003747.

Thermo Fisher Scientific. 2007. Model 5012 MAAP – Multi Angle Absorption Photometer. Franklin.

Thermo Fisher Scientific. 2007. Model 42i – Instruction Manual, Chemiluminescence NO-$NO_2$_$NO_x$ Analyser. Franklin.

Tiitta, P., Vakkari, V., Croteau, P., Beukes, J.P., Van Zyl, P.G., Josipovic, M., Venter, A.D., Jaars, K., Pienaar, J.J., Ng, N.L., Canagaratna, M.R., Jayne, J.T., Kerminen, V.-M. Kokkola, H., Kulmala, M., Laaksonen, A., Worsnop D.R. & Laakso, L. 2014. Chemical composition, main sources and temporal variability of PM1 aerosols in southern African grassland, *Atmospheric Chemistry and Physics*, 14:1909-1927, doi:10.5194/acp-14-1909-2014.

Toengas-Schuller, N., Stein, O., Rohrer, F., Wahner, A., Richter, A., Burrows, J.P., Bierle, S., Wagner, T., Plat, U. & Elvidge, C.D. 2006. Global distribution pattern of anthropogenic nitrogen oxide emissions: Correlation analysis of satellite measurements and model calculations. *Journal of Geophysical Research*, 111, doi: https://doi.org/10.1029/2005JD006068.

Tongwane, M., Mdlambuzi, T., Moeletsi, M., Tsubo, M., Mliswa, V. & Grootboom, L. 2016. Greenhouse gas emissions from different crop production and management practices in South Africa. *Environmental Development,* 19:23-35, doi: https://doi.org/10.1016/j.envdev.2016.06.004.

Tongwane, M.I. & Moeletsi, M.E. 2021. Provincial cattle carbon emissions from enteric fermentation and manure management in South Africa. *Environmental Research*, 195, doi: https://doi.org/10.1016/j.envres.2021.110833.

Tosen, G.R. & Jury, M. 1988. Climatology of the winter boundary layer over the eastern Transvaal. *South African Journal of Science*, 84(4), 247.

Tummon, F., Solmon, F., Liousse, C. & Tadross, M. 2010. Simulation of the direct and semidirect aerosol effects on the southern Africa regional climate during the biomass burning season, *Journal of Geophysical Research*, 115, D19206, doi:10.1029/2009JD013738.

Tyson, P.D. & D'abreton, P.C. 1998. Transport and recirculation of aerosols off Southern Africa: macroscale plume structure. *Atmospheric Environment*, 32:1511-1524, doi: https://doi.org/10.1016/S1352-2310(97)00392-0.

Van Der Merwe, C., Sukdeo, P., Peta, S. & Smit, D. 2017. Eskom low NOx burner combustion simulation experience*. 2017 ANSYS Engineering Simulation Conference*. https://www.researchgate.net/publication/329443440_ESKOM_Low_NOx_burner_combustion_simulation_experience_-_A_Low_NOx_burner_design_case_study.

Van Wilgen, B.W. & Richardson, D.M. 1985. The effects of alien shrub invasions on vegetation structure and fire behaviour in south African fynbos shrublands: A simulation study. *Journal of Applied Energy,* 22:955-966, doi: https://doi.org/10.2307/2403243.

Van Zyl, P.G., Beukes, J.P., Du Toit, G., Mabaso, D., Hendriks, J., Vakkari, V., Tiitta, P., Pienaar, J.J., Kulmala, M. & Laakso, L. 2014. Assessment of atmospheric trace metals in the western Bushveld Igneous Complex, South Africa, *South African Journal of Science*, 110(3/4), Art. #2013-0280, 11 pages, doi: https://doi.org/10.1590/sajs.2014/20130280.

Vakkari, V., Laakso, H., Kulmala, M., Laaksonen, A., Mabaso, D., Molefe, N. & Laakso, L. 2011. New particle formation events in semi-clean South African savannah. *Atmospheric Chemistry Physics*, 11:3333-3346. doi: https://doi.org/10.1002/2014GL059396.

Vakkari, V., Kerminen, V., Beukes, J.P., Tiits, P., Van Zyl, P.G., Josipovic, M., Venter, A.D., Jaars, K., Worsnop, D., Kulmala, M. & Laakso, L. 2014. Rapid changes in biomass burning aerosols by atmospheric oxidation. *Geophysical Research Letters*, 41, 2644-2651, doi: https://doi.org/10.1002/2014GL059396.

Vallero, D.A. 2014. Fundamentals of air pollution. Academic Press.

Vallero, D.A. 2021. Mapping exposure onto nanoscale toxicity measures. nanotoxicology in humans and the environment. Molecular and Integrative Toxicology. Springer, Cham. https://doi.org/10.1007/978-3-030-79808-6_6.

Venter, A.D., Vakkari, V., Beukes, J.P., Van Zyl, P.G., Laakso, H., Mabaso, D., Tiitta, P., Josipovic, M., Kulmala, M., Pienaar, J.J. & Laakso, L. 2012. An air quality assessment in the industrialised western Bushveld Igneous Complex, South Africa. *South Africa Journal of Science*, 108:1-10, doi: http://dx.doi.org/10.4102/sajs.v108i9/10.1059.

Venter, A.D., Van Zyl, P.G., Beukes, J.P., Josipovic, M., Hendriks, J., Vakkari, V. & Laakso, L. 2017. Atmospheric trace metals measured at a regional background site (Welgegund) in South Africa, *Atmospheric Chemistry and Physics*, 17:4251–4263, doi:10.5194/acp-17-4251-2017.

Venter, M., Beukes, J.P., Van Zyl, P.G., Vakkari, V., Virkkula, A., Josipovic, M., Kulmala, M. & LaaKSO, L. 2019. Long-term observations of aerosol optical properties at a southern African grassland savannah site, in preparation for *Atmospheric Chemistry and Physics*.

Venter, A.D. & Lourens, A.S.M. 2021. Ambient air quality data reported at Sasol Secunda monitoring stations during COVID-19 lockdown: Mpumalanga, South Africa. *Clean Air Journal,* 31, doi: http://dx.doi.org/10.17159/caj/2021/31/1.8954.

Viana, M., Kuhlbusch, T.A.J., Querol, X., Alastuey, A., Harrison, R.M., Hopke, P.K., Winiwarter, W., Vallius, M., Szidat, S., Prévôt, A.S.H., Hueglin, C., Bloemen, H., Wåhlin, P., Vecchi, R., Miranda, A.I., Kasper-Giebl, A., Maenhaut, W. & Hitzenberger, R. 2008. Source apportionment of particulate matter in Europe: A review of methods and results. *Journal of Aerosol Science,* 39:827-849, doi: 10/1016/j.jaerosci.2008.05.007.

Visser, H., Buring, E. & Breugel, P.B. 2001. Composition and origin of airborne particulate matter in the Netherlands. *National Institute for Public Health and the Environment*, RIVM.

Wagmuller, M. & Peterson, J. 1998. Method to quantify the $H_2S$ – Exposure for the urban area of Rotorua. AK98024, NIWA.

Wang, S. & Xiao, F. 2004. AHU sensor fault diagnosis using principal component analysis method. *Energy and Buildings*, 36(2):147-160, doi: 10.1016/j.enbuild.2003.10.002.

Wang, Y., Ali, M.A., Bilal, M., Qiu, Z., Mhawish, A., Almazroui, M., Shahid, S., Islam, M.N., Zhang, Y. & Haque, M.N. 2021. Identification of NO2 and SO2 pollution hotspots and sources in Jiangsu Province of China. *Remote Sensing*, 13(18):37-42, doi: https://doi.org/10.3390/rs13183742.

Wei, J., Li, Z., Wang, J., Li, C., Gupta, P. & Crib, M. 2023. Ground level gaseous pollutants (NO2, SO2 and CO) in China: daily seamless mapping and spatiotemporal variations. *Atmospheric Chemistry and Physics,* 23:1511-1532, doi: https://doi.org/10.5194/acp-23-1511-2023.

Wells, R., Lloyd, S. & Turner, C. 1996. National air pollution source inventory, in: Air pollution and its impacts on the South African highveld, (eds.) Held, G., Gore, B.J., Surridge, A.D., Tosen, G.R., Turner, C. R. & Walmsley, R.D., 3-9, *Environmental Scientific Association*, Cleveland.

Wenig, M., Spichtinger, N., Stohl, A., Held, G., Beirle, S., Wagner, T., Jähne, B. & Platt, U. 2003. Intercontinental transport of nitrogen oxide pollution plumes. *Atmospheric Chemistry and Physics*, 3:387-393, doi: https://doi.org/10.5194/acp-3-387-2003.

Williams, P.I. & Baltensperger, U. 2009. Particulate Matter In The Atmosphere. (*In* Hewitt, C.N. & Jackson, A.V., *eds. Atmospheric Science for Environmental Scientists*. Chichester, W. Sussex: Wiley-Blackwell. 168-197 p.)

Wold, S., Esbensen, K. & Geladi, P. 1987. Principal component analysis. *Chemometrics and Intelligent Laboratory Systems*. 2(1-3):37-52, doi: 10.1016/0169-7439(87)80084-9.

World Health Organization. 2003. Hydrogen Sulphide: Human health aspects. *Concise international chemical assessment document*; 53. ISBN: 92 4 1530537, ISSN: 1020-6167.
World Health Organization. 2016. Ambient air pollution: A global assessment of exposure and burden of disease.

World Health Organization. 2019. Ambient air pollution: training for health care providers (No. WHO/CED/PHE/EPE/19.12. 14). World Health Organization.

Xiao, Z. & Laplante, A.R. 2004. Characterizing and recovering the platinum group minerals-a review. *Minerals and Engineering*, 17:961-979 doi: 10.1016/j.mineng.2004.04.001.

Yarwood, G., Morris, R.E. & Wilson, G.M. 2007. Particulate Matter Source Apportionment Technology (PSAT) in the CAMx Photochemical Grid Model. *Air Pollution Modeling and its Application XVII.* Springer, Boston, MA, doi: https://doi.org/10.1007/978-0-387-68854-1_52.

Zunckel, M., Turner, C.R. & Wells, R.B., 1996. Dry deposition of sulphur on the Mpumalanga highveld: a pilot study using the inferential method. *South African Journal of Science*, 92(10):485-491, doi: http://hdl.handle.net/10204/719.

Zunckel, M., Robertson, L., Tyson, P.D. & Rodhe, H., 2000. Modelled transport and deposition of sulphur over Southern Africa. *Atmospheric Environment,* 34:2797-2808, doi: 10.1016/S1352-2310(99)00495-1.